NASA CR-72340
RCA 647DR-1220

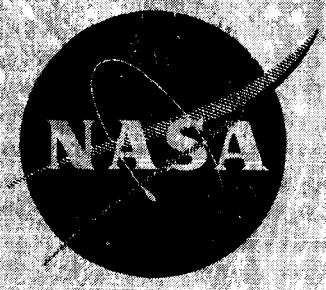

SOLAR THERMOELECTRIC GENERATOR DESIGN AND PANEL DEVELOPMENT PROGRAM (U)

(TASK III)

by

V. RAAG, R. E. BERLIN, and L. H. GNAU

Prepared for

NATIONAL AERONAUTICS AND SPACE ADMINISTRATION

CONTRACT NAS 3-10600

RADIO CORPORATION OF AMERICA
ELECTRONIC COMPONENTS AND DEVICES

Requests for copies of this report should be referred to

National Aeronautics and Space Administration
Office of Scientific and Technical Information
Attention: AFSS-A
Washington, D.C. 20546

NASA CR-72340
RCA 647DR-1220

DESIGN REPORT

SOLAR THERMOELECTRIC GENERATOR DESIGN AND PANEL DEVELOPMENT PROGRAM (U)

(TASK II)

by

V. RAAG, R. E. BERLIN, and L. H. GNAU

Prepared for

NATIONAL AERONAUTICS AND SPACE ADMINISTRATION

DECEMBER 20, 1967

CONTRACT NAS 3-10600

Technical Management
NASA Lewis Research Center
Cleveland, Ohio
Space Electric Power Office
WILLIAM BIFANO

TABLE OF CONTENTS

TABLE OF CONTENTS (Cont.)

LIST OF ILLUSTRATIONS

LIST OF ILLUSTRATIONS (Cont.)

LIST OF ILLUSTRATIONS (Cont.)

LIST OF TABLES

SYMBOLS

Section II

A - dummy integration variable pertaining to area

α - absorptivity of heat-reception plate

A_n - cross-sectional area of n-type thermoelement

A_p - cross-sectional area of p-type thermoelement

A_s - cross-sectional area of direct shunt heat transfer

A_T - area of heat-reception and heat-rejection plates

ΔT_C - average temperature difference of inner and outer surfaces of heat-rejection plate

ΔT_H - average temperature difference of outer and inner surfaces of heat-reception plate

ϵ_C - emissivity of outer surface of heat-rejection plate

ϵ_{CI} - emissivity of inner surface of heat-rejection plate

ϵ_H - emissivity of outer surface of heat-reception plate

ϵ_{HI} - emissivity of inner surface of heat-reception plate

E_L - load voltage

ϵ_S - net emissivity of inner surfaces of heat-reception and heat-rejection plates

η - efficiency of thermocouple

f - general function pertaining to temperature

I - current flowing through the thermocouple

k - thermal conductivity

K_C - thermal conductance of heat-reception plate

k_C - thermal conductivity of heat-rejection plate

K_{CS} - thermal conductance of cold stack

k_{CS} - thermal conductivity of cold stack

K_H - thermal conductance of heat-reception plate

k_H - thermal conductivity of heat-reception plate

K_{HS} - thermal conductance of hot stack

k_{HS} - thermal conductivity of hot stack

k_n - temperature averaged thermal conductivity of n-type thermoelement

k_p - temperature averaged thermal conductivity of p-type thermoelement

k_s - thermal conductivity of insulation

K_T - combined thermal conductance of n- and p-type thermoelements

SYMBOLS (Cont.)

ℓ - length of n- and p-type thermoelements

m - ratio of load to internal electrical resistance

μ - temperature averaged net Thomson coefficient of n- and p-type thermoelements

N - number of terms in a finite sum that approximates an integral

n - summation index

P_o - electrical power output

Q_I - total heat incident on heat-reception plate

Q_s - total amount of shunt heat

Q_T - total heat traversing the thermocouple

R - heat production per unit volume

r - radial coordinate

R_C - heat production per unit volume in heat-rejection plate

r_{Cn} - contact "resistivity" of n-type thermoelement and its metallic end piece

r_{Cp} - contact "resistivity" of p-type thermoelement and its metallic end piece

R_H - heat production per unit volume in heat-reception plate

R_I - total internal electrical resistance of thermocouple

r_i - radius of a circular plate of area equal to the combined areas of n- and p-type thermoelements

R_L - external electrical (load) resistance

ρ_n - temperature averaged electrical resistivity of n-type thermoelement

r_o - radius of a circular plate of area A_T

ρ_p - temperature averaged electrical resistivity of p-type thermoelement

R_S - extraneous electrical resistance of thermocouple

S - temperature averaged net Seebeck coefficient of n- and p-type thermoelements

σ - Stefan - Boltzmann constant

S_{HJ} - net Seebeck coefficient of n- and p-type thermoelements at hot junction

S_n - Seebeck coefficient of n-type thermoelement

S_p - Seebeck coefficient of p-type thermoelement

T - temperature

T_C - heat rejection plate temperature

t_C - thickness of the heat-rejection plate

T_{CJ} - cold junction temperature

SYMBOLS (Cont.)

t_{CS} - thickness of cold stack
T_H - heat-reception plate temperature
t_H - thickness of heat reception plate
T_{HJ} - hot junction temperature
t_{HS} - thickness of hot stack
t_s - insulation thickness
τ_n - Thomson coefficient of n-type thermoelement
τ_p - Thomson coefficient of p-type thermoelement
θ - angular coordinate
W - heat flux incident on heat-reception plate
W_C - weight of heat-rejection plate
W_{CS} - weight of cold stack
W_H - weight of heat-reception plate
W_{HS} - weight of hot stack
W_I - weight of insulation
W_S - weight of electrical connectors
W_T - weight of n- and p-type thermoelements
W_t - total weight of thermocouple
ξ - dummy variable pertaining to thermoelectric properties

Section III F

A, A_e - area of thermoelement
a - acceleration
a_o - amplitude of vibration
α_e - coefficient of linear thermal expansion of thermoelements
α_P - coefficient of linear thermal expansion of heat-reception plate
β - ratio of imposed to natural vibration frequencies
d - diameter of thermoelement
δ_H - density of hot shoe
δ_T - density of thermoelectric material
E - modulus of elasticity
E_e - modulus of elasticity of thermoelements
E_P - modulus of elasticity of heat-reception plate
F - force
I - moment of inertia
L - length of beam
ℓ - length of thermoelements
M - moment
m - mass
ν - magnification factor on force or on moment
ω_n - natural vibration frequency
ω - imposed vibration frequency
R - radius of thermoelement
σ - stress
θ - angular integration variable
T_e - temperature of thermoelements
t_H - thickness of hot shoe
T_P - temperature of heat-reception plate
V_H - volume of hot shoe
V_T - volume of thermoelement
W - load on beam, weight
W_1 - weight of thermocouple
w - weight per unit length

SYMBOLS (Cont.)

x,X	-	component of Cartesian coordinates
y,Y	-	component of Cartesian coordinates
$Y_{\text{subscript}}$		deflection of beam
z,Z	-	component of Cartesian coordinates

SOLAR THERMOELECTRIC GENERATOR DESIGN AND DEVELOPMENT PROGRAM

by

V. Raag, R.E. Berlin, and L.H. Gnau

ABSTRACT

A silicon-germanium solar thermoelectric generator has been designed for operation at a distance of 0.25 AU from the sun. The generator delivers 150 watts of electrical power at a nominal load voltage of 28 volts; produces 36.4 watts per square foot of generator area; and weighs 3.23 pounds per square foot. The design and analysis of both thermoelectric and mechanical performances of this generator are considered in detail. Engineering layout drawings of the generator and its components are also presented.

I. SUMMARY

The objectives of this program, as defined by Contract NAS3-10600, are: 1) the design of a 150-watt, 28-volt flat plate solar thermoelectric generator using silicon germanium as the thermoelectric material, and 2) the fabrication of three (3) representative sections of the generator (nine couples in a three-by-three array) for test by NASA. This report covers the design of the Solar Thermoelectric Generator prepared during Tasks I and II. A subsequent report, to be issued at the conclusion of Task III, will describe the panel fabrication program.

The potential applications of this generator design would include solar probes or interplanetary missions requiring the operation of spacecraft in the region between Mercury and the Sun. Either the use of solar thermoelectric generators alone or combined with solar photovoltaic power supplies would appear feasible. However, in the former case, little or no electrical power would be generated in transit, i.e., from Earth to design point.

A major design goal was to achieve a low-weight panel structure. A generator specific weight goal of 4 pounds per square foot was established, with a capability of producing a minimum of 35 watts of electrical power per square foot when operating at a distance of 0.25 astronomical units from the sun.

To achieve an optimal thermoelectric design configuration having a minimum system weight, there was need at the beginning of this program for analytic techniques better than those previously used. Prior analyses of thermoelectric devices operating with a constant heat source were not suitable for detailed performance calculations and for the design and optimization of thermoelectric generators because of over-simplification and/or the method of approach. (See Section II.) Therefore, the appropriate performance equations were derived in detail and programmed for solution on a high speed RCA 601 Computer.

The derived analysis which is discussed in detail in Section II, is unique in that it considers the heat-balance effects at the hot and cold sides of the

panel (the transverse heat flow in the hot shoe and radiator) and the generation of Thomson heat in the thermoelements. It also solves the resulting Poisson heat-flow equations instead of using a numerical approximation. In addition, the hot and cold junction temperatures are not assumed to be fixed.

The resulting analysis, after programming and debugging, was then available as a highly flexible and accurate tool for optimization. The procedure used to derive the reference design, which involved the calculation of some 1300 configurations, is described in Section III A. Briefly, the procedure involved varying four parameters (hot shoe area A_S, p-type element cross sectional area A_p, element length ℓ, and load ratio m), screening the resulting 1300 configurations to narrow the range of consideration by cross plotting of parameters, and then recalculating the couple to thermoelectrically optimize the configuration.

After the optimum thermoelectric couple configuration was selected, consideration of the state-of-the-art capability to fabricate extremes in hot shoe and element sizes dictated making minor modifications (increase the element length and cross section area) to the design to assure mechanical stability.

The reference design determined from the combined thermoelectric and mechanical analysis is as follows:

	Reference Design	Objective
No. of Couples	480	-
Current	5.63 amps	-
Voltage	26.6 volts	28
Power	150 watts	150
Efficiency	3.57 percent	-
Weight	13.3 lbs	-
Area	4.12 ft^2	-
Specific Weight	3.23 lb/ft^2	4.0
Power/Area	36.36 $watts/ft^2$	35
Power/Weight	11.27 watts/lb	-
Heat Transmitted	4190 watts	-

	Reference Design	Objective
Hot Junction Temperature	1063.8 °K (1456°F)	-
Cold Junction Temperature	702.8 °K (805°F)	-
Hot Plate Temperatures		nominal
Edge	1100.9 °K (1521°F)	1500°F
Center	1064.4 °K (1457°F)	-
Cold Plate Temperatures		
Edge	683.3 °K (784°F)	-
Center	687.5 °K (777°F)	-

The selected generator configuration consists of two panels of 240 couples each, each panel consisting of 20 sections fitted into a Beryllium frame.

Once the reference design was established, and approved by NASA, detailed design layouts of the generator and test sections were prepared (see Sections III E and IV A). A stress analysis of the thermoelectric generator components, assuming specified environmental loadings, was performed (Section III F). Acceleration, vibration, acoustic noise, and thermal cycling were considered. The analysis indicated that the stress levels are well below the allowable stresses.

In addition, the temperature profile (Section III B) and the component weight analysis (Section III C) on the panel were performed. The computer analysis was also utilized to determine the effect of varying the characteristics of the hot shoe absorber coating and the radiator coating on the performance of the generator (Section III D). Furthermore, it was possible to evaluate the off-design performance of the generator at distances other than 0.25 AU from the sun (Section III D).

In summary, the following are the achievements of this phase of the program:

A) A silicon germanium solar thermoelectric generator design has been determined which will produce 150 watts at a specific weight of 3.23 lb/ft^2 and 36.4 $watts/ft^2$, which can be utilized for missions operating in the range of 0.25 AU from the sun.

B) A rigorous and highly accurate thermoelectric analysis has been derived and computerized for use in design and evaluation of solar thermoelectric generators (and which can be adapted to isotope application with a minor modification).

C) Detailed design layouts of the generator and test panel have been prepared.

D) Supporting stress analyses have been prepared in depth.

E) Off-design generator performance conditions have been analyzed.

II. SOLAR PANEL THERMOELECTRIC GENERATOR PERFORMANCE CALCULATIONS

In the design and in the performance analysis of thermoelectric power generators, a variety of methods are commonly used. The most usual of these are based on the assumption that the generator operates between fixed hot- and cold-junction temperatures.[1,2] Fixed temperature operation implicitly assumes that the generator operates between a heat source and a heat sink of infinite capacity. Although this assumption permits considerable simplification in performance analyses, the results may be considered only approximate because in actual practice the assumption is not justified. In most applications, thermoelectric generators are coupled to finite heat sources supplying constant amounts of heat. This condition corresponds to the situation that is converse to the one usually assumed; namely, the hot- and cold-junction temperatures are variable and the heat input is fixed. Solar thermoelectric generators and radioisotope thermoelectric generators are examples of devices operating in this manner. As Castro and Happ[3] point out, the difference between the two types operation is analogous to that in the operation of an electrical network under constant voltage and constant current conditions.

A few treatments of the performance of thermoelectric devices have considered operation under conditions of constant heat input.[3,4,5] These treatments, however, are not generally suitable for detailed performance analyses and for the design and optimization of thermoelectric generators because of further simplifying assumptions and/or the method of approach. Castro and Happ[3] have outlined the method to be used in analyzing the performance of a thermoelectric device operating under conditions of fixed heat input but, for the case of a solar thermoelectric generator, have neglected reradiation effects at the hot side. Generally, they do not consider shunt heat losses or parasitic electrical losses in the device.

Fuschillo et al[4] have treated the case of a solar thermoelectric generator operating in space in the form of a panel. In their analyses, Fuschillo et al do account for reradiation effects at the hot side of the panel, but do not account for temperature drops in the thermoelectrically passive members of the thermal circuit; nor do they account for parasitic electrical losses. Moreover,

they make the implicit assumption that the n- and p-type legs of the thermocouples possess identical thermoelectric properties, a condition that is rarely, if ever, met in practice. The further assumption is made that maximum power is transferred to the load when the internal and load resistances are matched. This condition is not true for operation under fixed heat input conditions, and only applies under conditions of fixed temperature operation. Finally, Fuschillo et al[4] neglect the effects of transverse heat flow in the heat-collection and heat-rejection plates on the opposite faces of the panel, and implicitly assume the temperature independence of the Seebeck coefficient of the thermoelectric material by neglecting Thomson heat in the net heat balance of the thermoelements.

Lyon and Anderson[5] describe a solar thermoelectric energy conversion panel in terms of a simultaneous set of time-dependent, non-linear second-order differential equations. Because of non-analyticity, these equations are solved numerically on a computer. Although this treatment is considerably more sophisticated than most others and makes fewer simplifying assumptions, it is, nevertheless, unsuitable for designing a practical solar thermoelectric energy conversion panel and for characterizing the performance of that panel in terms of changing input conditions and panel properties. The reasons for this conclusion are: 1) that the treatment neglects the temperature drops across all thermoelectrically passive members (such as electrical insulators, current conductors, etc.) between the thermoelements and the heat-collection and heat-rejection plates that usually exist in an actual generator and 2) that the treatment is based on initially chosen hot- and cold-junction temperatures and calculated generator dimensions. It is more realistic to allow temperatures to vary and to fix the generator configuration because this is how a generator actually operates.[6] To study the behavior of a generator under conditions of varying input, such as varying values of incident solar heat flux, it is much more convenient to use the latter approach. This procedure is also true if it is desired to investigate the performance of a fixed configuration solar thermoelectric panel in terms of varying properties of component materials, such as the emittance characteristics of coatings, which may undergo change with time. Moreover, Lyon and Anderson[5] only treat the case in which direct heat transfer between the heat-reception and heat-rejection plates takes place by radiation. Many solar panel thermoelectric

generators, however, are designed with insulation in the space between the plates so that the actual mode of heat transfer is conduction rather than radiation.

Because of some of the shortcomings of most previous attempts to define the method of analysis of thermoelectric devices, it was concluded that a new analysis would be required to permit the design and optimization of practical solar thermoelectric generators operating in space. As a result, appropriate performance equations were derived in detail and programmed for solution on a high speed computer. The method used for doing this work will be developed later. Of all previous attempts to rigorously define the performance analysis of solar thermoelectric generators, that of Lyon and Anderson[5] probably most closely approximates the present treatment. Both treatments consider in detail the heat balance effects at the hot and cold sides of the panel and account for the generation (absorption) of Thomson heat in the thermoelements. Both of these effects are generally handled superficially or completely ignored in most other treatments. There are, however, basic differences between the present work and that of Lyon and Anderson[5]. Aside from the shortcomings already cited, which have been accounted for in the present treatment, Lyon and Anderson[5] obtain numerical solutions to their differential equations on a computer. In the present work, a simplification of the geometry of heat-reception and heat-rejection plates enables analytical solution of these differential equations. The simplification results in a slight loss of rigor, which in practice has almost negligible effects on the results, but permits considerably greater insight into the physics of the problem. Another basic difference between the two treatments is that Lyon and Anderson[5] solve the time-dependent problem, whereas the present work considers the time-independent situation. Time-dependence is important only in cases where there are rapid changes in the incident perpendicular heat flux on the heat-reception plate. Such changes may occur in the close proximity of a planet or if the generator rapidly alters its orientation with respect to the sun. The present treatment does not consider such short-time transient effects. Finally, modifications in the present development will also permit its use in the design and analysis of radioisotope thermoelectric generators.

The model used in developing the necessary equations which describe the performance of a solar thermoelectric generator is illustrated in Figure 1. The single thermocouple represents a building-block of the generator and serves as the unit on which all calculations are performed. Desired power

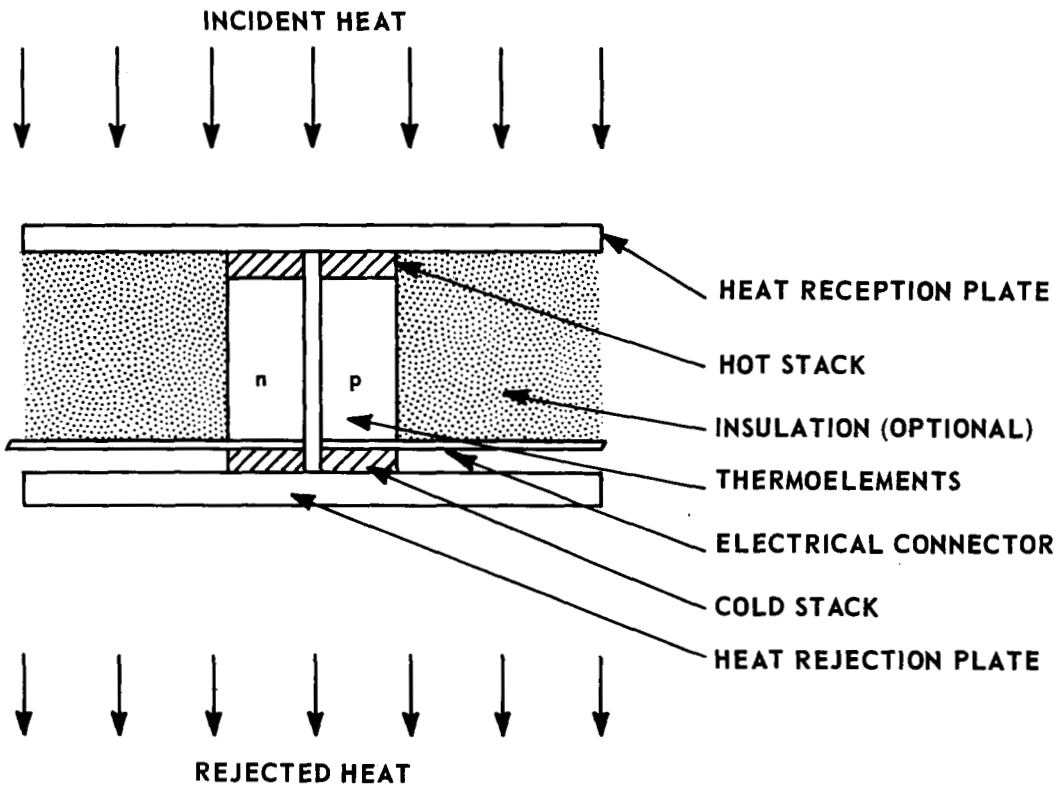

FIGURE 1. SCHEMATIC—CROSS SECTION OF THE THERMOCOUPLE

voltage characteristics of a system are obtained by appropriate combinations of single thermocouples. The thermocouple configuration consists of heat-reception and heat-rejection plates, in between which are the n- and p-type thermoelectric elements. Generally, on both ends of the thermoelements, there are so-called "stacks" which metallurgically connect the elements to the plates. The purpose of the stacks is to relieve stresses that arise from differential thermal expansion of the plates and the elements, and to afford low-loss thermal coupling between these members. If necessary, the stacks also include electrical insulators to isolate the electrical circuit from the remainder of the structure. To minimize shunt heat losses, the space between the plates not occupied by thermoelements may be filled with thermal insulation.

The thermocouple shown in Figure 1 has a fixed configuration and contains definite materials with their corresponding physical properties. The thermocouple configuration, although fixed, is completely arbitrary and the dimensions of its components have in no respect been optimized. One face of the thermocouple is assumed to be exposed to a perpendicular heat flux W. Because of the finite thermal resistance of the thermocouple configuration, the incident heat flux will establish a temperature difference across it. The heat appearing on the back side of the thermocouple will be dissipated by radiation into space at an assumed space temperature of zero degrees Kelvin.

The total heat incident on the thermocouple is given by

$$Q_I = W\alpha \quad A_T \tag{1}$$

where A_T is the area and α is the absorptivity of the heat-reception plate. The total heat, Q_T, flowing from the heat-reception to the heat-rejection plate is less than the incident heat, Q_I, because some of the heat absorbed by the heat-reception plate is reradiated into space, as expressed by

$$Q_T = Q_I - \sigma \epsilon_H \int_{A_T} T_H^4(A) \quad dA \tag{2}$$

where σ is the Stefan-Boltzmann constant, ϵ_H is the emissivity, and $T_H(A)$ is the temperature of the heat-reception plate surface. The temperature of the heat-reception plate surface is not constant because the heat received by the plate tends to preferentially flow towards the thermoelements which offer less thermal resistance to heat flow than does direct transfer between the heat-reception and heat-rejection plates. Direct transfer is inhibited either by the insertion of thermal insulation between the plates or by low emissivity coatings between or on the inside surfaces of the plates. The resultant transverse heat flow in the plates gives rise to temperature gradients. The A in the function $T_H(A)$ serves only temporarily as a dummy, indicating that the variables used must be compatible with those of the incremental area dA. The choice of variables or coordinates will be deferred until later. The total heat reradiated by the surface is therefore obtained by integration over the surface.

On the opposite face of the panel, the outer surface of the heat-rejection plate, also having an area A_T, is cooled by the radiation of heat that has been transported through the thermocouple. The quantity of such heat is less than Q_T by the amount that has been converted to electricity. Thus, it may be written

$$Q_T - P_o = \sigma \epsilon_C \int_{A_T} T_C^4(A) \quad dA \tag{3}$$

where P_o is the electrical power output, ϵ_C is the emissivity, and $T_C(A)$ is the temperature of the outer surface of the heat-rejection plate. Just as in the case of the heat-reception plate and for a similar reason, the temperature of the heat-rejection plate is position-dependent and the total heat radiated is obtained through integration over the surface.

To obtain expressions for the temperature functions $T_H(A)$ and $T_C(A)$, it is necessary to solve Poisson's equation for the heat-reception and heat-rejection plates. Poisson's equation describes steady heat flow in the presence of heat sources and heat sinks and is given by

$$\nabla^2 T = - \frac{R}{k} \tag{4}$$

where R represents the rate at which heat is supplied per unit volume and k is the thermal conductivity of the material. For the heat-reception plate, there are three contributions to R, viz., the incident heat from the sun, the heat reradiated from the face of the plate, and the shunt heat transferred directly between the heat-reception and heat-rejection plates. For the heat-reception plate, the quantity R, denoted as R_H, may therefore be written as

$$R_H = \frac{1}{t_H} \left[W \alpha - \sigma \epsilon_H T_H^4(A) - \frac{dQ_s(A)}{dA_s} \right] \tag{5}$$

where t_H is the thickness of the heat-reception plate, A_s is the area of the heat-reception and heat-rejection plates not covered by the n- and p-type thermoelements, and $dQ_s(A)/dA_s$ is the shunt heat per unit area directly transferred between the heat-reception and heat-rejection plates as a function of

position on these plates. Depending on the mode of shunt heat transfer, $dQ_s(A)/dA_s$ has the following forms:

$$\frac{dQ_s(A)}{dA_s} = \frac{k_s}{t_s}\left\{\left[T_H(A)-\Delta T_H(A)\right] - \left[T_C(A) + \Delta T_C(A)\right]\right\} \quad \text{(conduction)}$$

$$\frac{dQ_s(A)}{dA_s} = \sigma\epsilon_s\left\{\left[T_H(A)-\Delta T_H(A)\right]^4 - \left[T_C(A) + \Delta T_C(A)\right]^4\right\} \quad \text{(radiation)} \qquad (6)$$

where k_s is the thermal conductivity and t_s is the thickness of insulation. The emissivity, ϵ_s, is the net emissivity of the inner surfaces of the two plates and may be approximated by the expression for the net emissivity of two parallel surfaces

$$\epsilon_s = \frac{1}{\frac{1}{\epsilon_{HI}} + \frac{1}{\epsilon_{CI}} - 1} \qquad (7)$$

where ϵ_{HI} and ϵ_{CI} are the emissivities of the inner surfaces of the heat-reception and heat-rejection plates. The ΔT factors in Eqs. (6), identified by appropriate subscripts, account for the differences in the temperatures of the outer and inner surfaces of the heat-reception and the heat-rejection plates. Therefore, they may be approximated by Q_T/K_H, and $(Q_T-P_o)/K_C$, respectively, where K_H and K_C refer to the thermal conductances of the heat-reception and heat-rejection plates. This approximation effectively replaces the position-dependent axial temperature-drops in the two plates by their average values and is validated by the fact that such drops are typically of the order of a degree centigrade or less, depending on panel constructional materials and precise configuration. Eqs. (6) implicitly neglect the transverse heat flow in the insulation or the radiation space between the plates because integration of the equation in the calculation of total shunt heat, results in weighted average temperatures being used. This is a relatively minor approximation because in most thermocouples of practical interest, shunt heat forms only a very small portion of the total heat transmitted. Furthermore, in most cases, $T_H(A)$ and $T_C(A)$ are only relatively slowly-varying functions. Naturally, in the limit of vanishing k_s or ϵ_s, the approximation becomes exact.

In a manner similar to the case of the heat-reception plate, the quantity R for the heat-rejection plate, denoted by R_C, is given by

$$R_C = \frac{1}{t_C} \left[-\sigma \in_C T_C^4(A) + \frac{dQ_s(A)}{dA_s} \right] \tag{8}$$

where t_C is the thickness of the heat-rejection plate. In this instance, only two terms enter the equation: the heat radiated into space and the shunt heat directly transferred to the plate.

Eq. (4) with Eqs. (5) and (8) define the temperature distribution in the heat-reception and heat-rejection plates. The equations for the two cases, however, are nonanalytic in the sense that closed-form solutions are not generally possible. The way to proceed is to either obtain numerical solutions or to simplify the problem so that analytic solutions are possible. Adopting the latter approach for calculation purposes, it is assumed that the heat-reception and heat-rejection plates possess radial symmetry. In other words, for calculation purposes, the plates of square cross section are replaced by plates of circular cross section so that the total plate areas A_T remain the same. The thermoelements are combined into one of circular cross section, possessing an area equal to the combined areas of the n- and p-type thermoelements. The latter approximation is negligible in many cases because frequently the n- and p-type thermoelements are purposely designed with semicircular cross-sectional areas. Facing each other, with a small separation between them, the total cross-sectional area of the two thermoelements is already near-circular. Figure 2 schematically illustrates the assumed thermocouple configuration. The approximation resulting from the assumption of circular plates rather than of square plates is good because it directly enters into the calculation of only the transverse temperature distribution of the plates and, in most cases of practical interest, only has a second order effect on calculated thermocouple performance. This effect may be seen approximately by comparing the transverse temperature-drop in the plates with that across the active thermoelectric material. Usually, the former is only a few percent of the latter.

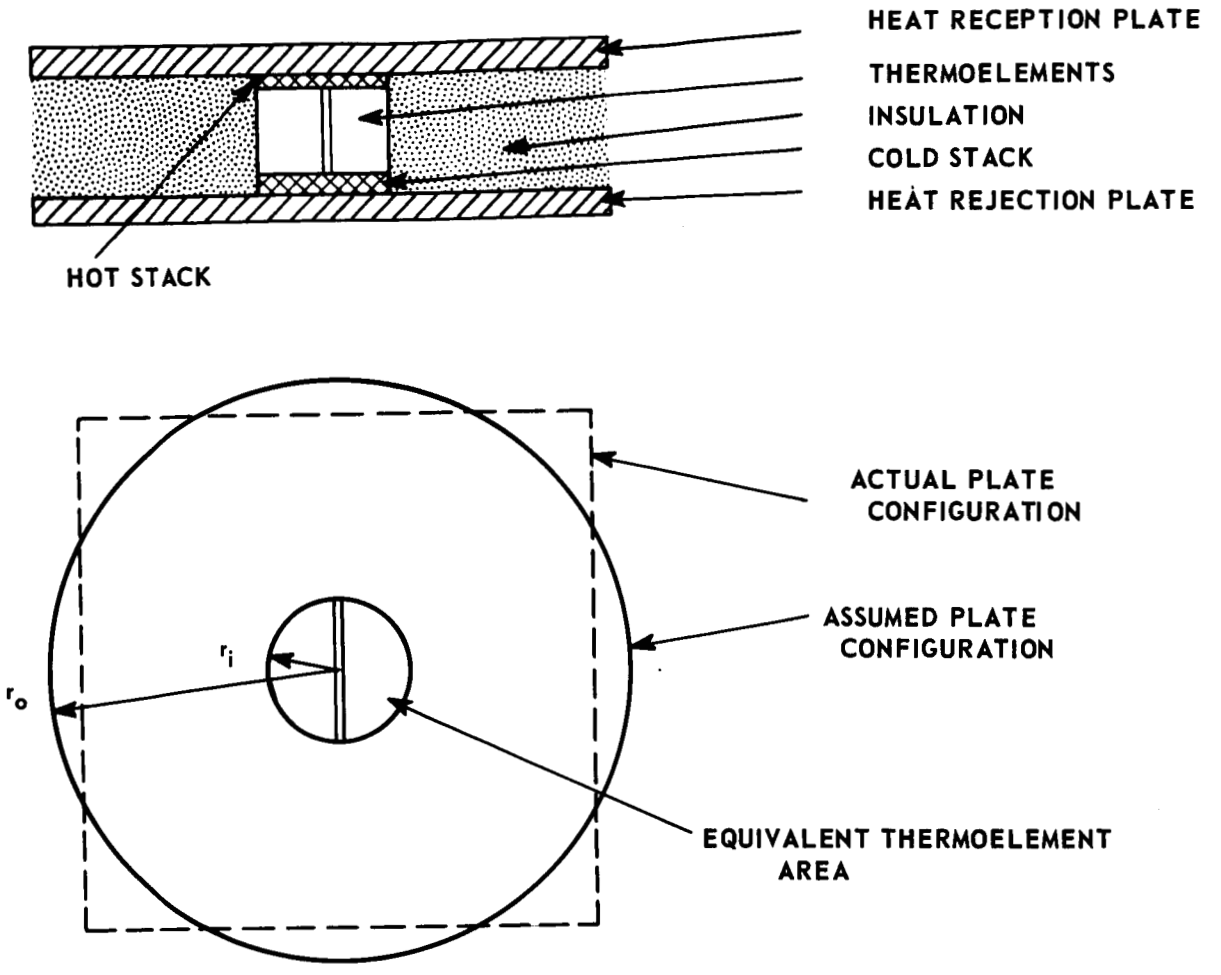

FIGURE 2. MODEL OF THERMOCOUPLE USED IN TRANSVERSE HEAT FLOW CALCULATIONS

Before proceeding with the mathematical development, it may also be well to emphasize the fact that the radial geometry adopted for transverse heat calculation in the plates has no effect on the geometry of the remainder of the thermocouple because, as already stated, the shunt heat directly transferred between the heat-reception and heat-rejection plates is assumed to be axially directed with no transverse component. A similar assumption will be made for heat flowing in the thermoelements. The results of these assumptions are that all the calculations performed for the portions of the thermocouple between the plates will be independent of the precise geometry of the components in the plane parallel to the plates. The only factor of interest is the cross-sectional area of the components, not their precise configuration.

Poisson's Eq. (4) in two-dimensional cylindrical coordinates may be written as

$$\frac{1}{r}\frac{\partial}{\partial r}\left(r\frac{\partial T}{\partial r}\right)+\frac{1}{r^2}\frac{\partial^2 T}{\partial \theta^2}=-\frac{R}{k} \tag{9}$$

Because of symmetry, the second term on the left hand side of Eq. (9) vanishes and the result is an ordinary second-order differential equation. Upon substitution from Eqs. (5) and (8), the differential equations for the heat-reception and heat-rejection plates may be written, respectively, as

$$\begin{aligned}
\frac{1}{r}\frac{d}{dr}\left(r\frac{dT_H}{dr}\right)&=-\frac{1}{k_H t_H}\left\{W\alpha-\sigma\in_H T_H^4(r)-\frac{dQ_s(r)}{dA_s(r)}\right\}\\
\frac{1}{r}\frac{d}{dr}\left(r\frac{dT_C}{dr}\right)&=-\frac{1}{k_C t_C}\left\{-\sigma\in_C T_C^4(r)+\frac{dQ_s(r)}{dA_s(r)}\right\}
\end{aligned} \tag{10}$$

where k_H and k_C are the thermal conductivities of the two plates. Eqs. (6) indicate that the shunt heat transfer terms Q_s are functions of both $T_H(r)$ and $T_C(r)$; therefore, Eqs. (10) are simultaneous. In principle, the method of solution is to set $T_C(r)$ in the first of Eqs. (10) equal to a constant and solve for $T_H(r)$. Substitution of this $T_H(r)$ in the second of Eqs. (10) enables a solution to be found for $T_C(r)$ which is now substituted in the first equation so that a new solution for $T_H(r)$ may be found. The process is repeated as often as is necessary to obtain consistency of the functions for $T_H(r)$ and $T_C(r)$ between successive approximations.

Although in principle, Eqs. (10) may be conveniently solved; in practice, because of the nonlinearity of the right hand sides, the solutions are not easily obtained. A simpler and more effective method of solution becomes apparent after Eqs. (10) are rewritten as

$$\begin{aligned}
\frac{1}{r}\frac{d}{dr}\left(r\frac{dT_H}{dr}\right)&=-\frac{R_H}{k_H}\\
\frac{1}{r}\frac{d}{dr}\left(r\frac{dT_C}{dr}\right)&=-\frac{R_C}{k_C}
\end{aligned} \tag{11}$$

where R_H and R_C are given by

$$R_H = \frac{1}{t_H} \left[\frac{dQ_T}{dA_T} - \frac{dQ_s}{dA_s} \right]$$

$$R_C = \frac{1}{t_C} \left[- \frac{d(Q_T - P_o)}{dA_T} + \frac{dQ_s}{dA_s} \right] \qquad (12)$$

Eqs. (1), (2), and (3) have been used to write Eqs. (12). By replacing all the position-dependent heat transfer rates per unit area by their average values in Eqs. (12), it is possible to treat R_H and R_C as constants. The solution of Eqs. (11) is now trivial, being obtained by two successive integrations. After the first integration, use is made of the condition that the temperature gradient at the edge of the two plates vanishes. This condition corresponds to the assumption that plate edges are insulated and allows the evaluation of one of the two integration constants. The temperature distributions obtained for the two plates are given by the function

$$T(r) = \frac{R}{2k} \left[r_o^2 \ln \left(\frac{r}{r_i} \right) - \frac{1}{2} (r^2 - r_i^2) \right] + T(r_i) \qquad (13)$$

where r_i and r_o are the radii between which the temperature distribution is evaluated. Eq. (13) is general and applies equally to the heat-reception and the heat-rejection plates. The distinction between the two cases can be made by appropriate subscripts on $T(r)$, $T(r_i)$, R and k. The radius r_o corresponds to the outer edge of the plate, whereas r_i represents the radius of the combined n- and p-type thermoelements (Figure 2). The temperature, $T(r_i)$, corresponds to the temperature of the region on the surfaces of the heat-reception and heat-rejection plates immediately adjacent to the thermoelements. This region is assumed to be equal in area to the total area of the thermoelements and to have the constant temperature $T(r_i)$. This assumption is consistent with that made in regard to axial heat flow in the thermoelements when the axial-flow region is extended on the extremities of the thermoelements to include the hot and cold stacks and the central portions of each plate. The heat transfer rates, R_H and R_C, averaged over the portions of the heat-reception and heat-rejection plates not covered by the thermoelements, are given by

$$R_H = \frac{1}{t_H} \left\{ \frac{Q_T - \left[W\alpha - \sigma \epsilon_H T_H^4(r_i)\right]\left[A_n + A_p\right] - Q_s}{A_s} \right\}$$

$$R_C = \frac{1}{t_C} \left\{ \frac{Q_T - P_o - \sigma \epsilon_C T_C^4(r_i) \left[A_n + A_p\right] - Q_s}{A_s} \right\} \qquad (14)$$

where A_n and A_p are the cross-sectional areas of n- and p-type thermoelements. Eqs. (11) were solved by fixing the values of R_H and R_C. Because the solutions of these equations, represented by Eq. (13), are used successively in the solution of the over-all problem, as will be seen later, the fixed values of R_H and R_C will also be iterated. The values calculated for Q_T, Q_S, P_o, $T_H(r_i)$, and $T_C(r_i)$ in any given iteration will be used in Eqs. (14) to obtain new R_H and R_C values for use in the next iteration. Thus, it is possible to minimize the effects of replacing the position-dependent heat transfer rates per unit area by their average values in Eq. (12). The net result is that Poisson's Eqs. (11) are solved in effect through a method of successive approximations.

Radii r_i and r_o may now be expressed in terms of total plate areas A_T and the areas A_n and A_p, of the n- and p-type thermoelements as

$$r_i = \sqrt{\frac{A_n + A_p}{\pi}}$$

$$r_o = \sqrt{\frac{A_T}{\pi}} \qquad (15)$$

For sake of completeness, the area of shunt heat transfer, A_s, may be defined in terms of the other areas as

$$A_s = A_T - (A_n + A_p) \qquad (16)$$

The defined system of coordinates to be used in treating the heat-reception and heat-rejection plates and the expressions obtained for the temperature distributions on these plates, can now be used to rewrite Eqs. (2), (3), and (6). Eq. (2) may now be written as

$$Q_T = Q_I - 2\pi\sigma\epsilon_H \int_{r_i}^{r_o} T_H^4(r)\, r\,dr - \sigma \epsilon_H \left[A_n + A_p\right] T_H^4(r_i) \qquad (17)$$

Similarly, Eqs. (3) and (6) may now be expressed as

$$Q_T - P_o = 2\pi \epsilon_C \int_{r_i}^{r_o} T_C^4(r)\, r\,dr + \sigma \epsilon_C \left[A_n + A_p\right] T_C^4(r_i) \qquad (18)$$

and

$$Q_s = 2\pi \frac{k_s}{t_s} \int_{r_i}^{r_o} \left\{\left[T_H(r) - \frac{Q_T}{K_H}\right] - \left[T_C(r) + \frac{Q_T - P_o}{K_C}\right]\right\} r\,dr \quad \text{(conduction)}$$

$$Q_s = 2\pi \epsilon_s \int_{r_i}^{r_o} \left\{\left[T_H(r) - \frac{Q_T}{K_H}\right]^4 - \left[T_C(r) + \frac{Q_T - P_o}{K_C}\right]^4\right\} r\,dr \quad \text{(radiation)} \qquad (19)$$

Because some of the indicated integrations are not easily accomplished in actual use, it is convenient to replace the integrations by summations. To avoid rewriting Eqs. (17), (18), and (19) in terms of finite sums, only the general formula that applies to all of these equations is given

$$\int_{r_i}^{r_o} f(r)\, r\,dr = \sum_{n=1}^{N} f\left(r_i + (n-\tfrac{1}{2}) \frac{r_o - r_i}{N}\right) \left[r_i + (n-\tfrac{1}{2}) \frac{r_o - r_i}{N}\right] \frac{r_o - r_i}{N} \qquad (20)$$

where f(r) refers to any of the integrands in Eqs. (17), (18), and (19), n is the summation index, and N is the number of terms in each sum by which it is desired to approximate the integrals. Obviously, the greater the value of N, the more closely the integrals are approximated.

Eq. (17) represents the heat balance at the heat-reception plate. The corresponding relationship for the heat-rejection plate is given by Eq. (18). Eq. (19) describes the direct shunt heat transfer between the two plates. What is still needed, however, is a relationship describing the heat transfer between the plates that takes place through the thermoelements. This relationship is obtained from detailed heat balancing at either the hot or the cold junctions of the thermoelements. For the hot junction, the following relationship may be written

$$Q_T - Q_s = K_T \left[T_{HJ} - T_{CJ}\right] + I\, S_{HJ}\, T_{HJ} - \tfrac{1}{2} I^2 R_I - \tfrac{1}{2} I\mu \left[T_{HJ} - T_{CJ}\right] \qquad (21)$$

where K_T is the thermal conductance of the thermocouple, T_{HJ} and T_{CJ} are the hot and cold junction temperatures, respectively, I is the current flowing in the thermocouple, S_{HJ} is the absolute value of the Seebeck coefficient difference between the n- and p-type thermoelements at the hot junction, R_I is the total internal electrical resistance of the thermocouple, and μ is the temperature-averaged net Thomson coefficient of the thermoelements. The first term on the right hand side of Eq. (21) represents the heat conducted through the thermoelements. The second describes the heat absorbed at the hot junction as a result of the Peltier effect. The third accounts for the fact that one-half of the Joule heat generated in the legs of the thermocouple as a result of current flow is conducted to the hot junction, and the last term makes a similar assumption about the heat generated (absorbed) in the legs as a result of the Thomson effect.[7]

Current I in the thermocouple may be expressed in terms of electrical resistances, junction temperatures, and Seebeck coefficient values as

$$I = \frac{S}{R_L} \frac{m}{1+m} \left[T_{HJ} - T_{CJ}\right] \tag{22}$$

where S is the temperature-averaged absolute value of the difference between the Seebeck coefficients of the n- and p-type thermoelements, R_L is the value of electrical load resistance, and m is the ratio of load to internal electrical resistance. Substituting Eq. (22) in Eq. (21) and solving for T_{HJ}, it is found

$$T_{HJ} = \left[\frac{b^2}{4a^2} + \frac{c}{a}\right]^{\frac{1}{2}} - \frac{b}{2a} \tag{23}$$

where a, b, and c are given by

$$a = S_{HJ} - \frac{1}{2}\frac{S}{1+m} - \frac{1}{2}\mu$$

$$b = \frac{R_L}{S}\frac{1+m}{m} K_T - S_{HJ} T_{CJ} + \frac{ST_{CJ}}{1+m} + \mu T_{CJ}$$

$$c = \frac{R_L}{S}\frac{1+m}{m} K_T T_{CJ} + \frac{1}{2}\frac{ST_{CJ}^2}{1+m} + \frac{1}{2}\mu T_{CJ}^2 + \frac{R_L}{S}\frac{1+m}{m}(Q_T - Q_s)$$

Eq. (23) relates the hot and cold junction temperatures of the thermoelements in terms of thermocouple material characteristics, electrical load resistance, and the total heat transported to the hot junctions of the thermoelements.

Because the heat balance Eq. (23) is written in terms of the hot and cold junction temperatures, and because the remainder of the heat balance Eqs. (17), (18), and (19) are written in terms of the temperatures of the center portions of the heat-reception and heat-rejection plates, $T_H(r_i)$ and $T_C(r_i)$, it is necessary to relate these temperatures. This relationship is achieved by considering axial conduction of heat through the hot and cold stacks and the plates. On the cold side, the relationship may be expressed as

$$T_{CJ} = T_C(r_i) + \frac{Q_T - Q_s - P_o}{K_{CS}} + \frac{Q_T - P_o}{K_C} \tag{24}$$

where K_{CS} is the thermal conductance of the cold stacks and K_C is the axial thermal conductance of the heat-rejection plate. The corresponding equation on the hot side has the form

$$T_H(r_i) = T_{HJ} + \frac{Q_T - Q_s}{K_{HS}} + \frac{Q_T}{K_H} \tag{25}$$

where K_{HS} is the thermal conductance of the hot stacks and K_H is the axial thermal conductance of the heat-reception plate. Eqs. (24) and (25) are only approximate because for the axial temperature-drops across the heat-reception and heat-rejection plates, as already stated, they only represent average values. Because of the inherent smallness of such temperature-drops, however, the effect of this approximation on final results is negligible.

Implicit in the above development, is the assumption that both the n- and p-type thermoelements have identical junction temperatures. The validity of this assumption depends primarily on the relative thermal conductances of the hot and cold stacks of the thermocouple. The junction temperatures are very close to each other if the stacks are highly conductive in comparison to the thermocouple legs. Because this condition is basic to obtaining maximum performance from a thermocouple, only stacks which fulfill this requirement are generally

used in practical thermocouples. Moreover, in some instances, there are no stacks at one or both sides of the thermoelements; in other instances, both thermoelements share a common stack. In such cases, by definition, the junctions have to be at the same temperature. In all cases, however, the use of identical temperatures for the junctions of n- and p-type thermoelements is considered to be well justified.

One more equation is needed to complete the formal exposition of performance equations for a solar thermoelectric power generator. This equation is straightforward and relates electrical power output to the temperatures, the material characteristics, and the configuration of the thermocouple:

$$P_o = \frac{S^2}{R_L} \left(\frac{m}{1+m}\right)^2 \left[T_{HJ} - T_{CJ}\right]^2 \qquad (26)$$

Most of the performance equations in the foregoing treatment contain configuration-dependent quantities such as conductances and resistances. The precise definition of these quantities in terms of material properties and geometry is trivial and will be deferred until later. This condition also applies to the calculation of temperature-averaged thermoelectric property data and the computation of thermocouple weight.

An inspection of the above equations shows that there are basically five unknown quantities that must be determined so that thermocouple performance may be completely characterized. These quantities are Q_T, Q_s, P_o, $T_C(r_i)$, and $T_H(r_i)$. However, there are the same number of basic equations that relate these five quantities, viz. (17), (18), (19), (23), and (26). It is assumed that Eq. (23) may be expressed in terms of $T_C(r_i)$ and $T_H(r_i)$ instead of T_{CJ} and T_{HJ} by means of Eqs. (24) and (25). By combining and rewriting some of the five equations, it is possible to reduce the number of unknown quantities and the corresponding number of equations. However, this procedure does not change the basic problem which is one of a set of simultaneous equations. Because of the nature of the equations involved, it is not possible to reduce the set to one equation and one unknown through analytic techniques. The solution must be obtained by a method of successive approximations as follows:

A fixed thermocouple configuration is assumed. This configuration, in terms of component geometry, is completely arbitrary because it is not known a priori for what combination of component dimensions thermocouple performance is optimized or satisfies imposed boundary conditions. Values are assumed for all required material properties that enter into the related equations. Because most material properties are temperature-dependent and because, initially, the temperature range is unknown over which the thermocouple will actually operate, it is sufficient in the first approximation to choose property values that are averages in the temperature range over which it is reasonably expected to operate. After a solution has been obtained and more precise operating temperatures have thus been established, new values for the required properties may be substituted and the calculation repeated. Because the solution of the over-all problem, as will be shortly seen, is obtained by successive approximations, it will be sufficient to use the temperatures of a given approximation to calculate the temperature-averaged properties which will be used in the next approximation before the start of each new iteration. On a computer, this procedure is conveniently done by introducing property data as a function of temperature either at fixed temperature intervals or in the form of equations obtained from fitting the data. Because it is the thermoelectric property data that generally have the greatest effect on calculated thermocouple performance, it usually suffices if only these data are integrated after each iteration. The remainder of the properties may initially be given approximate average values that remain fixed throughout the calculation.

The use of Eq. (1) enables the calculation of the heat incident Q_I on the thermocouple for a given value of incident solar-heat flux W which is a function of the distance from the sun. Because only a portion of this heat is transported through the thermocouple, quantity Q_T is assigned some arbitrary value in the range of zero to Q_I. Although it is initially assumed that P_o and Q_s are zero, other equally arbitrary values could be used. With values assigned to Q_T, Q_s, and P_o, it is apparent that in Eq. (18) the only remaining unknown is $T_C(r_i)$. Because $T_C(r_i)$ occurs in the integrand, which is raised to the fourth power, as well as outside the integrand, it is not possible to solve Eq. (18) analytically for $T_C(r_i)$; graphical or numerical methods are needed. The value of $T_C(r_i)$ thus calculated, with the assigned values of Q_T, Q_s, and P_o, may now

be used to calculate T_{CJ} by Eq. (24) which, in turn, is used to calculate T_{HJ} in Eq. (23). Eq. (25) relates T_{HJ} to $T_H(r_i)$, which substituted in Eq. (17), enables the determination of Q_T. The calculated values of $T_C(r_i)$ added to the assigned values of Q_T, Q_s, and P_o, permit the calculation of Q_s by means of Eq. (19). The calculated values of T_{HJ} and T_{CJ} substituted in Eq. (26) allow the determination of P_o. The values thus determined for Q_T, Q_s, P_o, $T_H(r_i)$, and $T_C(r_i)$ form first approximation estimates. By use of these first approximation estimates just determined, the procedure is repeated to obtain second approximation values of these quantities. Further repetition of the procedure will yield higher order approximations. When the calculated values of the five quantities do not change within some prescribed limits between two successive approximations, the calculation is then complete because self-consistency has been obtained and the equations are simultaneously satisfied.

Depending on the relative importance of the various contributing terms to the equations, the previously described sequence of calculations is sometimes not self-convergent in that the values of the five quantities do not converge to fixed values as a function of successive iterations. Actually, the values diverge. In such cases, the further the initial value of Q_T is from its self-consistency value, the more rapid is the divergence of the five quantities between successive approximations. Conversely, the closer the initial value of Q_T is to its self-consistency value, the slower is the divergence rate. If the value of Q_T at self-consistency is used initially in the calculation, the five quantities do not change between successive approximations and the equations are therefore simultaneously satisfied. In cases of nonconvergency, it is therefore necessary to search for the proper value of Q_T to be used initially. This proper value will also give self-consistency in the calculations and will yield the appropriate values of Q_s, P_o, $T_H(r_i)$, and $T_C(r_i)$ for the thermocouple. The search is performed either graphically or numerically.

Once the five quantities Q_T, Q_s, P_o, $T_H(r_i)$, and $T_C(r_i)$ have been determined for a fixed thermocouple configuration, the remaining performance parameters follow immediately. The current which flows in the thermocouple is calculated from Eq. (22) and load voltage E_L is obtained from

$$E_L = \frac{P_o}{I} \tag{27}$$

The efficiency of the thermocouple is defined as

$$\eta = \frac{P_o}{Q_T} \tag{28}$$

The foregoing development contains various thermal conductance terms that contain the geometry as well as the thermal conductivity of the respective components. These are given by

$$\begin{aligned} K_H &= \frac{A_T}{t_H} k_H \\ K_{HS} &= \frac{A_n + A_p}{t_{HS}} k_{HS} \\ K_T &= \frac{k_n A_n + k_p A_p}{\ell} \\ K_{CS} &= \frac{A_n + A_p}{t_{CS}} k_{CS} \\ K_C &= \frac{A_T}{t_C} k_C \end{aligned} \tag{29}$$

The subscripts n and p in Eqs. (29) refer to n- and p-type thermoelements, respectively. The other subscripts have been previously defined. All t's refer to thicknesses; A's refer to cross-sectional areas; and k's refer to thermal conductivity values. The thermal conductivities k_n and k_p refer to values averaged over the temperature range of thermocouple operation. The symbol ℓ refers to the length of the thermoelements. The stacks at both ends of the thermoelements are assumed to have cross-sectional areas identical to those of the thermoelements. Furthermore, it is implicitly assumed that the n- and p-type thermoelements are situated on common stacks of areas $A_n + A_p$. As already discussed, such assumptions about the stacks have little bearing on thermocouple performance and therefore are permissible. Eqs. (29) indicate that in order to calculate K_{HS} and K_{CS}, values are needed for the respective thermal conductivities. Because stacks typically contain more than one material,

it will be necessary to use average thermal conductivity values. The average thermal conductivity of a multimember component is defined as

$$k = \frac{t}{\sum_i \frac{t_i}{k_i}} \tag{30}$$

where the subscript i denotes the i^{th} member and t is the total thickness of the component.

As previously, the factors m and R_L entering the above performance equations are related to the internal thermocouple resistance R_I by $m = R_L/R_I$. Therefore, for any desired value of m, it is necessary to calculate R_I in order that R_L may be specified. The internal resistance R_I of the thermocouple is given by

$$R_I = \ell\left[\frac{\rho_n}{A_n} + \frac{\rho_p}{A_p}\right] + \frac{2r_{Cn}}{A_n} + \frac{2r_{Cp}}{A_p} + r_S \tag{31}$$

where ρ_n and ρ_p are the electrical resistivities of the n- and p-type legs of the thermocouples (averaged over the temperature range of thermocouple operation) and r_{Cn} and r_{Cp} are the contact "resistivities" (units of ohm-cm^2) of the interfaces between the n- and p-type elements and their respective metallic end pieces. The quantity r_S represents the remaining extraneous internal electrical resistance and is primarily the result of resistance in current-carrying interconnects.

As previously indicated, the material property data used in the foregoing calculations should be averaged over the temperature range of thermocouple operation. Also discussed was the manner of incorporating the resultant average values in the over-all calculation by obtaining new averages after each iteration, and that it is essential to do this only with the thermoelectric property data of the n- and p-type thermoelements. For the sake of completeness, a general equation which defines the averaging method is given

$$\xi = \frac{\int_{T_{CJ}}^{T_{HJ}} \xi(T)\,dT}{\int_{T_{CJ}}^{T_{HJ}} dT} \tag{32}$$

where ξ represents the property of which the average is desired. Thus ξ applies equally to ρ_n, ρ_p, k_n, k_p, S, and μ. The Seebeck coefficient, S, is defined as $S = S_p - S_n$ and the net Thomson coefficient, μ, is defined as $\mu = \tau_p - \tau_n$, where the τ's are the Thomson coefficients of the individual legs. The definition of τ is $\tau = T\, dS/dT$.

The weight of the thermocouple follows directly from the dimensions and materials assumed for the components of the thermocouple. Thus, the total thermocouple weight W_t is given by

$$W_t = W_H + W_{HS} + W_I + W_T + W_{CS} + W_S + W_C \tag{33}$$

where the subscripts of the individual terms have been previously defined. The individual weight terms are calculated from

$$W_i = A_i t_i \delta_i \tag{34}$$

where i refers to the i^{th} component and δ is the density of the component. Because some components, such as the hot and cold stacks, contain more than a single member, the density used in calculating the weight must be an average. The average value of density for multimember components is defined as

$$\delta = \frac{\sum_i t_i \delta_i}{t} \tag{35}$$

where t is the total thickness of the component.

As has already been indicated, the performance calculations of a thermocouple are done by initially assuming arbitrary dimensions for the various components. In a practical power generator, however, it is important that performance be optimized with respect to some parameter, such as specific power (watts per

pound) or efficiency, which is directly related to the economics of producing electrical power in a space application. This optimization is done through the variation of parameters. The important parameters in this respect are the cross-sectional areas of the elements, A_n and A_p, the heat-collection and heat-rejection plate areas, A_T, the thermoelement length, ℓ, and the ratio of load to internal electrical resistance, m. Each of these parameters may be varied independently for fixed values of the other parameters. Thus the performance may be optimized with respect to all parameters. The whole procedure may be automated by programming a computer to search for the optima by itself.

III. SOLAR PANEL THERMOELECTRIC GENERATOR REFERENCE DESIGN

The primary objective of this program is to design a silicon-germanium solar panel thermoelectric generator weighing less than 4.0 pounds per square foot of panel area and producing 35 watts of electrical power per square foot when operating at a distance of 0.25 astronomical unit from the sun. Auxiliary objectives are the preparation of a detailed design of a generator that not only meets the primary objective but also produces approximately 150 watts of electrical power at a load voltage of about 28 volts. Because of the limited temperature of operation of the absorption coating to be used on the heat-reception plate, this plate is constrained to operate at a nominal temperature of 1500°F. Finally, several sections of the panel, representative of the reference design, are to be fabricated and supplied to the National Aeronautics and Space Administration for evaluation.

This section of the report discusses in detail how a reference design was formulated to meet the stated program objectives. A discussion is included of the detailed performance characteristics of this generator, together with weight and temperature profiling in terms of generator components. Engineering layout drawings of the generator and its components are also included. Detailed stress analyses of the generator and its components are presented in terms of anticipated shock and vibration, as well as temperature cycling conditions encountered during and subsequent to vehicle launch. Generator performance under a variety of off-design conditions will be discussed.

A. Performance of the Reference Design Generator

The method of calculating the performance of a solar panel thermoelectric generator outlined in Section II has been applied to the case of a generator operating at a distance of 0.25 astronomical unit from the sun. Because of the complexity of the general equations developed in Section II, the calculations have been programmed for solution on a high-speed RCA 601 computer. To optimize the performance of the generator, as discussed in Section II, it is necessary to vary a number of parameters that pertain to panel configuration. Every variation of parameters results in a modified thermocouple configuration which may be considered to represent a different generator.

Examination of many different cases enables the choice of the thermocouple configuration that corresponds to the optimum generator. Because of the complex equations, even on a high-speed computer, the design calculations for each thermocouple configuration take appreciable time which when multiplied by the many cases, becomes excessive. For this reason, the initial scanning of numerous thermocouple configurations, corresponding to extensive variations of pertinent parameters, was done with somewhat simplified equations. This procedure yielded real savings in computer time. The full complement of equations developed in Section II was used in the final detailed performance analysis of the optimum configuration thermocouple, as well as of the reference design thermocouple which, as noted below, deviates somewhat from the optimum. The simplification introduced into the initial calculations pertained primarily to the transverse heat flow in the heat-reception and heat-rejection plates. Thus, the initial calculations were performed essentially with equations that neglected the transverse component of heat flow in the plates. The resultant performance parameters calculated were optimistic in that a part of the temperature-drop that actually occurred in the heat-reception and heat-rejection plates was added to the temperature-drop across the thermoelements. Even though this simplification results in enhanced performance characteristics for a given thermocouple configuration and incident solar flux, it does, however, permit a reasonably accurate determination of the configuration with optimized performance.

If desired, after initial optimization with the simplified equations, the procedure may be repeated with the refined equations over a narrow range around the initially determined optimum. However, the procedure was not repeated because, as will be seen later, the optimum configuration was not selected for the reference design. Another simplification in the initial calculations pertained to the use of fixed values of average thermoelectric properties and to the neglect of the generation (absorption) of Thomson heat in the thermocouple legs. In addition, a few other minor simplifications were made. Of these, mention may be made of the use of the expression for the figure-of-merit in Eq. (23) of Section II. The use of the figure-of-merit defines the optimum ratio of n- and p-type thermoelement cross-sectional

areas and thereby replaces the two variables A_n and A_p by a single variable. Although this particular simplification has been made almost invariably in every past treatment of thermoelectric device performance (for example; in all of the references cited in Section II with the exception of Reference 5), including performance under both fixed heat input and fixed temperature operating conditions, it strictly applies only to the latter mode of operation. As already stated, the above simplifications in initial calculations were introduced to conserve computation time. Final calculations to determine the precise performance of the optimum configuration and the reference design thermocouples did not use these simplifications.

The thermoelectric property data used for the silicon-germanium alloys (Section V) do not pertain to the properties extant initially in the alloys, but to those present after the bulk of an initial adjustment has taken place. This adjustment occurs in the n-type alloy and results from the approach of dopant concentration in solid solution to its solid solubility equilibrium at the operating temperature. The process is exponential in time and, therefore, most of it occurs relatively early in life (approximately one half of the total change in five years of operation will have taken place in the first 1500 hours). The effect of this adjustment on the properties of the alloy is to slightly increase its electrical resistivity and Seebeck coefficient values so that the quantity S^2/ρ, which is proportional to the electrical power output, is slightly decreased. The use of property data that accounts for most of the initial adjustment, permits the performance characteristics calculated for the solar thermoelectric generator to correspond to the values anticipated after some operating time. Initial performance will be slightly higher.

As outlined in Section II, the method of optimizing the solar panel design has been to assume fixed panel configurations, with definite component materials and their associated physical properties, and to calculate the whole spectrum of performance characteristics for each configuration. Thus it has been possible to choose the configuration that yields optimum performance under specified heat-reception plate temperature conditions

(1500°F). The primary criterion for optimizing performance has been the specific power (watts per pound) delivered by the solar panel. To define the range of panel configurations in which optimum performance occurs, the following four parameters were initially varied over six different values each:

$$A_S = 2, 4, 8, 16, 32, 64 \text{ cm}^2$$
$$A_p = 0.05, 0.1, 0.2, 0.4, 0.8, 1.6 \text{ cm}^2$$
$$\ell = 0.2, 0.4, 0.8, 1.6, 3.2, 6.4 \text{ cm}$$
$$m = 0.2, 0.4, 0.8, 1.6, 3.2, 6.4$$

This variation resulted in the calculation of the performance of a total of $6 \cdot 6 \cdot 6 \cdot 6 = 1296$ different cases which correspond to 216 different thermocouple configurations operating under conditions of six different ratios of load-to-internal resistance. The whole sequence of calculations outlined in Section II subject to the simplifications discussed previously, was performed for each of the 1296 cases on the RCA 601 Computer at the David Sarnoff Research Center in Princeton. The shunt heat transfer which occurs directly between the heat-reception and the heat-rejection plates of the thermocouple was assumed to occur by conduction through insulation. The procedure used to solve Eq. (18) for $T_C(r_i)$ was the use of a root-finding method that has been programmed as a subroutine for the RCA 601 computer. In this method, an adaptive search is conducted by an extrapolation scheme, quadratic in nature, and root finding via Muller's method. Special care has been exercised to avoid by-passing near multiple zeros. The subroutine permits recursive use for solving nonlinear systems of equations. The following performance parameters were printed out for each case calculated: A_S, A_n, A_T, ℓ, m, $T_C(r_i)$, T_{CJ}, T_{HJ}, $T_H(r_i)$, Q_T, Q_I, P_o, I, E_L, W_t, η, P_o/A_T, W_t/A_T.

The results of the calculation of the initial 1296 cases were plotted and cross-plotted to establish the approximate ranges of A_S, A_p, ℓ, and m values in which thermocouple performance was optimized. This optimization occurred for the following ranges of the parameters: $0.4\text{cm} < \ell < 0.8\text{cm} < 1.6$, and $40 < A_S/A_p < 160$. The optimum performance values for A_S and A_p are indicated in terms of a range of values of the ratio A_S to A_p; the performance was practically independent of the individual values of A_S and A_p for a fixed

ratio of A_S to A_p. This condition essentially removed another variable from the initial optimization of thermocouple performance. However, it strictly applies only to the simplified initial calculation, and is not as valid in the case of the more rigorous calculations. The optimization of the ratio A_S/A_p and the fixing of either of the two variables enabled an optimum value to be determined for the other variable. The fixed value chosen for either A_S or A_p depends on such mechanical considerations as strength of the thermocouple. Thus, it would not be desirable to make A_p unduly small and thereby obtain a thermoelement that possesses an extreme value of ℓ/A. Conversely, a large value of A_S implies a large value for the areas of the heat-reception and heat-rejection plates. If, as in this case, the heat-reception plate is made of a semiconductor material, there is usually an upper limit caused by manufacturing techniques on how large an area is practically feasible.

After determining the ranges of the parameters for which the performance of the solar panel thermocouple optimizes, the procedure was repeated for fine variation of the parameters over the indicated ranges, still using the simplified design equations. The parameters were now given the following values

$$A_S = 8,\ 12,\ 18,\ 27,\ 40.5\ cm^2$$
$$A_p = 0.2\ cm^2$$
$$\ell = 0.4,\ 0.5,\ 0.6,\ 0.7,\ 0.8,\ 0.9,\ 1.0\ cm$$
$$m = 1.0,\ 1.2,\ 1.4,\ 1.6$$

Only one value was used for A_p. As already indicated, the important factor in A_S-and A_p-variation is the ratio A_S/A_p. Thus, the optimization of A_S/A_p for the fixed value of $A_p = 0.2$ enables the choice of any other value for A_p so long as the ratio A_S/A_p remains at its optimum value.

To illustrate how the optimum values of the parameters for the solar panel thermocouple were determined, the sequence of operations will be outlined in detail. The computer results, similar to those in the first run in which 1296 cases were calculated, were plotted and cross-plotted. Figure 3 shows a plot of specific power P_o/W_t as a function of A_S/A_p for the different

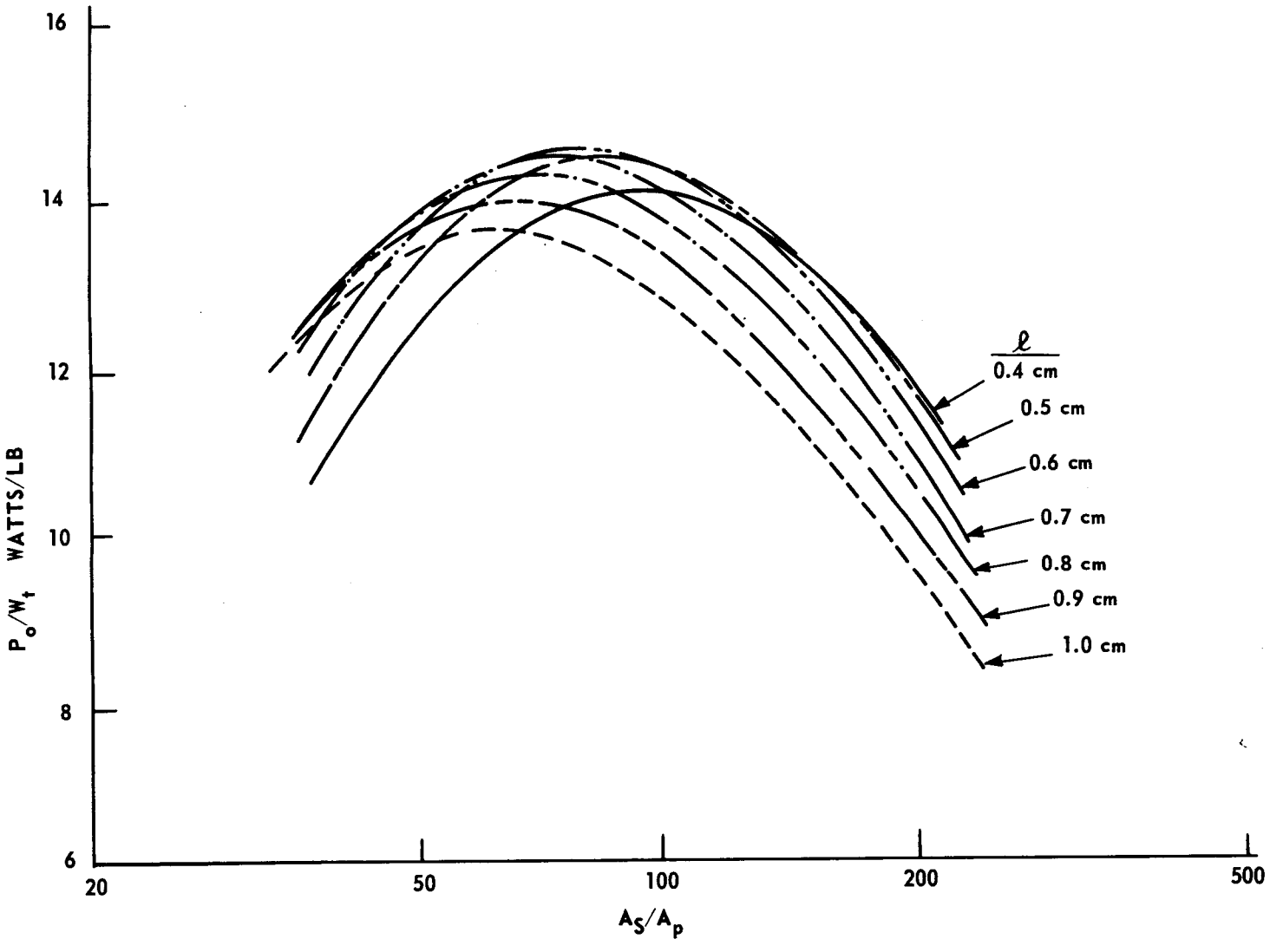

FIGURE 3. SPECIFIC POWER AS A FUNCTION OF A_S/A_p FOR DIFFERENT VALUES OF THERMOELEMENT LENGTH (ℓ) AND THE FIXED VALUE m = 1.2

values of thermoelement length. The value of 1.2 has been used for m. As will become apparent later, 1.2 is the approximate value of m for which performance is optimized. The optimum P_o/W_t values of the individual curves shift to decreasing A_S/A_p values for increasing values of ℓ. In addition, the highest value of P_o/W_t occurs at a value of $A_S/A_p = 80$ and appears to correspond to a thermoelement of length close to 0.6 cm. To more precisely determine the optimum value of thermoelement length, the data of Figure 3 have been cross-plotted in Figure 4 with the thermoelement length as the independent variable and A_S/A_p as a parameter. Values of ℓ are now chosen for which the various A_S/A_p curves are at their maxima. These ℓ values are plotted as a function of A_S/A_p in Figure 5. When $A_S/A_p = 80$, the optimum value of ℓ is exactly 0.6 cm. Because there exists the independent requirement that the heat-reception plate temperature be 1500°F (1089°K)*, it is necessary to plot this temperature as a function of A_S/A_p for different values of ℓ (Figure 6). Where $A_S/A_p = 80$ and $\ell = 0.6$, the heat-reception plate temperature is a little higher than specified. In order to obtain the required temperature it will be necessary to slightly decrease either the value of A_S/A_p or of ℓ. Maintaining the value of ℓ and decreasing A_S/A_p to 77 satisfies the temperature requirement. To see the effect of this change on the main performance indicator P_o/W_t, Figure 3 has been partly replotted in Figure 7 with largely expanded scales. Under these conditions, the reduction of A_S/A_p from 80 to 77 at a thermoelement length of 0.6 cm. has practically no effect on the specific power. Superimposed on Figure 7, is a plot of the 1500°F heat-reception plate temperature contour. The optimum thermocouple configuration is immediately determined when either A_S or A_p is specified. Because it is impractical, for fabrication reasons, to make heat-reception plates larger than 2.825 cm. on the side, the total area A_T can have a maximum value of 7.975 cm.^{2} Employment of the relation[1], which gives the optimum ratio of thermoelement leg areas in terms of the figure-of-merit relationship and of the properties of the silicon-germanium alloys, yields $A_n = 1.644\ A_p$. Making use of this relation between leg areas in Eq. (16) of Section II along with $A_S = 77A_p$ and $A_T = 7.975$ cm.^{2}, enables the determination of $A_p = 0.100$ cm.^{2} Based on previous experience, the cold stack thickness has been set at 0.368 cm. and the thickness of the heat-reception and the heat-rejection plates is constant at 0.1457 and 0.1650 cm.,

*Neglect of transverse heat flow in initial calculations causes the calculated value of heat-reception plate outer-surface temperature to be constant over the whole plate area.

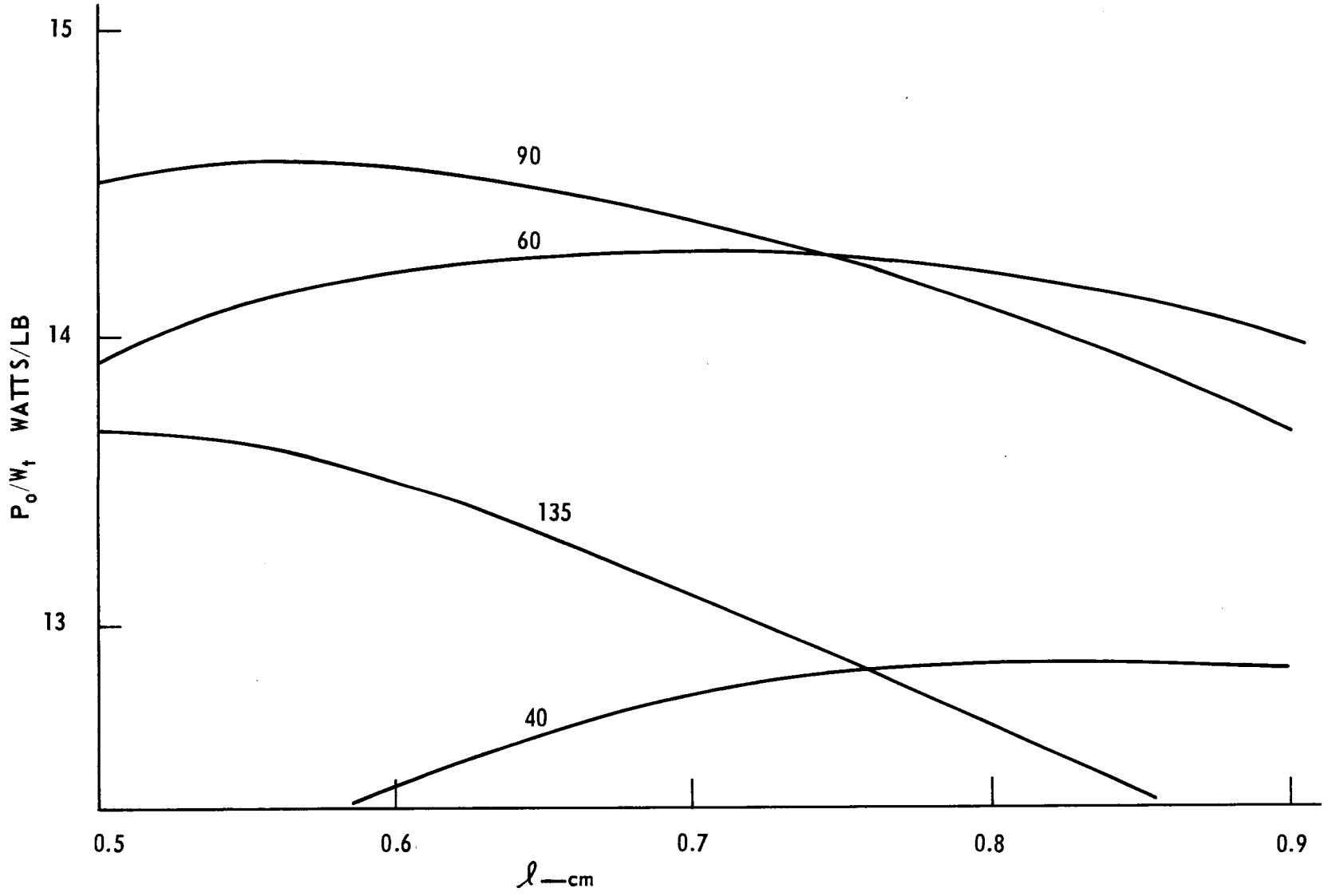

FIGURE 4. SPECIFIC POWER AS A FUNCTION OF ELEMENT LENGTH, ℓ (cm), FOR DIFFERENT VALUES OF A_S/A_p AND FIXED VALUE m = 1.2

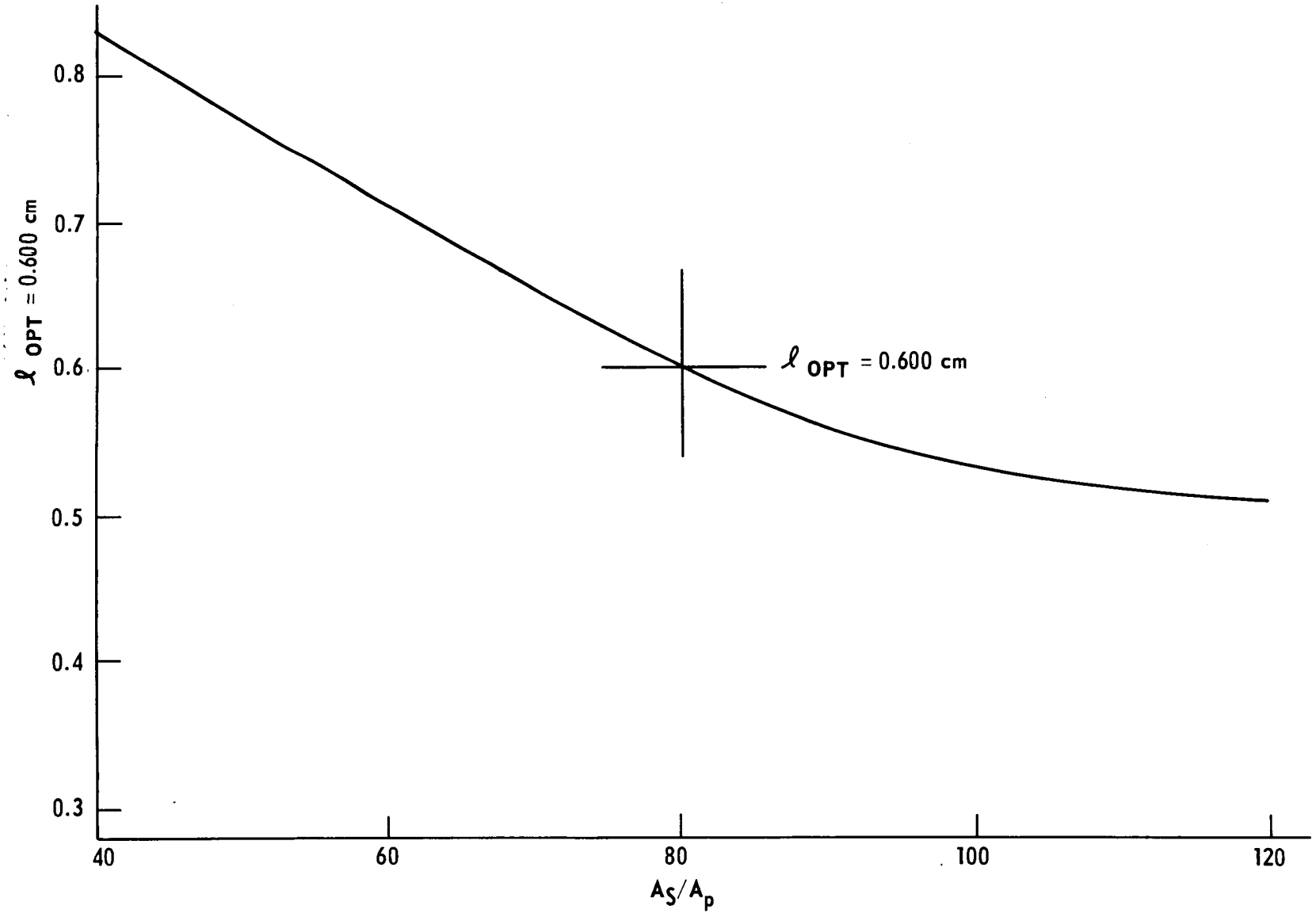

FIGURE 5. OPTIMUM ELEMENT LENGTH AS A FUNCTION OF A_S/A_p AND FIXED VALUE m = 1.2

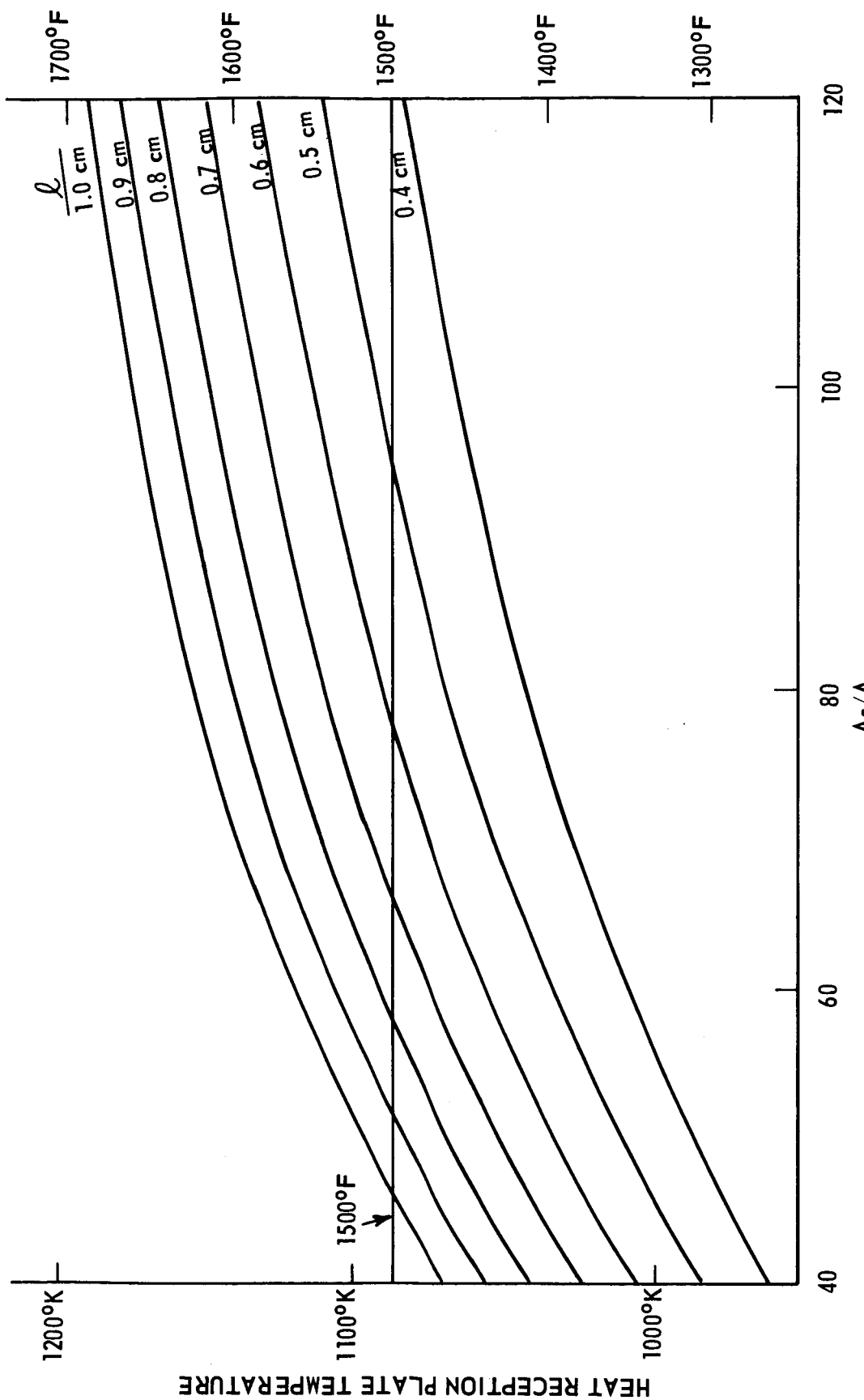

FIGURE 6. AVERAGE HEAT RECEPTION PLATE TEMPERATURE AS A FUNCTION OF A_S/A_p FOR DIFFERENT VALUES OF ELEMENT LENGTH (ℓ) AND FIXED VALUE $m = 1.2$

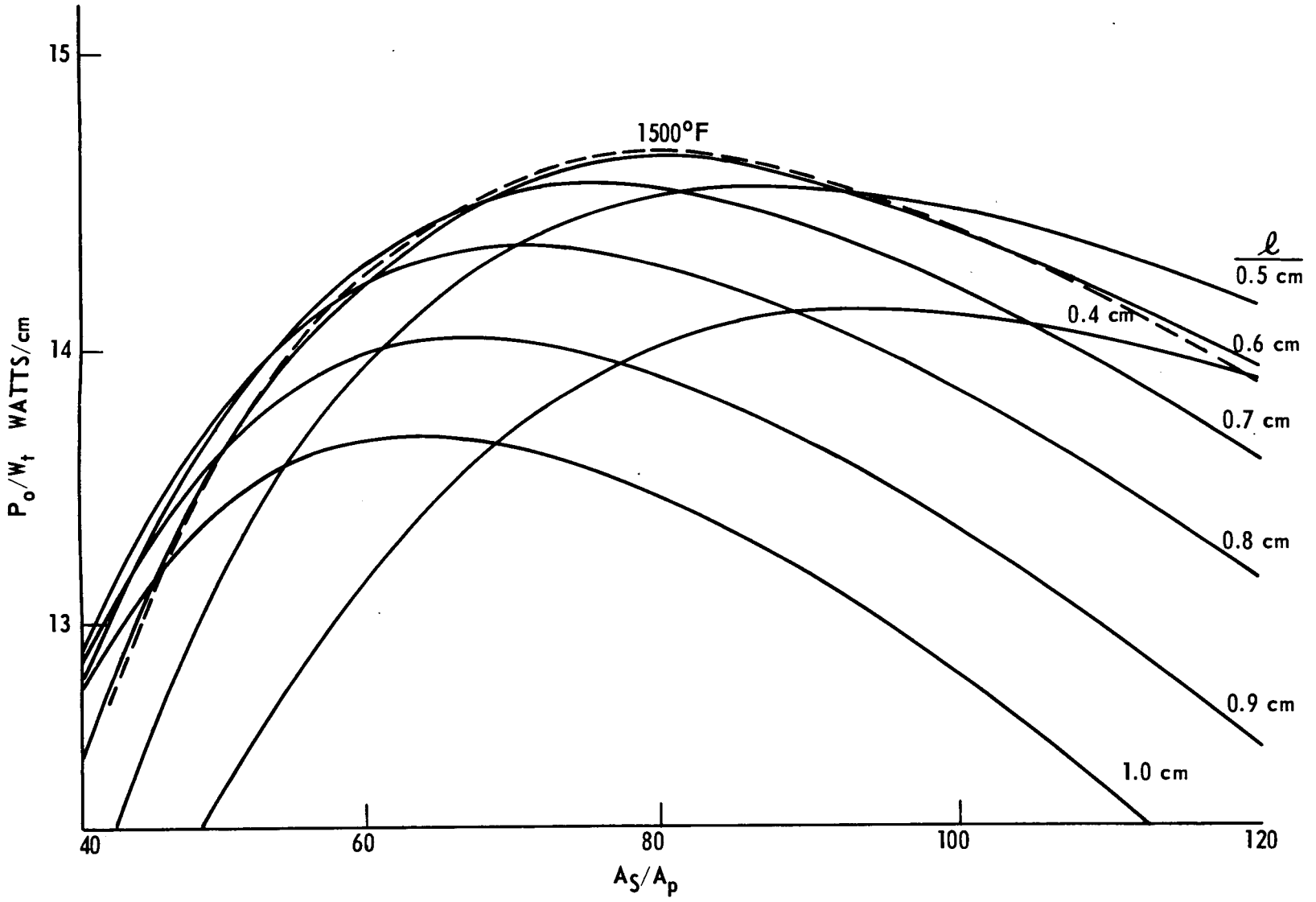

FIGURE 7. DETAIL OF THE GENERAL PLOT OF SPECIFIC POWER AS A FUNCTION OF A_S/A_p FOR DIFFERENT VALUES OF ELEMENT LENGTH (ℓ) AND FIXED VALUE m = 1.2

respectively. There is no hot stack. Even though the heat-reception plate has a pyramidal shape in the reference design, it has been replaced for calculation purposes by a flat plate having the same cross-sectional area and volume.

The chosen solar panel thermocouple configuration has optimum performance characteristics in terms of the simplified equations. The final optimization would be normally performed with the total set of equations in Section II by varying the configuration over a narrow range around that just established. This procedure, however, was not followed because after the approximate optimum design was reviewed in detail by RCA and NASA project personnel at the Lewis Research Center, it was concluded that this design was somewhat extreme in relation to the present development program. Therefore a thermocouple configuration that was more capable of fabrication within the framework of the present program was chosen for the reference design. This step meant the choice of a configuration with a smaller value for the ratio of the areas of the heat-reception plate and the thermoelements; it also meant an increase in thermoelement length. The net result was that the thermocouple performance was no longer at its optimum.

For the sake of completeness, before continuing the discussion of the reference design, the configuration corresponding to the approximate optimum performance was used in detailed calculations with the full set of equations in Section II. The results of this calculation, for m = 1.2, are listed in Table I:

TABLE I

OPTIMUM PERFORMANCE

Heat-Reception Plate Outer Edge Temperature	1099.0°K
Heat-Reception Plate Center Temperature	1055.9°K
Hot Junction Temperature	1055.2°K
Cold Junction Temperature	713.9°K
Heat-Rejection Plate Center Temperature	690.0°K
Heat-Rejection Plate Outer Edge Temperature	685.0°K
Thermocouple Efficiency	3.13%
Specific Power	12.49 w/lb

TABLE I (Cont.)

Power Output/Couple	0.274 watt
Weight/Area	2.56 lb/ft^2
Power Output/Area	31.97 w/ft^2
Load Voltage/Couple	0.1051 volt
Load Current/Couple	2.612 amps

For a generator to produce 150 watts at 28 volts, 548 couples must be combined in series-parallel. This arrangement, in addition to giving the desired voltage, enhances the reliability of the system. The characteristics of a generator with 548 couple at m = 1.20 will be:

Power Output	150.1 watts
Load Voltage	28.8 volts
Load Current	5.22 amps
Total Area	4.70 ft^2
Total Weight	12.02 lbs

The total area and the weight of the generator do not include contributions from the mounting frame and the ribs on the heat-rejection plates. Moreover, the approximate optimum-performance (in terms of watts per pound) generator does not meet the objective of 35 watts per square foot of panel area; whereas the reference design generator does, but at a slightly increased generator weight. Also apparent is the fact that the heat-reception plate does not possess a uniform 1500°F (1089°K) temperature because of transverse heat flow. Except for the peripheral areas of the plate, the temperature is generally less than 1500°F. The belief is that the slightly higher temperature that exists at the periphery has no adverse effects on the characteristics of the emittance and the absorption coating.

As already stated, because of greater compatibility with the present state-of-the-art fabrication techniques, a thermocouple configuration was selected for the reference design with relative component dimensions less extreme than those determined for the approximate optimum thermocouple. The thermoelement length was fixed at 1.0 cm. and detailed design calculations, similar to the ones discussed previously, were repeated to precisely

define a new configuration. The use of a heat-reception plate of maximum size (A_T = 7.975 cm.^{2}) showed that the thermoelement areas of A_n = 0.2684 cm.^{2} and A_p = 0.1632 cm.^{2} resulted in heat-reception plate temperatures that closely correspond to those determined for the thermocouple which possesses the approximate optimum configuration. On the average, such temperatures satisfy the criterion of 1500°F heat-reception plate temperature. The detailed performance characteristics of the reference design thermocouple for m = 1.2 are listed in Table II:

TABLE II

REFERENCE DESIGN PERFORMANCE

Heat-Reception Plate Outer Edge Temperature	1100.9°K
Heat-Reception Plate Center Temperature	1064.4°K
Hot Junction Temperature	1063.8°K
Cold Junction Temperature	702.8°K
Heat-Rejection Plate Center Temperature	687.5°K
Heat-Rejection Plate Outer Edge Temperature	683.3°K
Thermocouple Efficiency	3.57%
Specific Power	11.27 w/lb
Power Output/Couple	0.312 watt
Weight/Area	3.23 lb/ft^2
Power Output/Area	36.36 w/ft^2
Load Voltage/Couple	0.1108 volt
Load Current/Couple	2.817 amps

To obtain a generator with the desired power and voltage characteristics (approximately 150 watts and 28 volts) 480 couples are used in a series-parallel arrangement. Two identical panels of 240 couples each are set up; each panel consists of 20 sections, and each section has 12 couples.

The over-all performance of the reference design generator at m = 1.20 will be:

Power Output	149.8 watts
Load Voltage	26.6 volts
Load Current	5.63 amps

Total Area	4.12 ft^2
Total Weight	13.29 lbs

The total area and the weight of the generator do not include contributions from the mounting frame and the ribs of the heat-rejection plates.

Figure 8 shows the power output of the generator for a variable load in terms of the ratio of load-to-internal resistance. The curve further shows that power output maximizes in the range of m = 1.2 to 1.3. This plot illustrates the incorrectness of the assumption frequently made that maximum power is delivered to the load when the load and internal resistances are equal. Finally, the over-all performance characteristics of the reference design generator are graphically illustrated in Figure 9 as a function of load current. Figure 9 shows that if the desired operation is to be at a load voltage of 28 volts, rather than at the 26.6 volts corresponding to m = 1.20 given in the tabulation, all that need be done is to increase the load resistance slightly. The resultant effect on power output is negligible.

B. Temperature Profile of the Reference Design Thermocouple

As a part of the performance analyses of the reference design thermocouple, detailed calculations were performed of the temperatures at a variety of key places as follows:

Outer edge of outer surface of heat-reception plate	1100.9°K
Center of outer surface of heat-reception plate	1064.4°K
Center of inner surface of heat-reception plate	1063.8°K
Hot junction of the thermoelements	1063.8°K
Cold junction of the thermoelements	702.8°K
Center of inner surface of heat-rejection plate	687.6°K
Center of outer surface of heat-rejection plate	687.5°K
Outer edge of outer surface of heat-rejection plate	683.3°K

The center of the inner surface of the heat-reception plate and the hot junctions of the thermoelements are noted to be at the same temperature.

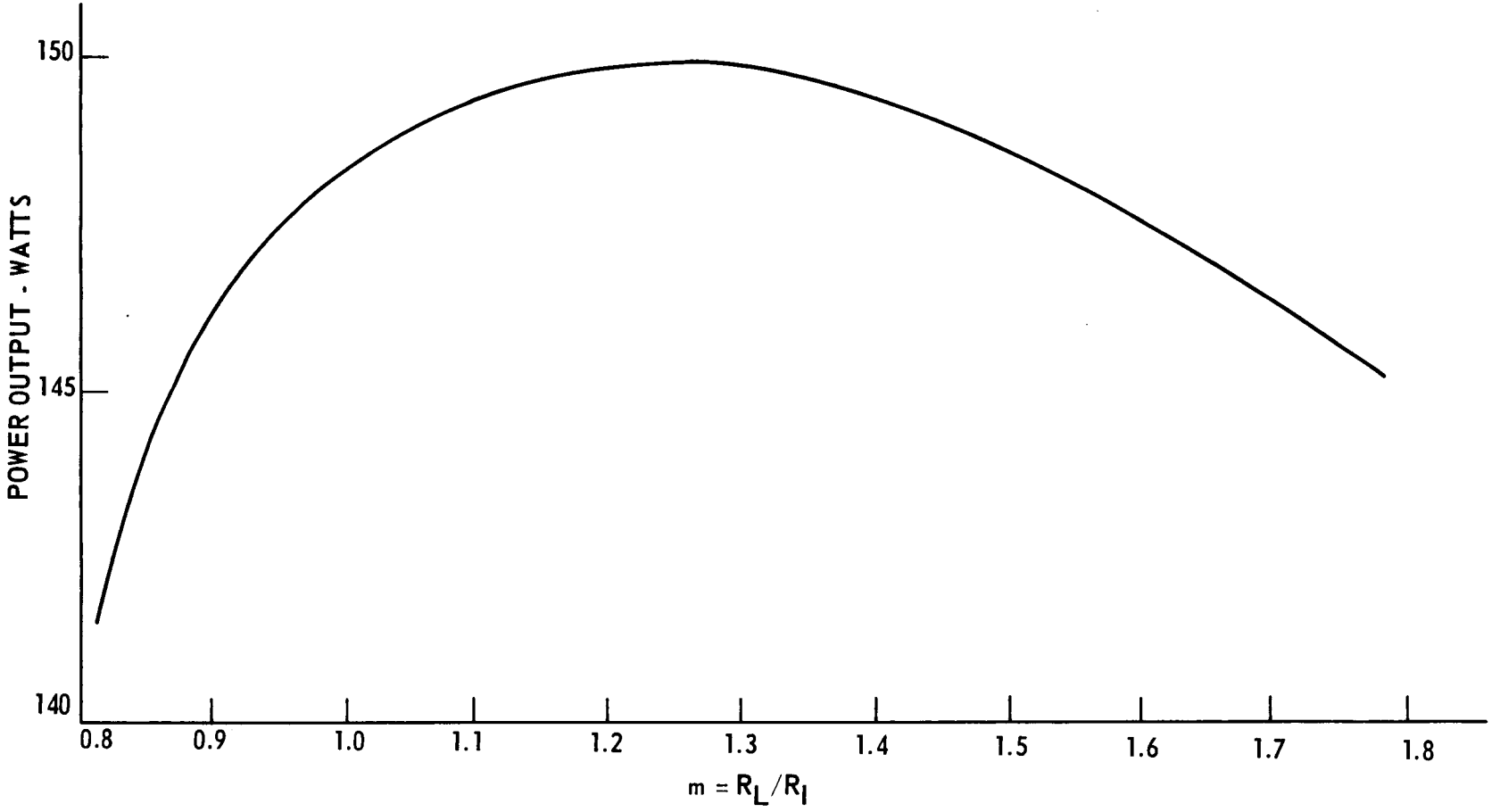

FIGURE 8. REFERENCE DESIGN GENERATOR POWER OUTPUT AS A FUNCTION OF THE RATIO OF LOAD TO INTERNAL ELECTRICAL RESISTANCE

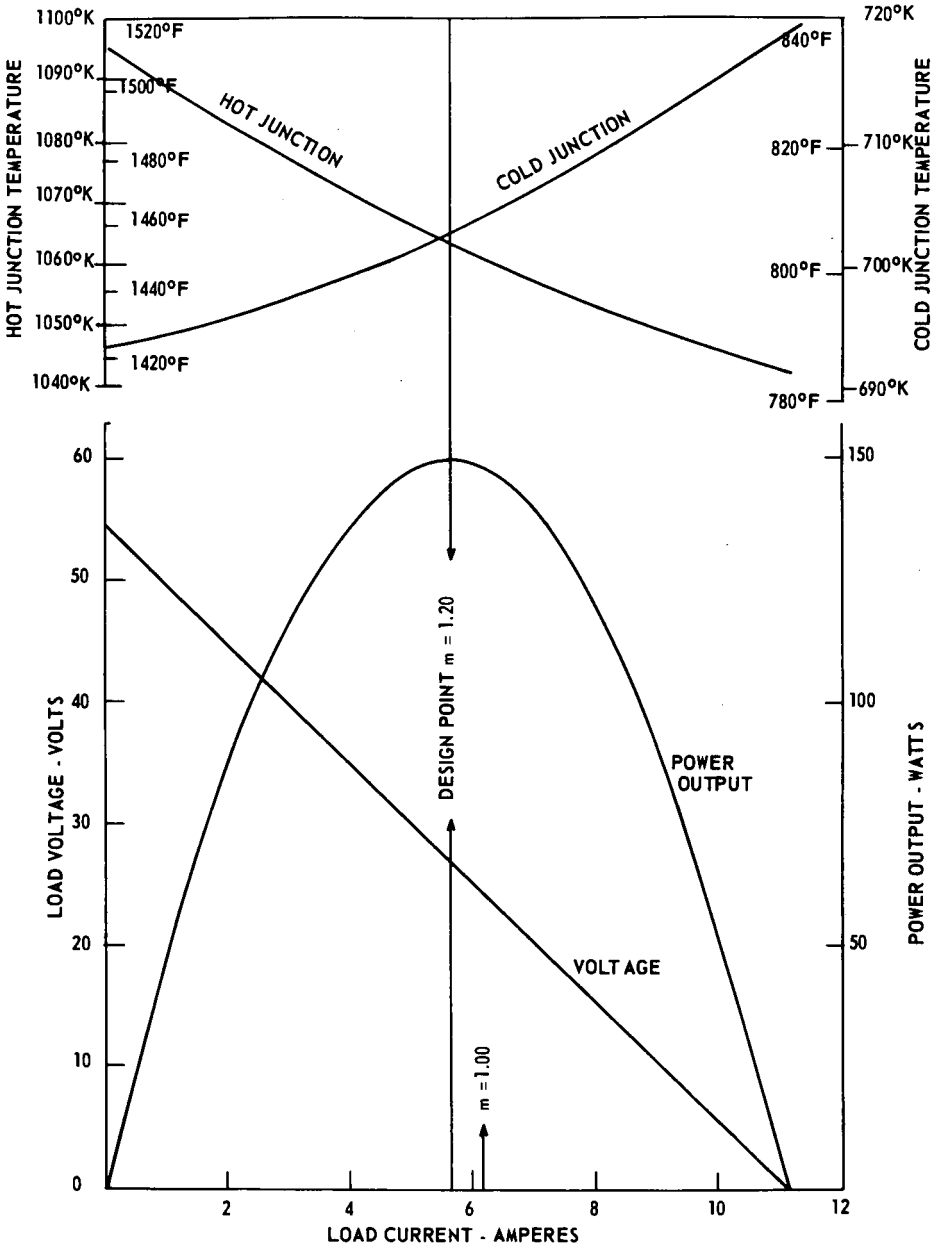

FIGURE 9. REFERENCE DESIGN GENERATOR PERFORMANCE CHARACTERISTICS AS A FUNCTION OF LOAD CURRENT

This condition exists because there is no stack at the hot end of the structure. The temperature profile of the structure is illustrated in Figure 10. Because of the radial geometry assumed for the heat-reception and heat-rejection plates for calculation purposes, the temperature profiles shown for these plates represent averages.

C. Weight Analysis of the Reference Design Generator

A detailed weight analysis of any given thermoelectric structure is made as a part of the performance calculations outlined in Section II. The results of such a weight analysis for the reference design solar thermoelectric generator are tabulated as follows:

Member	Weight per Thermocouple	Generator Weight (480 couples)
Heat-reception plate	0.007170 lb	3.441 lbs
Insulation	0.007250 lb	3.479 lbs
Thermoelements	0.003369 lb	1.617 lbs
Cold Stack	0.003786 lb	1.817 lbs
Electrical connector	0.000752 lb	0.361 lb
Heat-rejection plate	0.005363 lb	2.575 lbs
Total	0.027690 lb	13.290 lbs

In a total generator, there are additional members that have not been included in the previous table. The detailed weights of these additional components are listed below:

Member	Weight per Thermocouple	Generator Weight (480 couples)
Studs	0.000034 lb	0.016 lb
Nuts	0.000053 lb	0.026 lb
Panel Section Ribs	0.002740 lb	1.315 lbs
Mounting Frames	0.006080 lb	2.918 lbs
Total	0.008907 lb	4.275 lbs

Because the ribbing on the panel sections and the mounting frames for the sections have not been subjected to design optimization, the listed weights of these components are preliminary and probably only represent, at best,

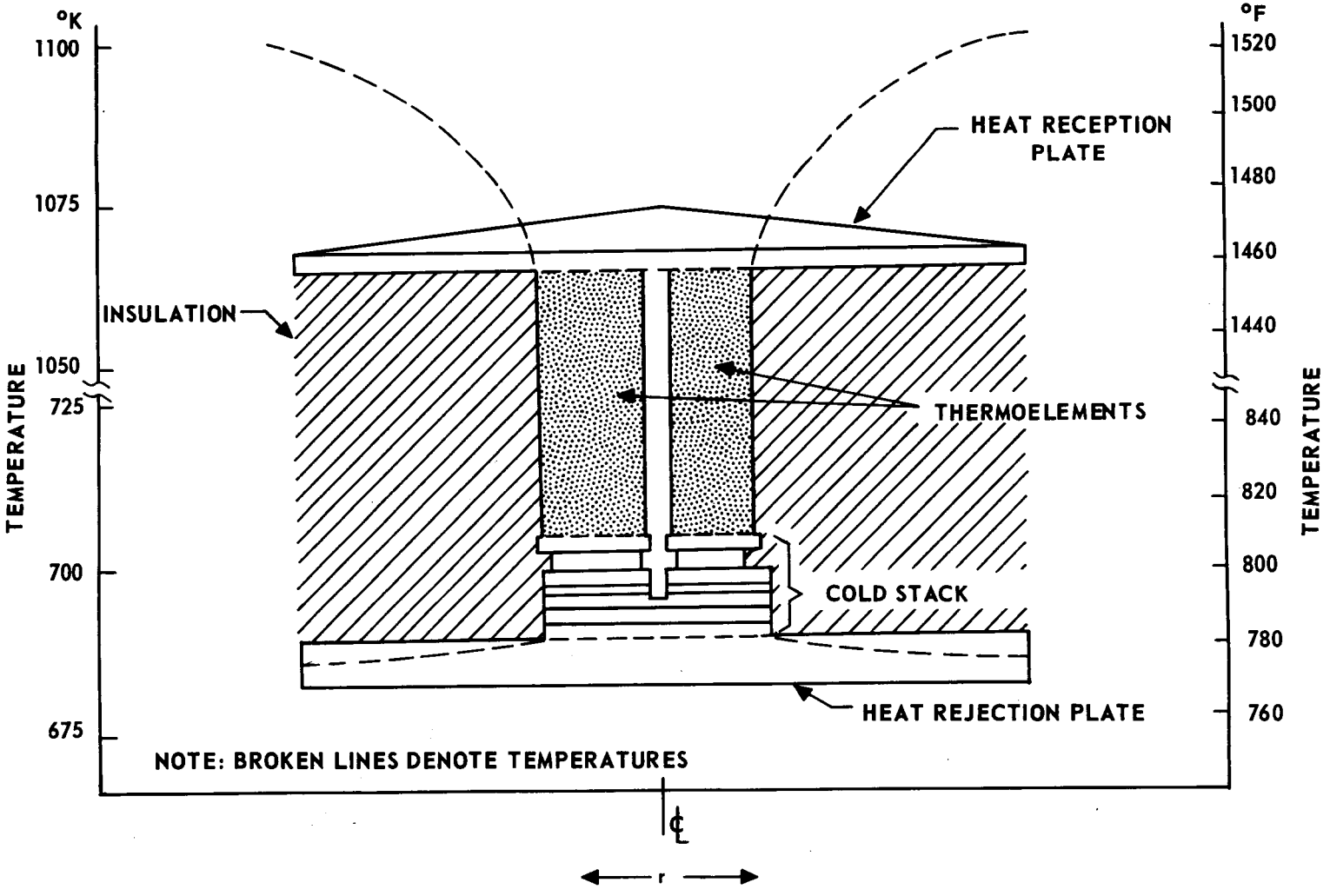

FIGURE 10. GRAPHIC ILLUSTRATION OF TEMPERATURE PROFILE OF REFERENCE DESIGN THERMOCOUPLE

upper limit values. It is expected that upon optimization, the weights of these components will be considerably reduced. Just as in the case of generator weight, the total generator area has contributions from factors other than the thermocouples. These factors are the edges of the mounting frames and the spacings between the heat-reception plates of adjacent thermocouples. Thus, whereas the combined area of all of the thermocouples is 4.12 square feet, the total area of the generator, including the factors just mentioned, is 4.49 square feet.

D. Off - Design Performance of Reference Design Generator

It is apparent from the equations in Section II that the performance of a solar thermoelectric generator is strongly dependent on the emittance and absorption characteristics of the coatings on the heat-reception and heat-rejection plate surfaces as well as on the solar heat flux incident on the generator. The present reference design has been developed with the following assumed values for these properties:

$$\alpha = 0.85$$
$$\epsilon_H = 0.10$$
$$\epsilon_C = 0.85$$
$$W = 2.24 \text{ watts/cm.}^2$$

The incident flux value of 2.24 watts/cm.^{2} corresponds to the perpendicular flux at a distance of 0.25 astronomical unit from the sun.

Because the properties of the coatings may change with time, it is valuable to know how such changes would affect the performance of the reference design generator. Moreover, inasmuch as the solar flux incident on the generator depends on the distance and/or the orientation of the panel with respect to the sun, it is also of interest to know how the performance of the reference design generator depends on incident flux. Detailed performance calculations of the reference design generator, using the equations of Section II, were accordingly performed for variable values of α, ϵ_H, ϵ_C, and W. Some of the results of these "off design" calculations have been plotted in the included figures.

Figures 11 to 14 pertain to the incident solar flux of 2.24 watts/cm.^{2} at the design distance of 0.25 astronomical unit from the sun, and show the effects of varying values of α, ϵ_H and ϵ_C on the reference design generator performance and temperatures. Of the three properties, it is the emissivity of the heat-rejection plate, ϵ_C, that has the least effect on generator performance. By the same token, it is the emissivity of the heat-reception plate, ϵ_H, that has the greatest effect. In addition to illustrating generator performance under varying conditions of emittance and absorption coatings, the results of these "off-design" studies are useful in indicating which parameters are most critical and, therefore, which properties should receive the greatest attention in development work on coatings.

If design values are assumed for the properties of the coatings, as listed previously, it is also of interest to know how the performance and temperatures of the reference design generator depend on the incident solar flux. For example, assumed perpendicularity of incidence indicates the expected performance of the generator as a function of its distance from the sun. Conversely, at the design distance of 0.25 astronomical unit from the sun, or at any other distance for that matter, the dependence of performance on incident flux may be interpreted as giving the performance as a function of generator tilt angle with respect to incident radiation. At any distance from the sun, nonperpendicularity of the plane of the generator to incident radiation will naturally reduce the incident flux. Figure 15 shows the results of performance calculations as a function of incident solar flux. The results have been presented as a function of the distance from the sun which implicitly assumes perpendicularity of the plane of the generator to incident radiation. For greater generality, Table III relates distance from the sun to the incident perpendicular solar flux (solar constant):

TABLE III

INCIDENT SOLAR FLUX VS. DISTANCE FROM THE SUN

Distance From Sun-Astronomical Units	Distance From Sun - Miles	Solar Constant-Watts/cm.^{2}
0.1	9.3×10^6	14.00
0.2	18.6×10^6	3.50
0.4	37.2×10^6	0.88

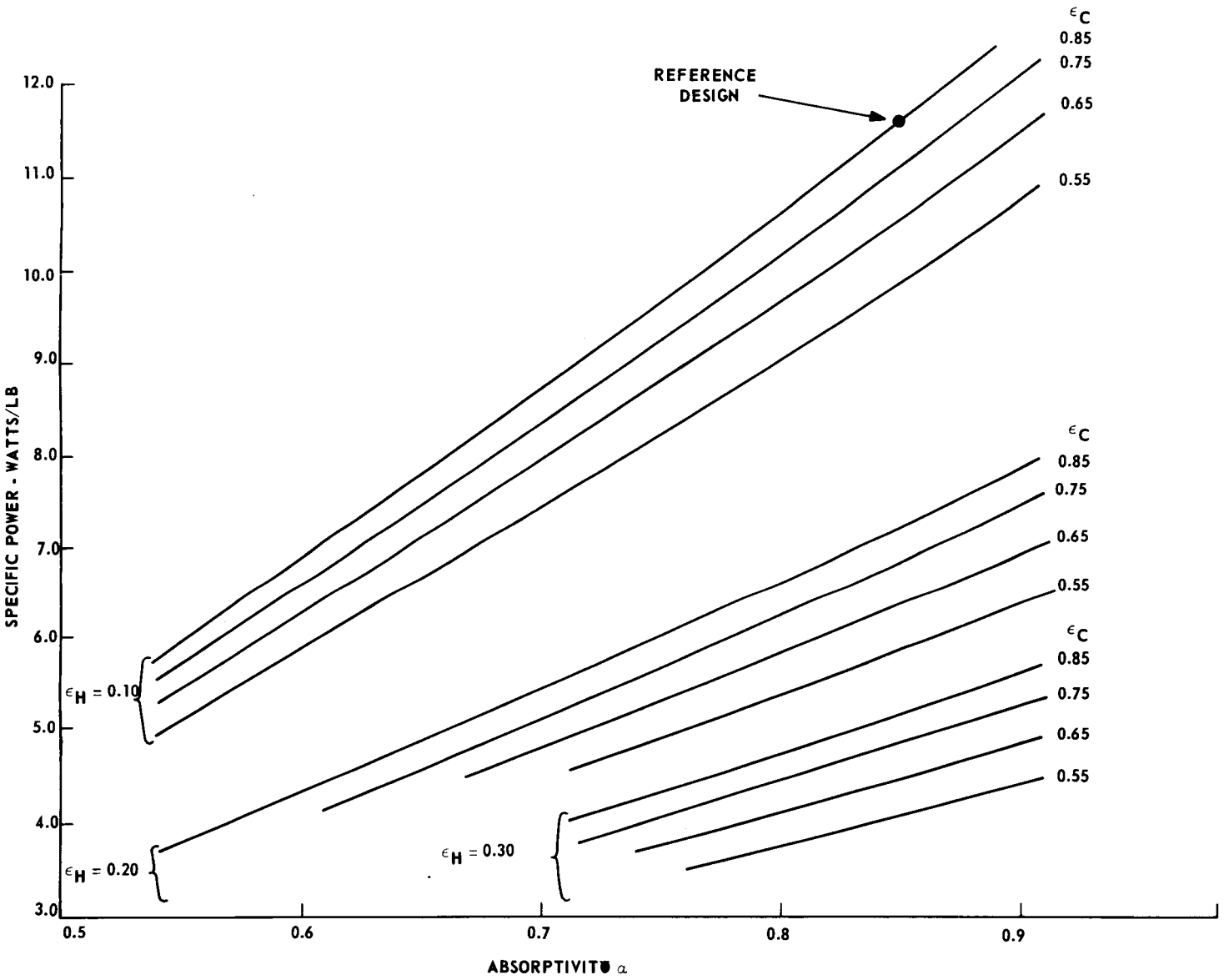

FIGURE 11. SPECIFIC POWER OF REFERENCE DESIGN GENERATOR AS A FUNCTION OF HEAT RECEPTION PLATE ABSORPTIVITY FOR DIFFERENT VALUES OF HEAT RECEPTION AND HEAT REJECTION PLATE EMISSIVITIES AND FOR FIXED VALUES, W = 2.24 WATTS/cm^2 AND m = 1.20

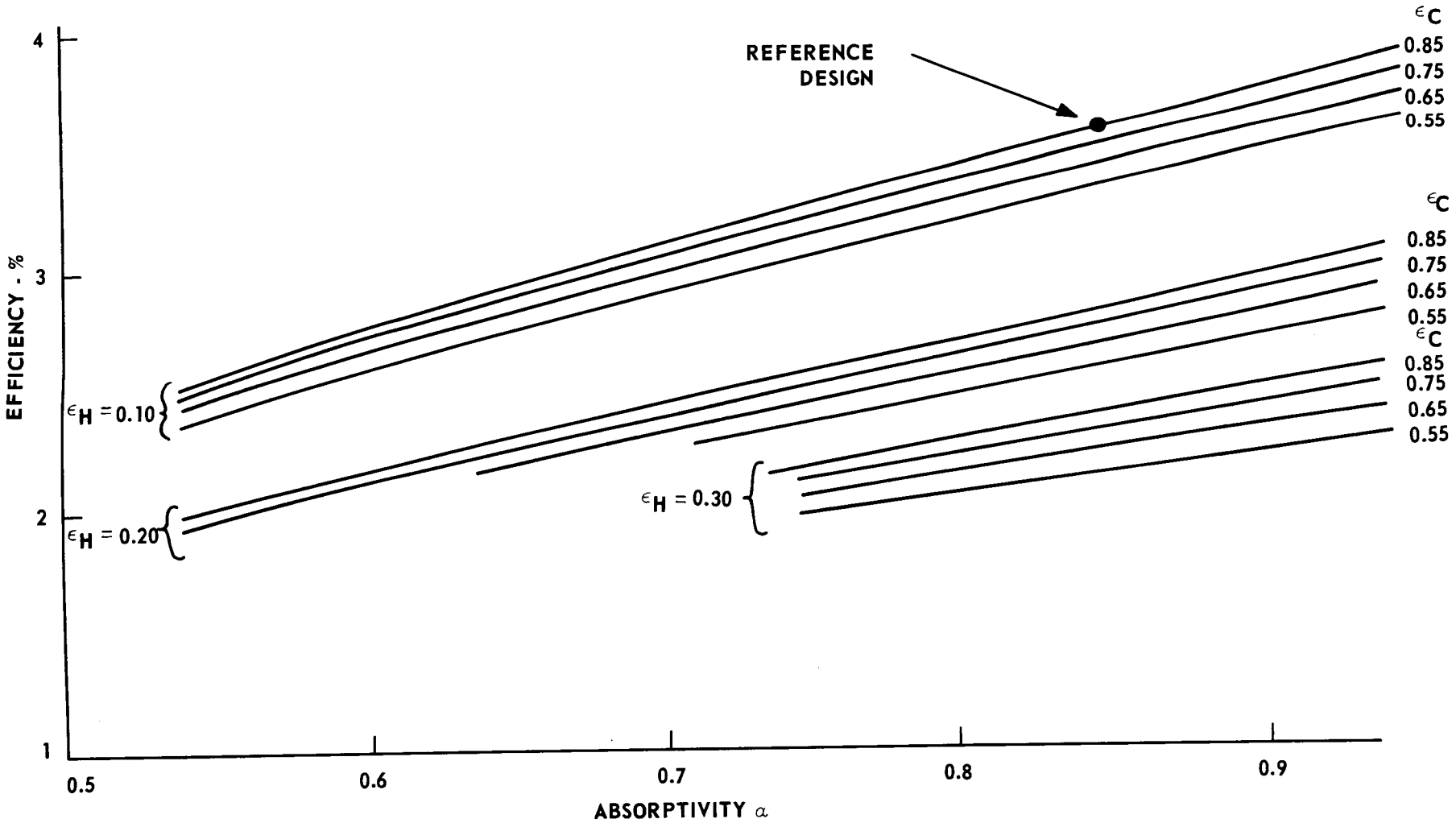

FIGURE 12. EFFICIENCY OF REFERENCE DESIGN GENERATOR AS A FUNCTION OF HEAT RECEPTION PLATE ABSORPTIVITY FOR DIFFERENT VALUES OF HEAT RECEPTION AND HEAT REJECTION PLATE EMISSIVITIES AND FOR FIXED VALUES, W = 2.24 watts/cm^2 and m = 1.20

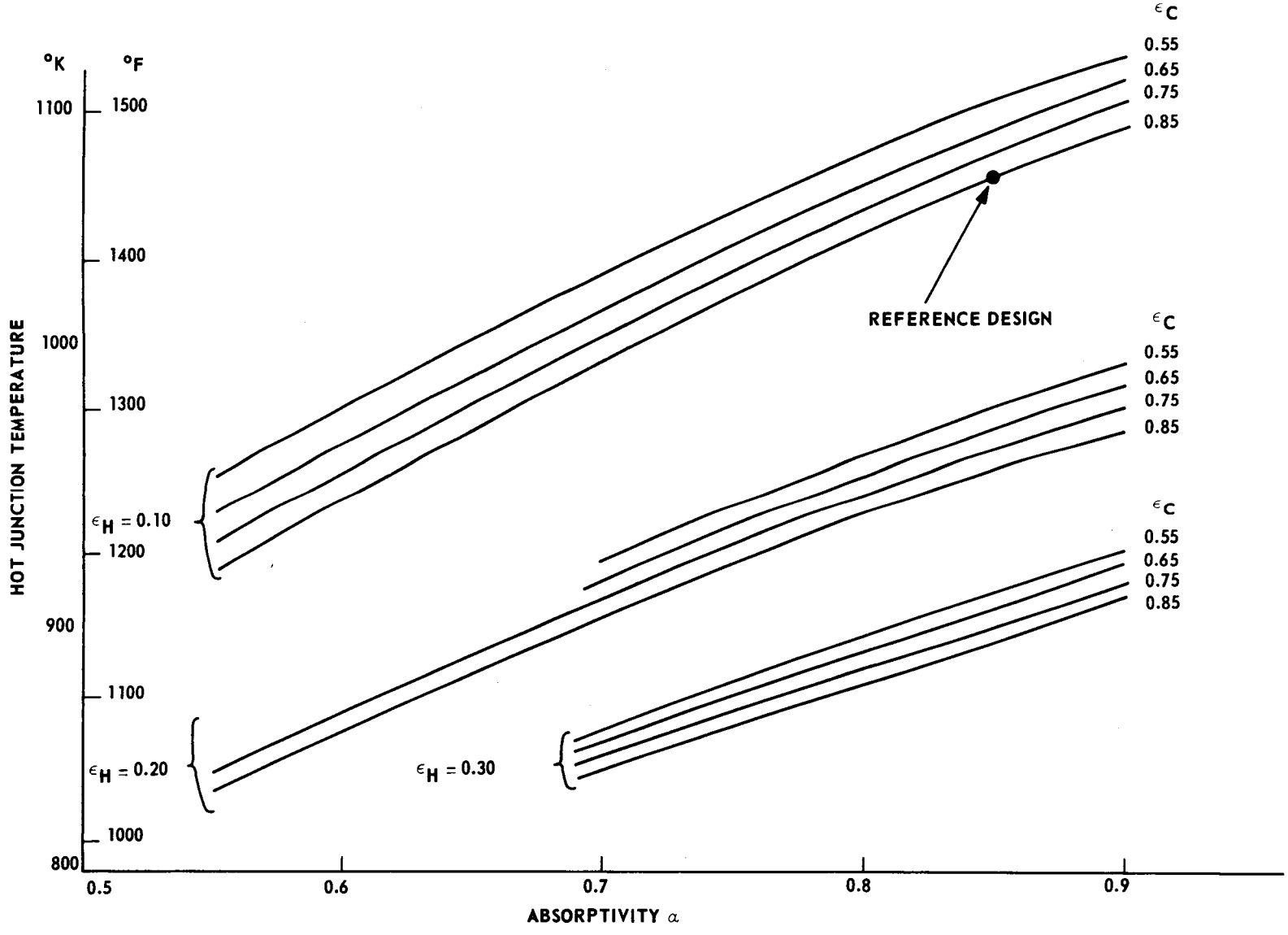

FIGURE 13. HOT JUNCTION TEMPERATURES OF REFERENCE DESIGN GENERATOR AS A FUNCTION OF HEAT RECEPTION PLATE ABSORPTIVITY FOR DIFFERENT VALUES OF HEAT RECEPTION AND HEAT REJECTION PLATE EMISSIVITIES AND FOR FIXED VALUES, W = 2.24 WATTS/cm^2 AND m = 1.20

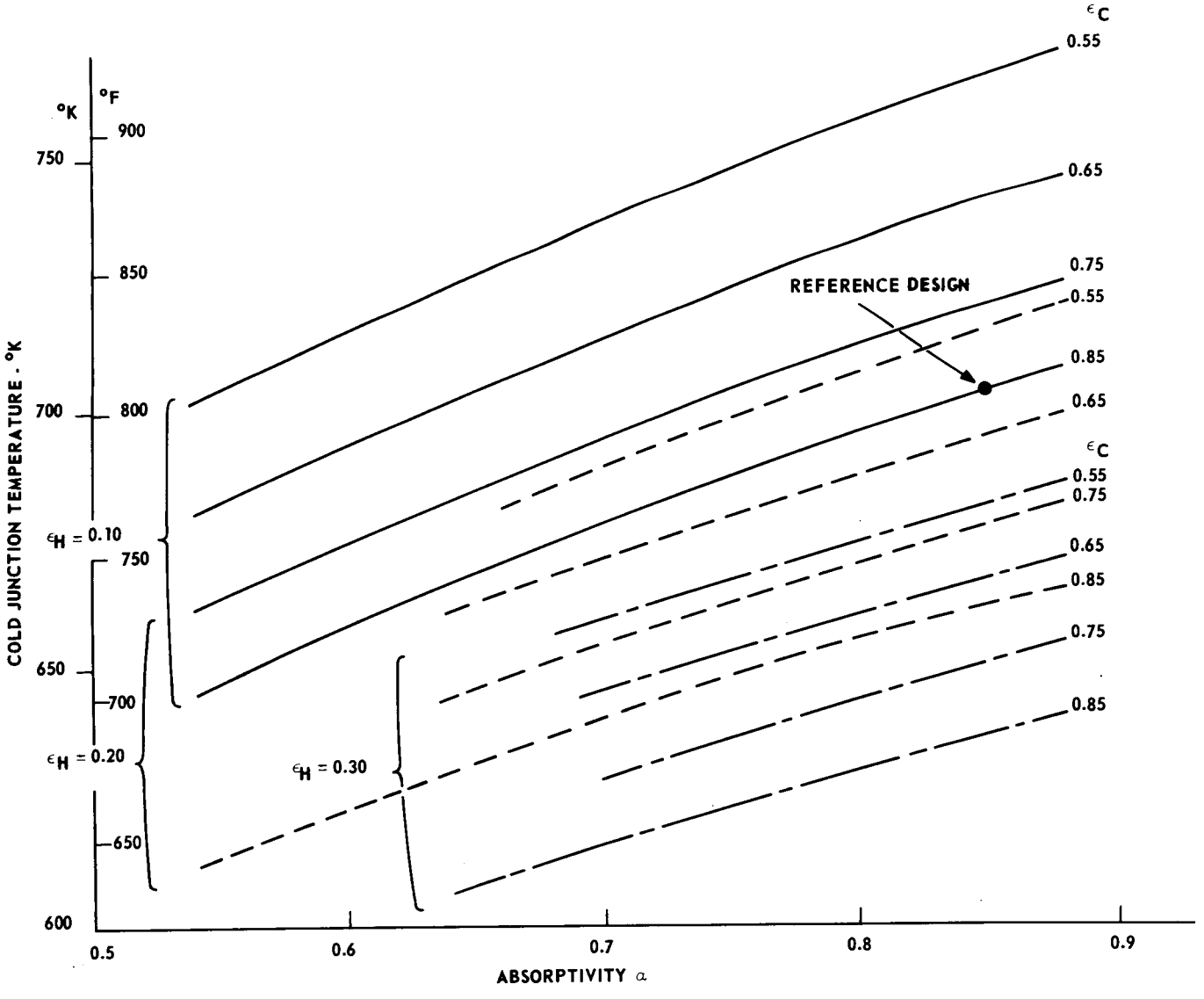

FIGURE 14. COLD JUNCTION TEMPERATURES OF REFERENCE DESIGN GENERATOR AS A FUNCTION OF HEAT RECEPTION PLATE ABSORPTIVITY FOR DIFFERENT VALUES OF HEAT RECEPTION AND HEAT REJECTION PLATE EMISSIVITIES AND FOR FIXED VALUES, W = 2.24 WATTS/cm^2 AND m = 1.20

TABLE III (Cont.)

Distance From Sun- Astronomical Units	Distance From Sun - Miles	Solar Constant- Watts/cm.^{2}
0.6	55.7×10^6	0.39
0.8	74.3×10^6	0.22
1.0	92.9×10^6	0.14

This table may be used in conjunction with Figure 15 to determine the performance of the reference design generator as a function of generator tilt angle. Thus, if the generator is at some distance from the sun but it is tilted such that the incident flux is less than the solar constant at that distance, a new effective distance corresponding to the actual heat flux at the generator may be obtained. This effective distance, used in Figure 15, enables the actual generator performance to be determined. Figure 15 shows plots of hot and cold junction temperatures, values of total heat transmitted per couple, and generator efficiency in terms of distance from the sun. Electrical power output per couple may be easily obtained from the data in Figure 15 by multiplying the efficiency by the heat transmitted per couple. Total generator power is 480 times that product.

E. Layout Drawings of the Reference Design Generator

The detailed layout of the solar thermoelectric reference design generator and its components is shown in Figures 16 to 21. A brief description of each drawing follows:

Figure 16 - Couple Assembly: shows the detailed layout of the thermoelement assembly with the heat-reception plate and the pedestals attached to the cold shoes.

Figure 17 - Cold End Assembly: shows the configuration and composition of the cold stack with electrical interconnects and the stud for mounting the thermocouple on the heat-rejection plate.

Figure 18 - Thermocouple Subassembly: shows the detailed configuration of the total reference design thermocouple, with the exception of the heat-rejection plate.

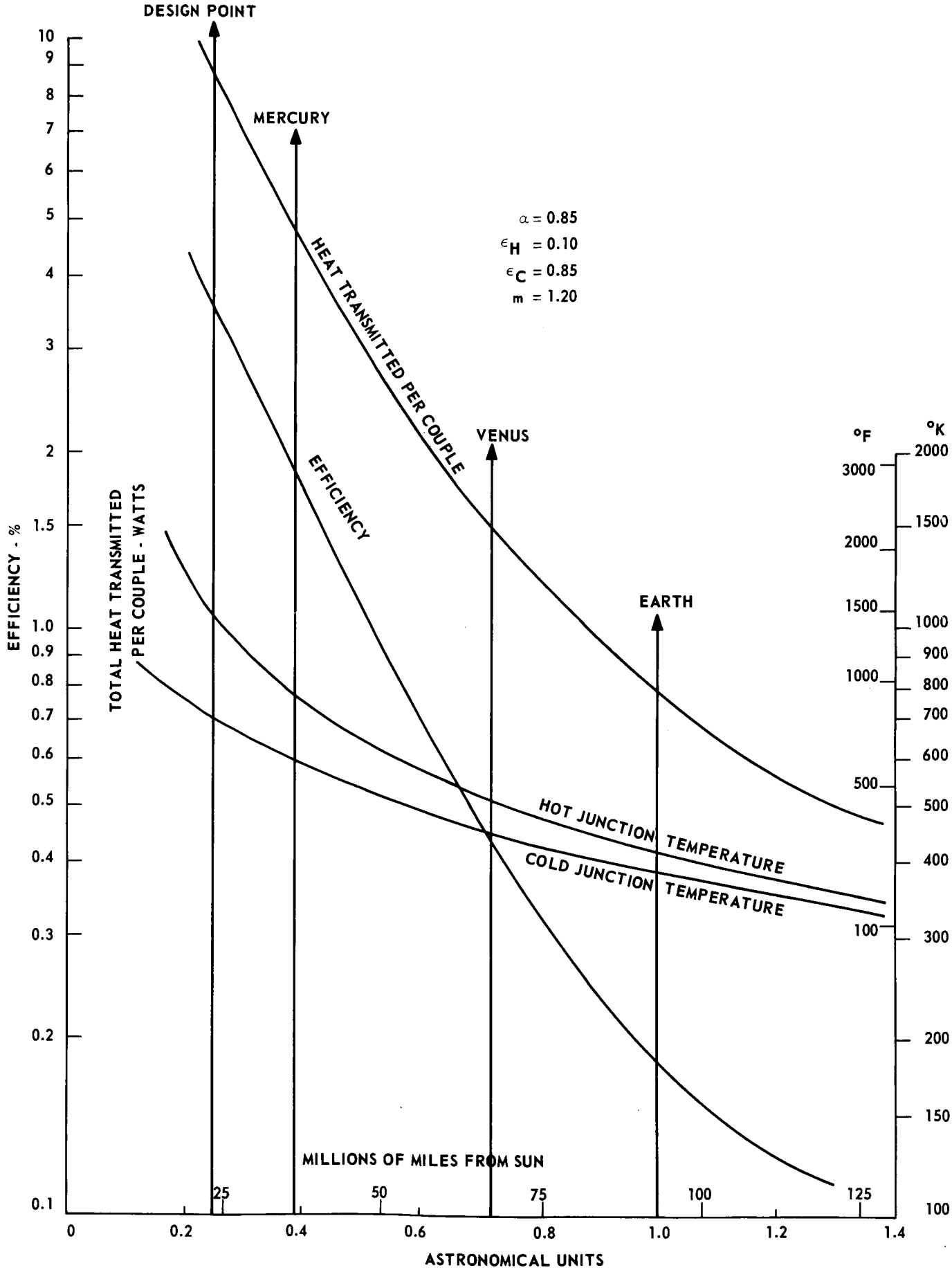

FIGURE 15. REFERENCE DESIGN GENERATOR PERFORMANCE CHARACTERISTICS AS A FUNCTION OF DISTANCE FROM THE SUN

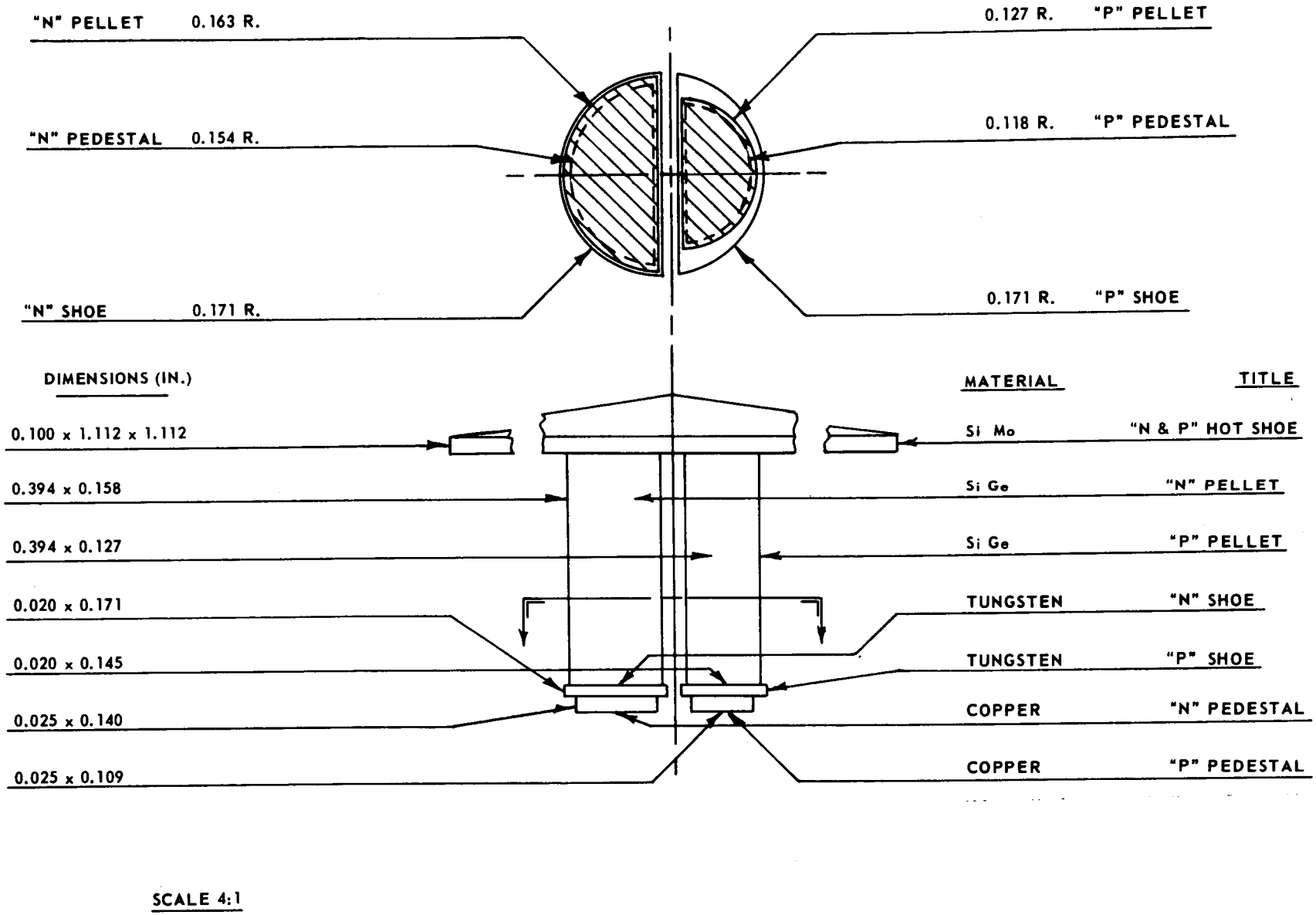

FIGURE 16. REFERENCE DESIGN COUPLE ASSEMBLY

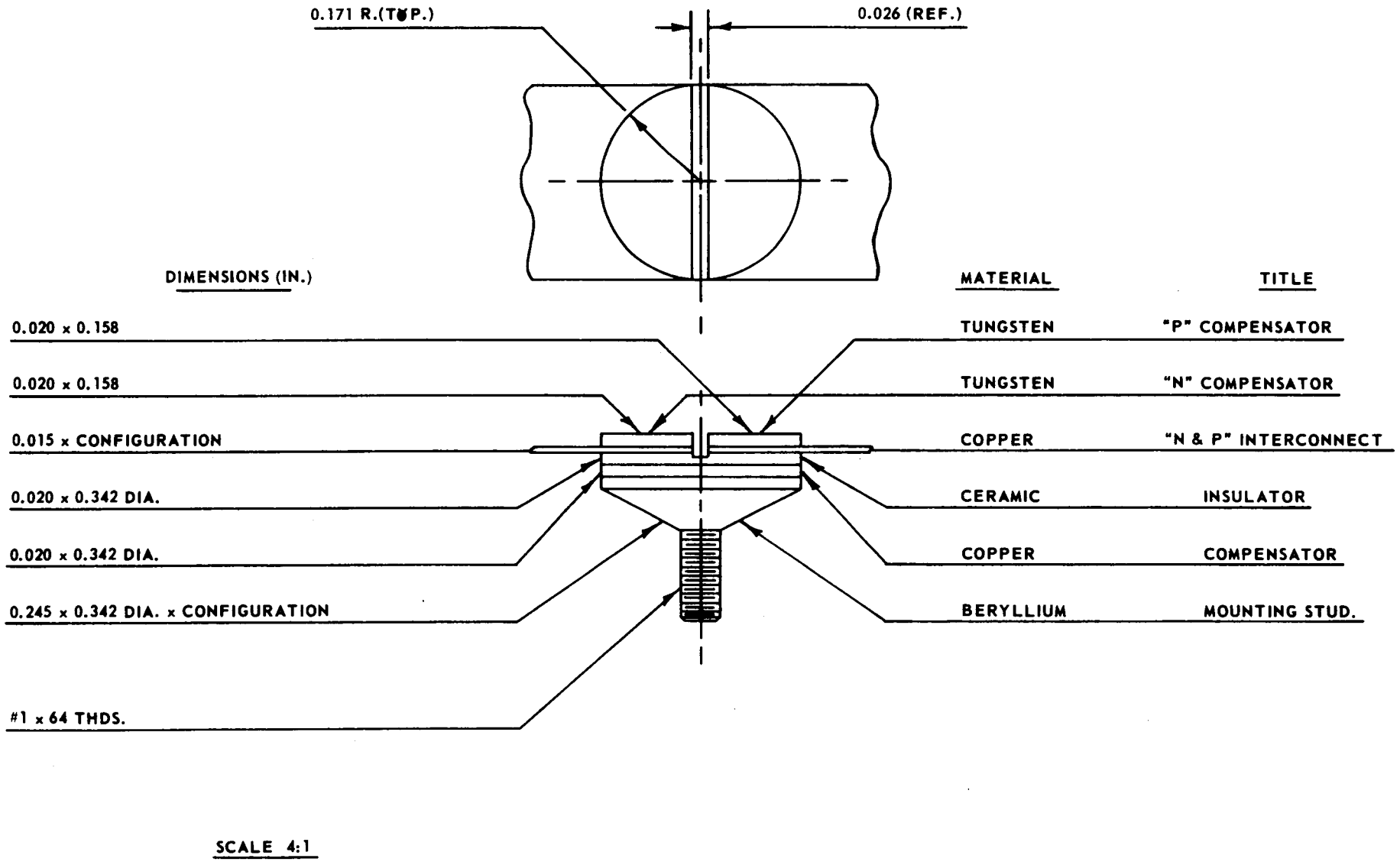

FIGURE 17. REFERENCE DESIGN COLD END ASSEMBLY

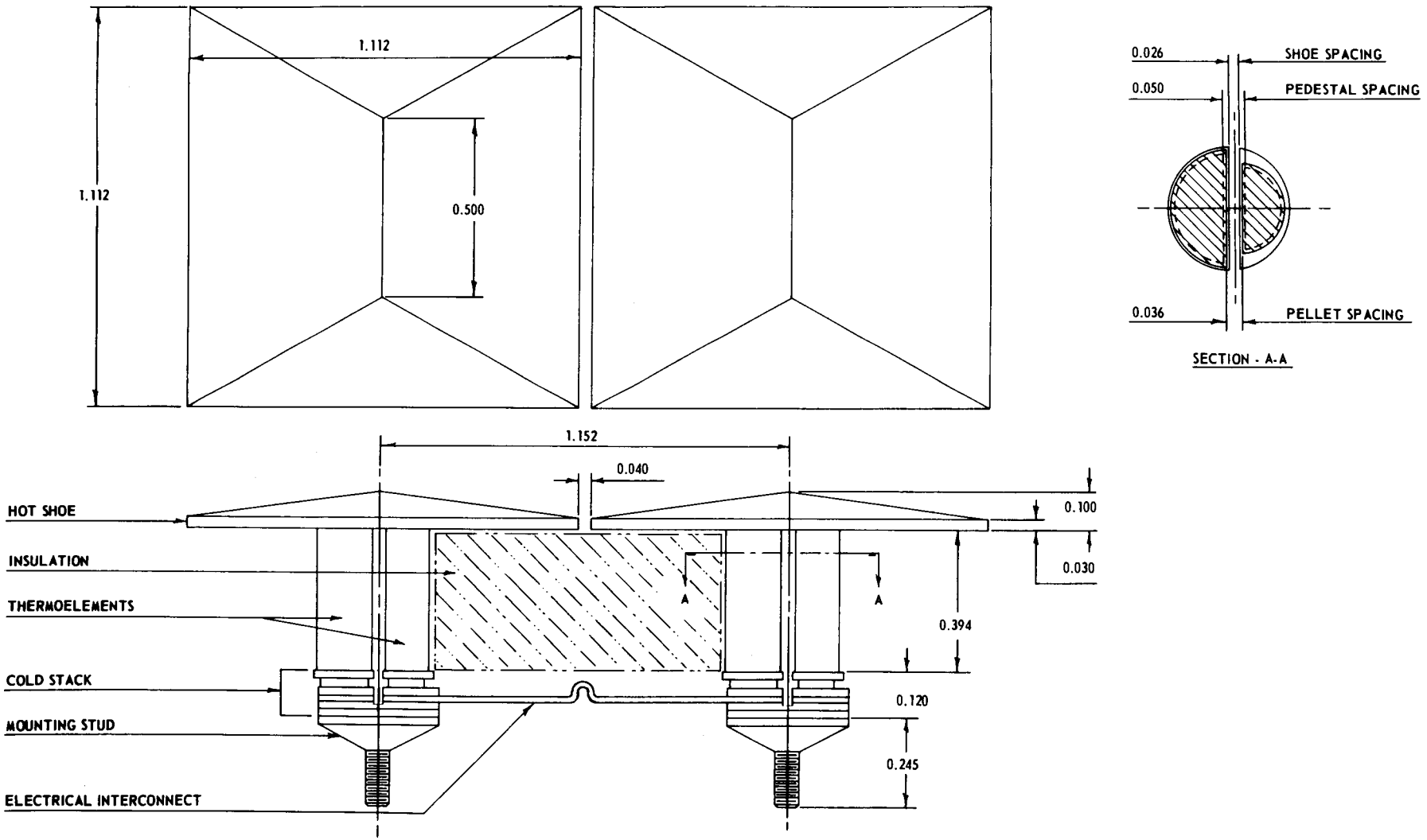

FIGURE 18. REFERENCE DESIGN—THERMOCOUPLE ASSEMBLY

Figure 19 - Generator Panel Section Assembly: shows the layout of the reference design generator panel section, including the heat-rejection plate.

Figure 20 - Generator Panel Assembly: shows the combination of panel sections to form a panel of the reference design generator. Two such panels form the total generator.

Figure 21 - Generator Panel Electrical Schematic: illustrates the electrical combination of the thermocouples of a reference design generator panel to give series - parallel redundancy.

F. Stress Analysis of Solar Thermoelectric Generator Panel Components

The reference thermoelectric couple and panel configurations have been structurally analyzed to determine the maximum stress levels to be anticipated when the panel generator is subjected to the following individual or combined environmental loading requirements:

1) Acceleration: The panel shall withstand 7 g's acceleration for five minutes in both directions along three mutually perpendicular axes.

2) Vibration: The panel shall withstand vibration of a 5-g peak at the resonant frequencies between 16 and 2000 H_z for 15 minutes along three mutually perpendicular axes.

3) Acoustic Noise: The panel shall withstand for five minutes a total integrated sound pressure level of 148 decibels referred to 0.0002 dyne per $cm.^2$, with the frequency spectrum specified in Contract NAS3-10600.

4) Thermal Transient: The panel shall withstand two cycles of the following thermal transient test: The panel shall be heated to an absorber surface temperature of 1500°F as rapidly as possible when subjected to the thermal flux required to achieve this hot junction temperature. Immediately after temperature equilibrium has been established, heating

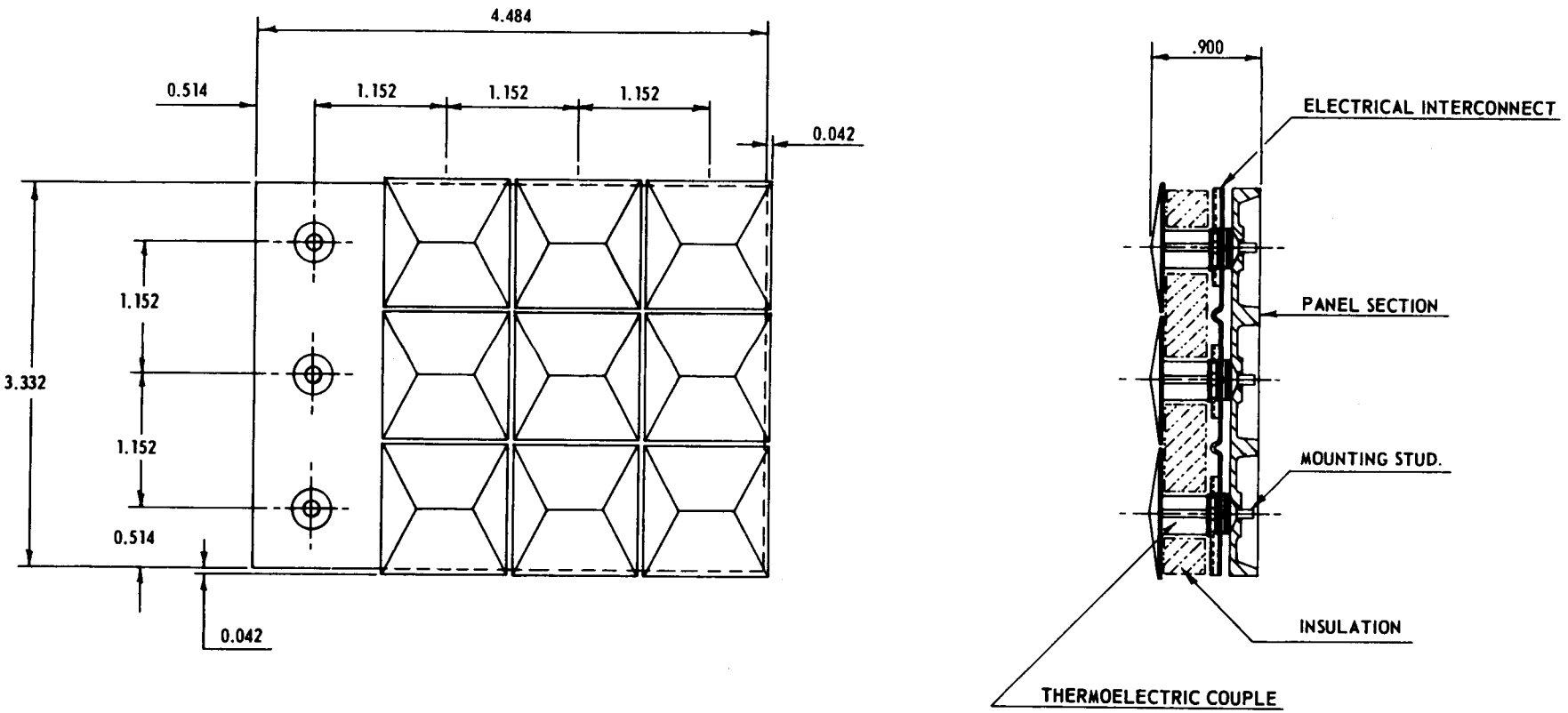

FIGURE 19. REFERENCE DESIGN—GENERATOR PANEL SECTION ASSEMBLY

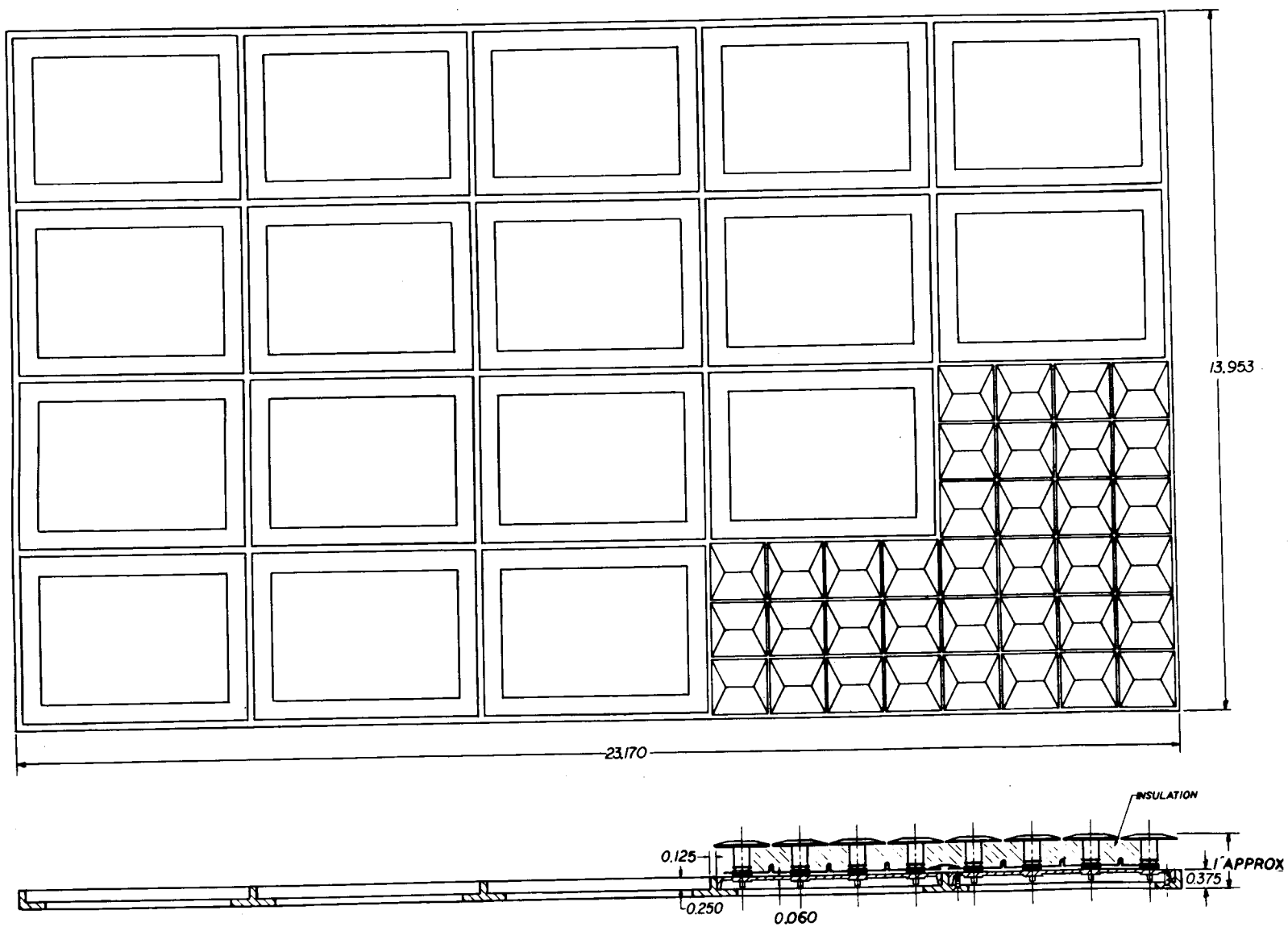

FIGURE 20. REFERENCE DESIGN—GENERATOR PANEL ASSEMBLY

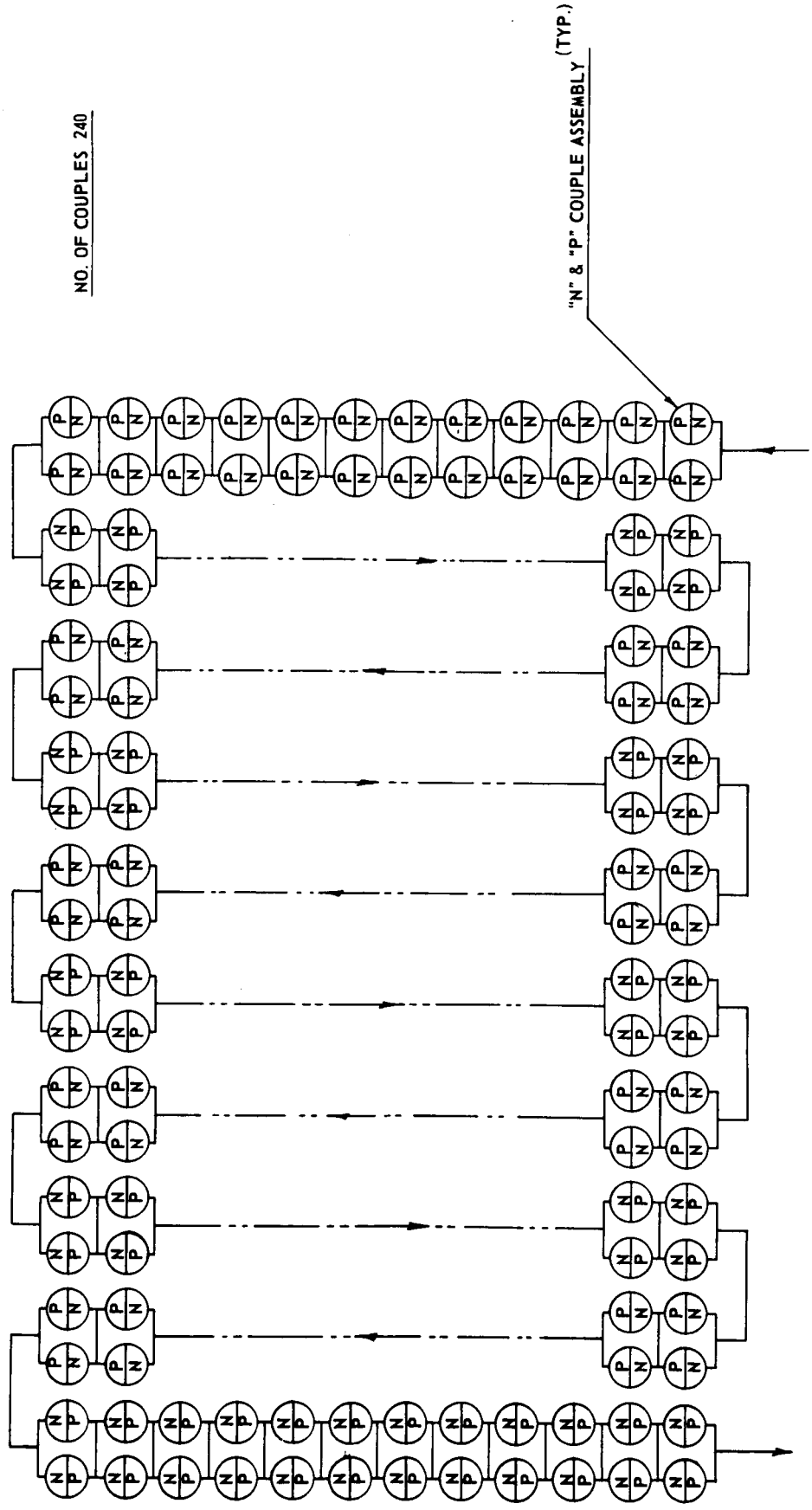

FIGURE 21. REFERENCE DESIGN—GENERATOR PANEL ELECTRICAL ASSEMBLY

shall cease. The panel shall be allowed to cool to an equilibrium temperature by radiating to the surrounding walls of a liquid-nitrogen-cooled chamber. When an equilibrium temperature has been obtained, the absorber surface shall be reheated to an equilibrium temperature of 1500°F. The panel shall again be allowed to cool to an equilibrium temperature dictated by the surroundings.

The results of the detailed stress analysis are described after the following account of the analysis procedure. The conclusions indicate that a substantial margin of safety exists between the calculated maximum stresses for each condition and for the material strength capability. (Tables IV and V.)

This procedure was followed in performing the analysis: Attention was concentrated on the analysis of the maximum stress levels for the thermoelectric couple and the radiator base plate. A less detailed analysis was made of the generator frame because 1) the program objectives required emphasis on the details of the thermoelectric configuration rather than on the generator configuration and 2) because no specific satellite orientation had been defined. To a large extent, the specific satellite configuration and the method of attachment of the panels to the satellite will control the stress levels in the generator frame. For example, potentially excessive stresses caused by vibration can be reduced to within the allowable level by either relocating the point of attachment of the frame to its hinge attachment or struts, or by placing a damping mechanism in the strut between the panel and the satellite. Therefore, a vibration analysis of the generator frame has not been performed. Consequently, the analysis of the generator frame has been confined to a determination of the severest potential acceleration stress levels for conservative approximations of the actual loading conditions.

The analysis considered only elastic response of the material. Inasmuch as the thermoelectric material is a semiconductor which would tend to experience little plastic deformation prior to failure, the plastic effects are not being considered.

1. Capability of the Structure to Withstand Acceleration Requirement

Requirement: The panel shall withstand 7 g's acceleration for five minutes in both directions along three mutually perpendicular axes.

Analysis: The stresses at the bond of the SiGe element to the tungsten shoe at the cold end were selected as the most critical acceleration-induced stresses in the thermocouple because

a) The stresses in the region of the hot end bond will be substantially less, resulting from a significantly smaller moment being induced by a smaller mass (hot shoe) acting through a shorter arm.

b) Though the moment in the region of the couple (cold stack) below the cold shoe is slightly larger than at the cold end bond, the moment of inertia of the members is greater, and the material is capable of withstanding higher stresses in tension than SiGe.

Thus the relatively high moment, produced by acceleration at the point of the couple where the material is least capable of withstanding tensile stresses, makes this the most critical region to analyze.

a. Acceleration-Induced Stresses in Thermocouple

Case I. Acceleration in the X-Direction

In this case, the primary stress is induced by the bonding moment. An acceleration in the X-direction will generate a moment about point O. (Figure 22.) This moment must be resisted by a bond stress. The moment caused by acceleration will be determined initially: total amount = $M_{element} + M_{hot\ shoe}$

where

$$M_{hot\ shoe} = (F_{hot\ shoe})\ (\text{moment arm}) = a\ V_H\ \delta_H\ (\ell + \frac{t_H}{2}) \qquad (36)$$

where V_H is volume of hot shoe, δ_H is density of hot shoe material, a is acceleration; and to find $M_{element}$, consider a small increment of the element, dm.

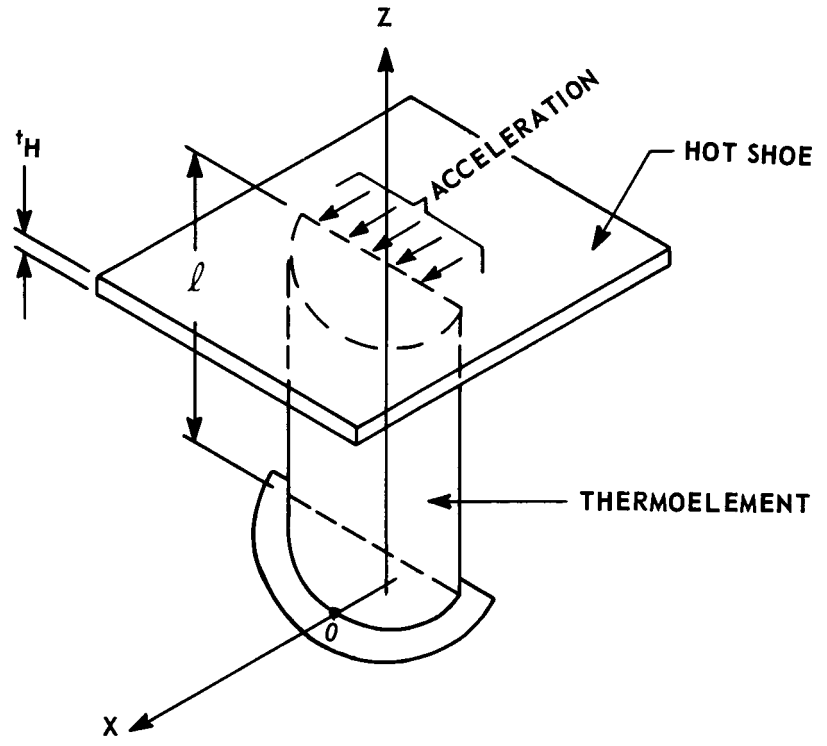

FIGURE 22. LOAD DISTRIBUTION IN X-DIRECTION

$$dF = adm = a\,\delta_T dV_T = a\,\delta_T \int_o^{\pi} \frac{R^2 d\theta}{2} \quad dZ = \frac{a\,\delta_T \pi R^2 dZ}{2}$$

$$dm = ZdF = \frac{a\,\delta_T\,\pi R^2 Z dZ}{2}$$

and $$M_{element} = \frac{a\,\delta_T\,\pi R^2}{2} \int_o^{\ell} ZdZ = \frac{a\,\delta_T\,\pi R^2 \ell^2}{4} \qquad (37)$$

TABLE IV

CALCULATED MAXIMUM STRESS LEVELS IN PANEL COMPONENTS

Environmental Loading	Component and Maximum Stress Level	
1. Acceleration	Thermoelement bond to cold shoe -	Max-X = 12.2 psi
		Max-Y = 7.0 psi
		Max-Z = 2.2 psi
	Generator Frame	Max-X = 3875 psi
		Max-Y = 5360 psi
2. Vibration	Thermocouple	Max-X = 9.0 psi
		Max-Y = 18.3 psi
	Radiator Base Plate	Max = 103 psi
3. Acoustic Noise	Thermocouple	Max-X = 25.5 psi
		Max-Y = 51.8 psi
	Radiator Base Plate	Max = 660 psi
4. Thermal Stresses	Thermocouple-Element	Max = 11,900 psi compression
	Hot Shoe	Max = 10,600 psi tension

TABLE V

MECHANICAL PROPERTIES OF COMPONENT MATERIALS

Material	Modulus of Elasticity	Ultimate Tensile Strength	Ultimate Compression Strength
Silicon Germanium	18×10^6 psi	p-type 3900 psi n-type 4400 psi	150,000 psi
Beryllium (at 400°C)	42×10^6 psi	30,000 psi	--
Silicon Molybdenum	18×10^6 psi	20,500 psi (as determined for conditions of thermal stress)	--

The detailed analyses which support the previously discussed conclusions are:

where δ_T is density of SiGe, V_T is volume of element, R is radius of element and θ is the angular coordinate used in integration. Therefore, adding (36) and (37) we get

$$\text{Total Moment} = \frac{a\delta_T \pi R^2 \ell^2}{4} + aV_H \delta_H \left(\ell + \frac{t_H}{2}\right) \qquad (38)$$

Now, the resisting moment, or the moment due to the bond stress will be determined. Consider a strip in the plane of the bond as shown in Figure 23. (Force acts perpendicular to the plane of the paper.)

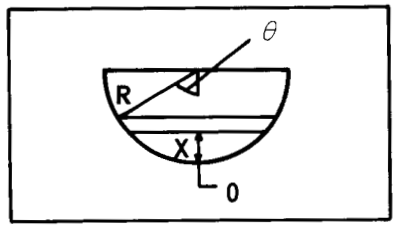

FIGURE 23. SECTION IN PLANE OF BOND

Strip Area $dA = 2R \sin\theta \, dx$
where $x = R - R\cos\theta = R(1-\cos\theta)$
and $dx = R \sin\theta \, d\theta$
therefore $dA = 2R^2 \sin^2\theta \, d\theta$
and the incremental force dF is
$dF = \sigma dA = 2\sigma R^2 \sin^2 d\theta$,
where σ is the bond stress, and
$dM = xdF = 2R^3 \sigma (1-\cos\theta)\sin^2\theta d\theta$.

Integrating between the limits 0 and $\pi/2$ gives

$$M = 2R^3 \sigma \left[\frac{\pi}{4} - \frac{1}{3}\right] \qquad (39)$$

Now we can equate (38) and (39) and solve for σ to obtain

$$\sigma = \frac{\frac{a\delta_T \pi R^2 \ell^2}{4} + aV_H \delta_H \left(\ell + \frac{t_H}{2}\right)}{2R^3 \left[\frac{\pi}{4} - \frac{1}{3}\right]}, \qquad (40)$$

now substituting the following constants

$\ell = 1.0$ cm.; $\delta_T = 3.53$ g/cm.^{3}; $a = 7(980) = 6.86 \times 10^3$ cm./sec^2;
$R_{nleg} = 0.414$ cm.; $R_{pleg} = 0.322$cm.; $\delta_H = 2.6$ g/cm.^{3}; $\ell + \frac{t_H}{2} = 1.127$cm.;
$t_H = 0.254$ cm.
$V_H = 1.162$ cm.^{3}

we obtain

$$\sigma\, p_{leg} = 840 \times 10^3 \text{ dynes/cm.}^2 = 12.2 \text{ psi}$$
$$\sigma\, n_{leg} = 416 \times 10^3 \text{ dynes/cm.}^2 = 6 \text{ psi}$$

(assuming, conservatively, that either leg may be required to absorb the entire weight of the hot shoe).

The above-calculated maximum stresses for the n- and p-legs are negligibly small.

Case II - Acceleration in the Y-Direction (Figure 24)
As in Case I, the primary stress is induced by the bending moment.

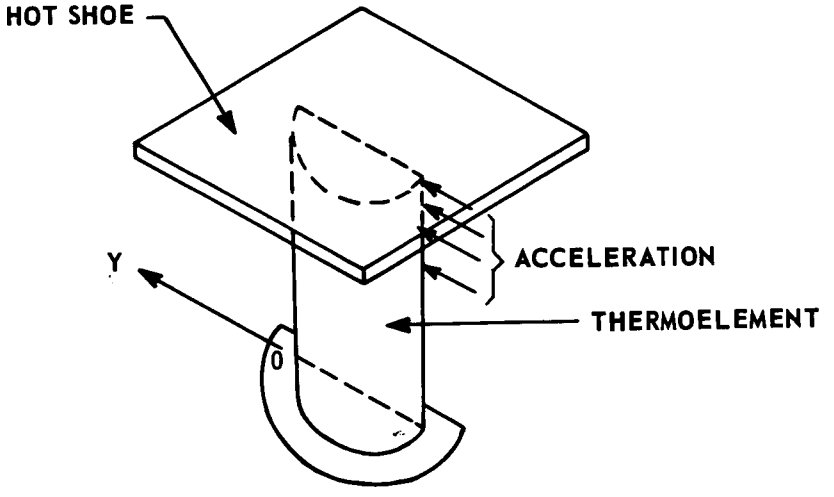

An acceleration in the Y-direction will generate a moment about point 0 which must be resisted by the bond stress. (Point 0 may be located at any position that simplifies calculation of moments.)

FIGURE 24. LOAD DISTRIBUTION IN Y-DIRECTION

The Moment M which results from acceleration will be the same as in Case I (Eq. (38) because the mass increment and the acceleration are the same, as in the distance the force acts through.

The moment caused by bond stress will, however, be different from that of Case I. Consider a strip in the plane of the bond, as shown in Figure 25. (Force acts perpendicular to the plane of the paper.)

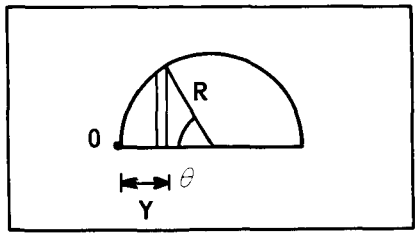

FIGURE 25. SECTION IN PLANE OF BOND

$$\text{Strip Area } dA = R \sin\theta \, dy$$

$$\text{where } y = R - R\cos\theta \text{ is } R(1-\cos\theta)$$

$$dy = R \sin\theta \, d\theta$$

$$\text{therefore } dA = R^2 \sin^2\theta \, d\theta$$

and the incremental force

$$dF = \sigma \, dA = \sigma R^2 \sin^2\theta \, d\theta$$

$$\text{and } dM = y\,dF = R^3 \sigma (1-\cos\theta) \sin^2 d\theta$$

integrating between the limits 0 and $\pi/2$ gives

$$M = \frac{\pi R^3 \sigma}{2} , \qquad (41)$$

equating moments by Eqs. (38) and (41), and solving for σ gives

$$\sigma = \frac{\frac{a \delta_T \pi R^2 \ell^2}{4} + a \delta_H V_H \left(\ell + \frac{t_H}{2}\right)}{\pi R^3/2} , \qquad (42)$$

using the previously denoted constants, we obtain

$$\sigma p_{leg} = 483 \times 10^3 \text{ dynes/cm.}^2 = 7.0 \text{ psi}$$
$$\sigma n_{leg} = 240 \times 10^3 \text{ dynes/cm.}^2 = 3.5 \text{ psi}$$

(again, making the conservative assumption that either leg may be required to absorb the entire weight of the hot shoe).

The above calculated maximum stresses for the n- and p-legs are negligibly small.

Case III - Acceleration in the Z-Direction

In this case, a normal tensile (or compressive) load is placed on the bond.

$$\text{Total Force, } F = ma \tag{43}$$

$$= (\delta_T V_T + \delta_H V_H)\, a$$

and the normal force F causes a stress

$$\sigma = F/A \tag{44}$$

where A is cross sectional area of element (πR^2) and substituting (43) into (44) gives

$$\sigma = \frac{(\delta_T V_T + \delta_H V_H)\, a}{A} \tag{45}$$

substituting the previously denoted constants in (45) we obtain

$$\sigma p_{leg} = 151 \times 10^3 \text{ dynes/cm.}^2 = 2.2 \text{ psi}$$
$$\sigma n_{leg} = 101 \times 10^3 \text{ dynes/cm.}^2 = 1.5 \text{ psi}$$

(again, making the conservative assumption that either leg may be required to absorb the entire weight of the hot shoe).

The above calculated stresses for the n- and p-legs are negligibly small.

Finally, acceleration at any angle can be resolved into X, Y, and Z components. Because the maximum accelerations on each axis generate negligible stresses at the region of the bond, a resolved acceleration in any direction will also generate a trivial stress.

b. Acceleration-Induced Stresses in Generator Frame

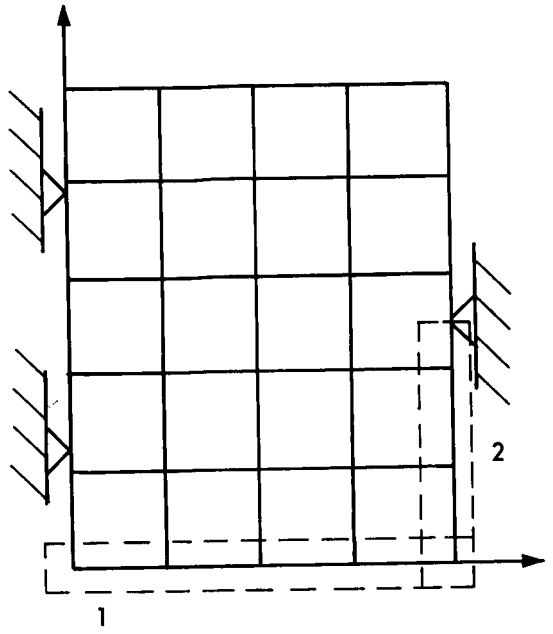

FIGURE 26. PANEL ATTACHMENT MECHANISM

As a conservative approximation of actual stress state in the generator frame, two critically located sections of the frame are isolated as fixed-end cantilever beams, and are assumed to carry a fraction of the panel weight greater than a proportional distribution would require. The two sections selected are shown in Figure 26 which also shows the assumed method of attachment of the panel to the generator frame (hinged at two points on one long edge, and supported by a collapsible strut (boom) at the center of the other long edge).

Case I: Treat as a fixed-end beam carrying an accelerated uniform load equivalent to one-fifth of the panel weight (the full weight of one-fifth of the panel corresponding to a transverse row of 4 sections). Figures 27A and 27B.

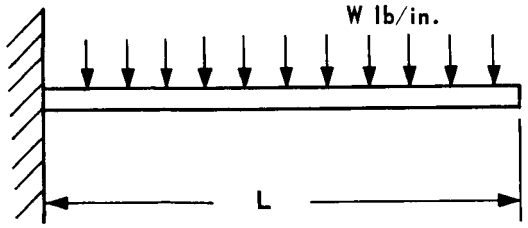

FIGURE 27A. LOADING ON SECTION OF FRAME

The properties of the channel cross section of the beam are[8]

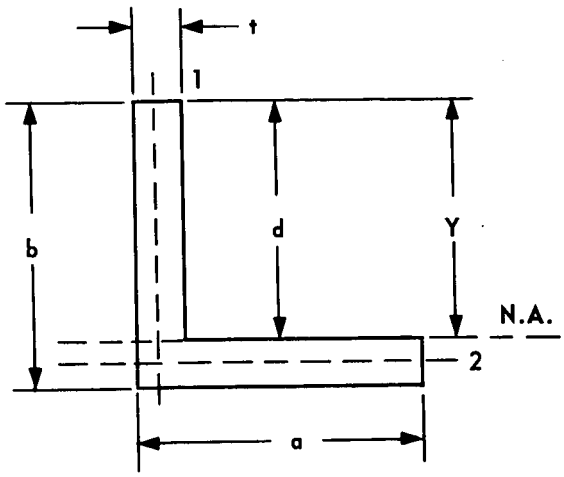

$$y = b - \frac{t(2d + a) + d^2}{2(d + a)} \qquad (46)$$

$$I_y = \frac{1}{3} t_y^3 + a(b-y)^3 - (a-t)(b-y-t) \qquad (47)$$

where y is the distance from the neutral axis to extreme fiber and

Iy is the moment of inertia of the section.

FIGURE 27B. LOADING ON SECTION OF FRAME

Substituting the following constants

$$b = 0.375 \text{ in.}, \; t = 0.125 \text{ in.},$$
$$d = 0.250 \text{ in.}, \; a = 0.500 \text{ in.}$$

we obtain

$$y = 0.250 \text{ in.}$$
$$I_y = 5.53 \times 10^{-3} \text{ in.}^4$$

and for a fixed-end cantilever the maximum moment

$$\text{max. } M = \frac{1}{2} W L \qquad (48)$$

where W is the total load on the beam.

For L = 13.95 in., $W = \frac{8.783 \text{ lb/panel}}{5} = 1.757$ lb., and considering an acceleration of 7 g's, we obtain max. M = 85.7 in. lb

and max. stress $\sigma = \frac{M_Y}{I_y} = 3875 \text{ lb/in}^2$ in tension at the topmost fiber of the beam.

Case II: Treat as a fixed-end beam carrying an accelerated uniform load equivalent to one-third of the panel weight (assuming support of the entire portion of the panel below a line drawn between one hinge support and the center edge support).

W = 2.93, L = 11.59 in., acceleration = 7 g's.
max. moment = 159.4 in-lbs
max. σ = 5360 psi
The allowable tensile stress for Beryllium at 400°C is approximately 30,000 psi.

2. Capability of Structure to Withstand Vibration Requirement

Requirement: The panel shall withstand vibration of a 5-g peak at the resonant frequencies between 16 and 2000 H_z for 15 minutes along three mutually perpendicular axes.

Analysis: The vibration-induced stresses in the couple and the radiator support plate were analyzed. Because of the preliminary nature of the panel frame design, and the lack of knowledge as to method of attachment to the satellite and the nature of the transmitted loads, a vibration analysis has not been made of the frame. The following assumptions have been made in performing the analysis of the couple and radiator support plate:

a) No credit has been taken for damping at any point in the structure. Because damping will exist within the component structure, the calculated stresses are more severe than the actual stress state. In addition, damping mechanisms (e.g. between the panel frame and the satellite struts) could be used, if required, to reduce high stresses in the frame.

b) In the couple, the stresses at the bond of the SiGe element to the tungsten shoe at the cold end were selected as the most critical stresses induced by vibration (see discussion under analysis of Acceleration-Induced Stresses).

c) The radiator support plate has not been rigorously analyzed as a plate. It has been broken down into a series of fixed edge beams (with point loadings) which, it is assumed, behave equivalently to

each other for loads along the same axis. The analysis was made of a typical section in both the X- and Y-directions.

a. Maximum Vibration-Induced Stresses in Couple

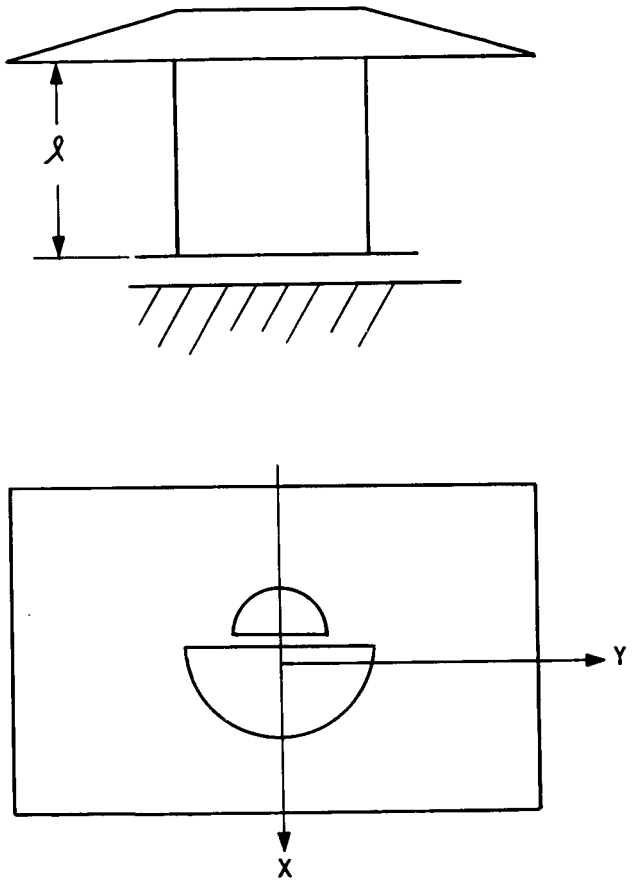

Treat the couple as a fixed-end cantilever at the point of bonding to the cold stack (Figure 28).

The natural frequency of vibration for a cantilever beam, with an end-load W, supporting its own weight, $w\ell$, is[9]

$$\omega_n(H_z) = \frac{3.13}{\sqrt{\frac{(W+0.236\ w)\ \ell^3}{3EI}}} \qquad (49)$$

where E is modulus of elasticity and I is moment of inertia.

The moment of inertia about each axis is given by[8]

$$I_X = 0.007d^4$$
$$I_Y = 0.0245d^4$$

FIGURE 28. COUPLE AS FIXED END CANTILEVER

Now, assuming the weight of the shoe is supported equally by the n- and p-legs for loads along either the X- or Y-axis, and utilizing the following constants

ℓ = 1.0 cm.; E = 18 x 10^6 psi, W = 3.02 gm (.00666 lb.), $(w\ell)$ n_{leg} = 0.00209 lb., $(w\ell)$ p_{leg} = 0.00127.; d_{nleg} = 0.828 cm.; d_{pleg} = 0.644 cm.

we obtain

$$(I_X)_{n_{leg}} = 2.76 \times 10^{-4} \text{ in.}^4; \quad (I_Y)_{n_{leg}} = 7.90 \times 10^{-5} \text{ in.}^4$$

$$(I_X)_{p_{leg}} = 1.01 \times 10^{-4} \text{ in.}^4; \quad (I_Y)_{p_{leg}} = 2.90 \times 10^{-5} \text{ in.}^4$$

and

$$(\omega_n X)_{n_{leg}} = 25{,}000 \text{ H}_z \quad ; \quad (\omega_n Y)_{n_{leg}} = 13{,}390 \text{ H}_z$$

$$(\omega_n X)_{p_{leg}} = 15{,}530 \text{ H}_z \quad ; \quad (\omega_n Y)_{p_{leg}} = 8{,}300 \text{ H}_z$$

To avoid the imposition of synchronous vibrations which are developed in component by the condition of resonance, the natural frequency of vibration of every part should be considerably higher than the number of impulses which the part receives during operation. This condition of avoiding resonant frequencies is met in all instances examined above; the closest the imposed frequency ω approaches to the natural frequency ω_n is where $(\omega_n Y)_{p_{leg}} = 8300 \text{ H}_z$ compared to $\omega = 2000 \text{ H}_z$.

Expressing the above as[10,11]

$$\beta = \omega / \omega_n \tag{51}$$

and $$\upsilon = \frac{1}{1 - \beta^2} = \text{magnification factor on force or} \tag{52}$$

moment, the relationship between the imposed amplitude of vibration and beam static deflection can be determined from[10,11]

$$\frac{Y_o}{a_o} = \frac{\left(\frac{\omega}{\omega_n}\right)^2}{1 - \left(\frac{\omega}{\omega_n}\right)^2} = \upsilon \beta^2 \tag{53}$$

where Y_o is the relative deflection of beam and a_o is the amplitude of motion due to vibration of frequency ω.

To determine a_o, we assume a sinusoidal mode of vibration,[10,11]

$$\begin{aligned} X &= a_o \sin \omega t \\ \dot{X} &= a_o \omega \cos \omega t \\ \ddot{X} &= -a_o \omega^2 \sin \omega t \end{aligned} \qquad (54)$$

amplitude of acceleration $= a_o \omega^2$

$$a_o = 5g/\omega^2$$

therefore for extremes of frequency specified

$$a_o = 0.1912 \text{ in.} \quad (\text{for } \omega = 16 \text{ H}_z)$$
$$a_o = 12.25 \times 10^{-6} \text{ in.} \quad (\text{for } \omega = 2000 \text{ H}_z)$$

and therefore, substituting the appropriate constants we obtain

$$(Y_{o-x})_{n_{leg}} = 7.84 \times 10^{-8} \text{ in.} \qquad (Y_{o-y})_{n_{leg}} = 28 \times 10^{-8} \text{in.}$$

$$(Y_{o-x})_{p_{leg}} = 20.65 \times 10^{-8} \text{in.} \qquad (Y_{o-y})_{p_{leg}} = 75.45 \times 10^{-8} \text{in.}$$

The maximum deflection and moment of a cantilever beam, with an end-load w , supporting its own uniform weight, $w\ell$, are[8]

$$\text{max. } Y_o = \frac{W\ell^3}{3EI} + \frac{(w\ell)\ell^3}{8EI} \qquad (55)$$

$$\text{max. } M = W\ell + (w\ell)\left(\frac{\ell}{2}\right) \qquad (56)$$

(at cold joint bond)

Solving for W (substituting the values of Y_o previously calculated), and then for maximum moment, we obtain

$$(\text{max.Mx})_{n_{leg}} = 0.0076 \text{ in.lb} \qquad (\text{max.My})_{n_{leg}} = 0.0078 \text{ in.lb}$$

$$(\text{max.Mx})_{p_{leg}} = 0.0072 \text{ in.lb} \qquad (\text{max.My})_{p_{leg}} = 0.0073 \text{ in.lb}$$

The maximum bending (fiber) stress is

$$\sigma \text{ max} = \frac{(\text{max.M})C}{I} \tag{57}$$

where C is distance from neutral axis to extreme fiber. Using the relationships, $C = d/_2$ (about X-axis) and $C_{max.} = 0.5756\ R$ (about Y-axis)[9] (58)

and substituting the appropriate values for M and I, we obtain

$$(\sigma_x)_{n_{leg}} = \pm 4.5 \text{ psi} \qquad (\sigma_y)_{n_{leg}} = \pm 9.3 \text{ psi}$$

$$(\sigma_x)_{p_{leg}} = \pm 9.0 \text{ psi} \qquad (\sigma_y)_{p_{leg}} = \pm 18.3 \text{ psi}$$

The maximum stresses in the SiGe legs caused by the vibration loading are negligibly small. Because the stresses at the hot junction will be even smaller, and the capability of the cold stack to absorb stresses even greater, assumption b would appear valid.

b. Maximum Vibration-Induced Stresses in Radiator Support Plate

The analyses of stresses induced in the radiator base plate, Figure 29, are covered in the following cases A and B.

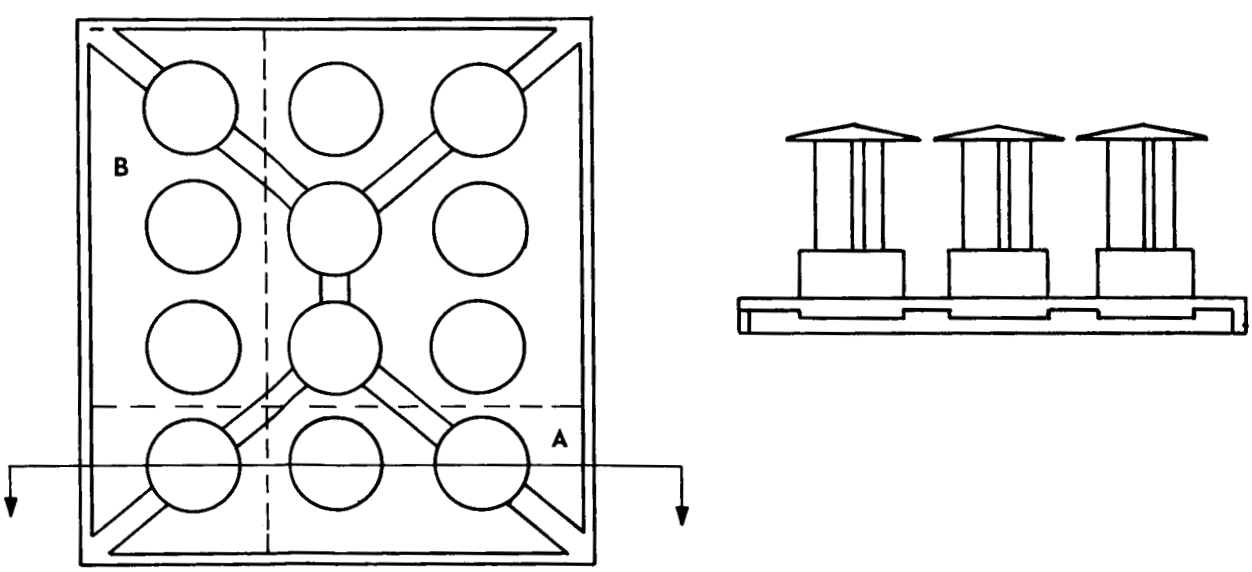

FIGURE 29. SCHEMATIC-RADIATOR BASE PLATE

Case A: Treat as a fixed-edge beam of uniform width, thickness (equivalent), and weight with three concentrated loads corresponding to three thermocouples (Figure 30).

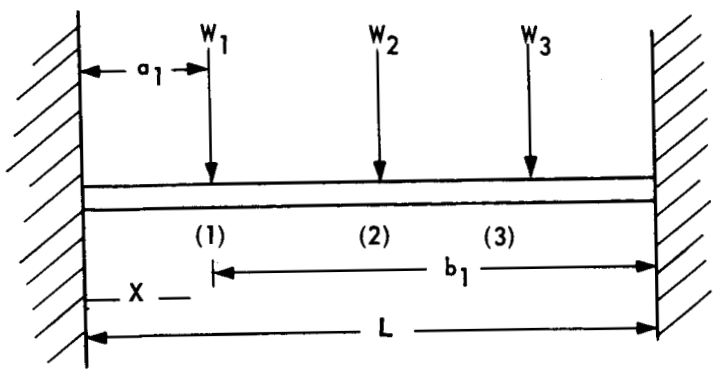

To find the natural frequency of a fixed-end beam which supports several concentrated loads, the Rayleigh method, using energy principles, is applied.[12]

FIGURE 30. LOAD DISTRIBUTION ON FIXED END BEAM

The static deflection equation of a fixed-end beam with a single concentrated load is given by

$$Y = \frac{Wb^2x^2}{6EI\,L^3}\,(3Ax + bx - 3aL), \text{ from } 0 \le X \le a \qquad (59)$$

and $$Y = \frac{Wa^2(L - x)^2}{EI\,L^3}\,(3\,b + a)\,(L - x) - 3\,b\,L, \text{ from}$$

$$a \le x \le L \quad (8)$$

Where W is the weight of one thermocouple plus one-third the weight of the beam (this assumption can be used since the deflection caused by the equivalent concentrated load is very nearly equal to the deflection caused by the weight of the beam) and equals $W_1 + \frac{wL}{3}$.

Now, substituting the following constants into Eq. (59)

$$W_1 = 0.0274 \text{ lb},\ a_1 = 0.370 \text{ in.},\ b_1 = 2.674 \text{ in.},\ L = 3.044 \text{ in.}$$

we obtain for point (1) in Figure 30

$$Y_{11} = \frac{0.002705}{EI} \quad , \quad Y_{12} = \frac{0.00516}{EI} \quad , \quad Y_{13} = \frac{0.000560}{EI}$$

and $$Y_1 = Y_{11} + Y_{12} + Y_{13} = \frac{0.001404}{EI} \quad , \tag{60}$$

now, applying the same method to points (2) and (3) in Figure 30 and using the following constants

$W_2 = W_3 = 0.0274$ lb., $a_2 = 1.522$ in., $a_3 = 2.674$ in., $b_2 = 1.522$ in., $b_3 = 0.370$ in.,

we obtain

$$Y_{21} = Y_{23} = \frac{0.00086}{EI} \quad , \quad Y_{22} = \frac{0.00563}{EI}$$

$$Y_2 = Y_{21} + Y_{22} + Y_{23} = \frac{0.00735}{EI} \tag{61}$$

and

$$Y_3 = Y_1 = \frac{0.001404}{EI} \quad . \tag{62}$$

Now, to find the natural frequency of the beam, we use[12]

$$\omega_n^2 = \frac{g \sum_{i=1}^{3} W_i Y_i}{\sum_{i=1}^{3} W_i Y_i^2} \tag{63}$$

where g is the acceleration constant.

For this case, $W_1 = W_2 = W_3$; therefore Eq. (63) reduces to

$$\omega_n^2 = \frac{g(Y_1 + Y_2 + Y_3)}{Y_1^2 + Y_2^2 + Y_3^2} \tag{64}$$

and substituting the values for Y_1, Y_2, and Y_3 from Eqs. (60)-(62) respectively, we obtain

$$\omega_n^2 = 0.0476 \times 10^6 \, EI$$

where $E = 42 \times 10^6$ psi (for Beryllium at 400°C).

The moment of inertia of the equivalent uniform beam (Figure 31) is,[13]

$$I = \frac{BC_1^3 - bh^3 + aC_2^3}{3} \qquad (65)$$

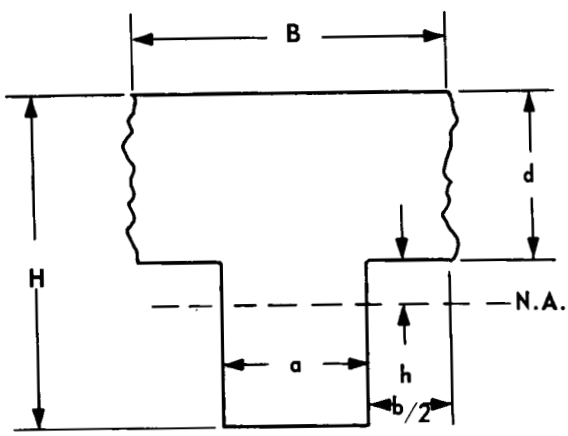

FIGURE 31. SECTION OF BASE PLATE RIB

where h is C_1-d

and $C_1 = \frac{aH^2 + bd^2}{2(aH + bd)}$, $C_2 = H - C_1$

using the constants
B = 1.152 in., H = 0.260 in.,
b/2 = 0.536 in., a = 0.080 in.,
d = 0.060 in.,
we obtain
C_1 = 0.1122 in., C_2 = 0.1478 in.,
h = 0.0522 in.

and substituting in (65), we obtain $I = 578.5 \times 10^{-6}$ in.^{4}
which when substituted in Eq. (64) gives

$$\omega_n = 5430 \text{ H}_z \text{ .}$$

Because the natural frequency is well above the range of imposed frequencies, there is no chance of resonance occurring.

Now, using Eqs. (51) - (54) and the imposed vibration requirements, we obtain

$\beta = \omega/\omega_n = 0.368$ (for ω = 2000 H_z being the more severe case)
$\nu = 1/1 - \beta^2 = 1.159$
$a_o = 12.25 \times 10^{-6}$ in. (for ω = 2000 H_z)

which gives

$$Y_o = a_o \nu\beta^2 = 1.94 \times 10^{-6} \text{ in.}$$

Now, the maximum deflection of the beam occurring at point (2) is given by Eq. (61): $Y_2 = 0.00735/EI = 0.331 \times 10^{-6}$ in.; the static deflection is therefore amplified by the factor $Y_o/Y_2 = 5.86$. Therefore, the Maximum Moment in the beam at the fixed edge, resulting from the vibration loading, is

$$M_{max.} = \left(\frac{WL}{8} + \frac{Wab^2}{2} + \frac{Wa^2b}{2}\right)\left(Y_{o/Y_2}\right) \qquad (66)$$

where a is 0.370 in., b is 2.674 in., L = 3.044 in.
which gives $M_{max.} = 0.1019$ in. lb.
The maximum fiber bending stress is

$$\sigma = \frac{MC}{I}$$

where C_1 is 0.1122 in., C_2 is 0.1478 in., I is 578.5×10^{-6} in.^{4}
or σ max. = 26.2 psi.

The ultimate tensile strength of Beryllium at 400°C is approximately 30,000 psi. The calculated stress is therefore negligible by comparison.

Case B: Treat as a fixed-edge beam of uniform width, thickness (equivalent), and weight with four concentrated loads corresponding to four thermocouples (Figure 32).

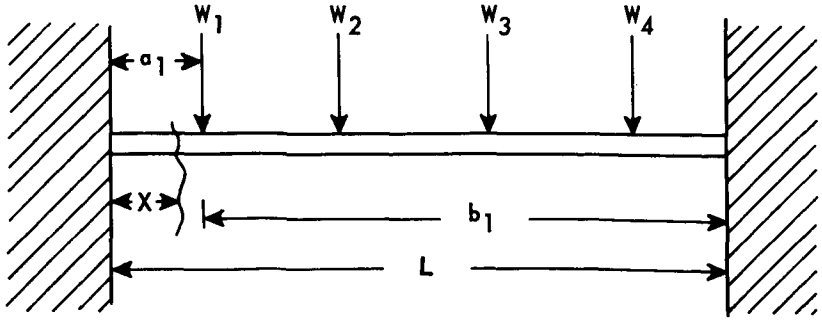

The same procedure is followed in this case as in Case A.

FIGURE 32. LOAD DISTRIBUTION ON FIXED END BEAM

The constants in this instance are:

$W_1 = W_2 = W_3 = W_4 = 0.0259$ lb
$a_1 = 0.370$ in., $a_2 = 1.522$ in., $a_3 = 2.674$ in., $a_4 = 3.826$ in.
$b_1 = 3.826$ in., $b_2 = 2.674$ in., $b_3 = 1.522$ in., $b_4 = 0.370$ in.,
$L = 4.196$ in.

which, from Eq. (59), gives

$Y_{11} = 3.315 \times 10^{-4}/EI$, $Y_{12} = 9.4 \times 10^{-4}/EI$, $Y_{13} = 5.56 \times 10^{-4}/EI$
$Y_{14} = 0.4745 \times 10^{-4}/EI$

and

$Y_1 = Y_{11} + Y_{12} + Y_{13} + Y_{14} = 18.75 \times 10^{-4}/EI$
$Y_{21} = 9.42 \times 10^{-4}/EI$, $Y_{22} = 78.8 \times 10^{-4}/EI$, $Y_{23} = 59.9 \times 10^{-4}/EI$,
$Y_{24} = 5.56 \times 10^{-4}/EI$
$Y_2 = Y_{21} + Y_{22} + Y_{23} + Y_{24} = 153.68 \times 10^{-4}/EI$
$Y_3 = Y_2 = 153.68 \times 10^{-4}/EI.$
$Y_4 = Y_1 = 18.75 \times 10^{-4}/EI$

substituting Y_1-Y_4 into Eq. (64) yields

$$\omega_n^2 = 2.78 \times 10^4 EI$$

where E is 42×10^6 psi and I is 578.5×10^{-6} in.^{4}

and therefore $\omega_n = 3445$ H_z.

The natural frequency of 3445 H_z is considerably greater than the maximum imposed frequency of 2000 H_z. There is no danger of a resonant condition being imposed.

From Eqs. (51)-(54) we obtain

$$\beta = 0.616;\ \upsilon = 1.61;\ a_o = 12.25 \times 10^{-6} \text{ in.};\ Y_o = 7.5 \times 10^{-6} \text{ in.},$$

now the maximum deflection of the beam occurring at point (2) is given by Eq. (61)

$$Y_2 = 153.86 \times 10^{-4}/EI = 0.633 \times 10^{-6} \text{ in.}$$

The static deflection is therefore amplified by the factor

$$Y_o/Y_2 = 11.85$$

and the maximum moment in the beam at the fixed edge, resulting from the vibration loading, is

$$\text{max. } M = \frac{W a_1 b_1^2}{2} + \frac{W a_2 b_2^2}{2} + \frac{W a_3^2 b_3}{2} + \frac{W a_4^2 b_4}{2} \qquad (67)$$

which gives max. M = 0.4035 in. lb.

The maximum fiber bending stress

$$\sigma_{max.} = M_{max.} C/I = 103 \text{ psi}$$

This stress is also negligibly small.

3. Capability of Structure to Withstand Acoustic Noise Requirement

Requirement: The panel shall withstand for five minutes a total integrated sound pressure level of 148 decibels referred to 0.0002 dynes per cm.^{2} with the frequency spectrum shown in the Figure 3 in the specification.

Analysis: Sound is essentially a vibration of audible frequency, and therefore this requirement will be analyzed in the same manner as in Section 2, with the same assumptions applied.

To convert the specified sound pressure level to a unit pressure loading, the following expression is used:(16)

$$\text{Sound Pressure Level (db)} = 20 \log_{10} \frac{P}{0.0002 \text{ microbar}} \qquad (68)$$

where 1 microbar = 1 dyne/cm.^{2}, and P is the sound pressure or total instantaneous pressure at that point in the presence of a sound wave (minus the static pressure)

now for SPL = 148 dbs, we get from Eq. (68)

$P = 0.11$ psi

In addition, the natural frequencies of the couple and radiator base plate determined in Section 2 are (along X- and Y-axes) far in excess of the range of imposed frequencies shown in the specified frequency spectrum. There is, therefore, no possibility of a resonant condition being imposed at any time during operation.

Utilizing the same analyses that were applied in Section 2, we can determine that instantaneous application of the 0.11 psi pressure loading along the X- or Y-axes will create the following approximate maximum stresses:

1. In the SiGe couples:

   $(\sigma_X)_{n_{leg}} = 12.7$ psi $(\sigma_Y)_{n_{leg}} = 26.4$ psi

   $(\sigma_X)_{p_{leg}} = 25.5$ psi $(\sigma_Y)_{p_{leg}} = 51.8$ psi

2. In the radiator support plate:

   Case A: σ max. = 160 psi

   Case B: σ max. = 660 psi

The stresses caused by noise loading are also negligible in relation to the allowable stresses. In addition, the total stress levels along the X- and Y-axes for a simultaneous imposition of acceleration, noise, and vibration loading are quite small, and well within the allowable ranges.

4. Capability of Structure to Withstand Thermal Stresses

Two conditions will be examined: 1) the maximum thermal stresses induced in the structure during normal steady state operation

2) the maximum thermal stresses imposed by the thermal transient test requirement.

The following assumptions are made in performing the analysis:

a) No stress relaxation caused by creep or plastic flow is assumed. The thermal stresses are not assumed to be reduced by material displacement or flow at elevated temperatures.

b) The thermal stresses induced in the couple in the SiMo hot shoe and the SiGe elements are assumed to be the most severe under conditions of constant temperatures, or of the imposed operating temperature gradient. The cold end junction between the SiGe and the cold stack is subjected to smaller temperature extremes, and is of the same construction as the SNAP-10A hot side, which has undergone environmental thermal shocks, gradients, and cycling far more severe than the requirements of this program without ever experiencing a failure. In addition, the thermal stresses in the radiator plate, stud, and frame will be small, because none of these components are subject to large temperature gradients or have any materials expansion mismatch.

a. Maximum Thermal Stresses in Couple During Normal Operation

For the bonding of two members, a zero stress state will exist at the bonding temperature. At any other temperature, the non-uniform thermal expansion of the two members will result in a stressed condition. At room temperature, the differential expansion of the two members is greatest (furthest removed from bonding temperatures), and the stresses induced in the region of the bond are therefore a maximum at room temperature.

The couple structure of the hot shoe bonded to the element can be approximated by the structural element in Figure 33. The plate is heated to temperature T_p and the element is at temperature T_e. Assuming no bowing or buckling, the thermal stresses in plate σ_p, and in element σ_e are given by[15]

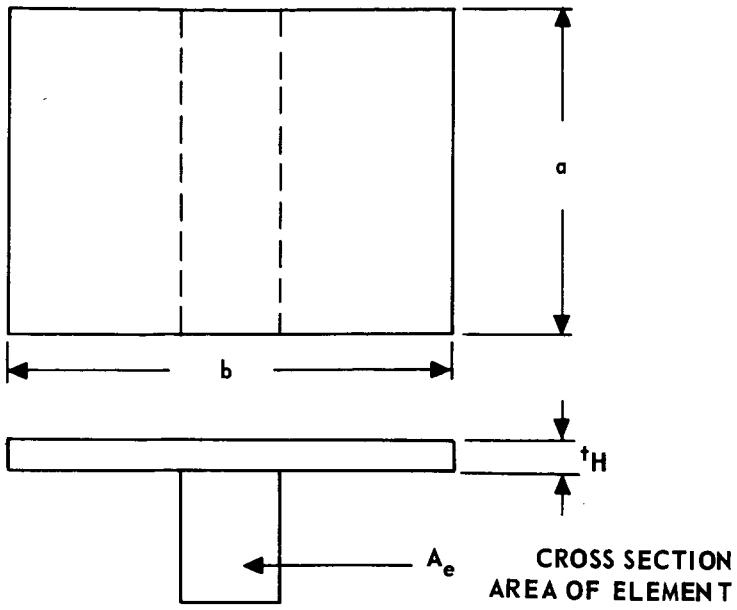

FIGURE 33. APPROXIMATION OF HOT SHOE-TO-ELEMENT CONFIGURATION

$$\sigma_P = \frac{-E_P (\alpha_P T_P - \alpha_e T_e)}{1 + \frac{b\, t_H\, E_P}{A_e E_e}} \qquad (69)$$

and

$$\sigma_e = \frac{-bt_H}{A_e} \sigma_P \qquad (70)$$

where E_P, α_P, and E_e, α_e are the moduli of elasticity and coefficients of thermal expansion of the plate and element, respectively.

The SiMo-to-SiGe bonding temperature is approximately 1200°C, therefore, for isothermal room temperature conditions

$$T_P = T_e = 1200 - 25 = 1175°C$$
$$E_P = E_e = 18 \times 10^6 \text{ psi}$$
$$\alpha_P = 4.0 \times 10^{-6}/°C$$
$$\alpha_e = 4.7 \times 10^{-6}/°C$$

and $t_H = 0.1457$ cm., $b = 2.825$ cm., $A_e = 0.322$ cm.^{2}(p_{leg}); 0.414 cm.^{2}(n_{leg})

when substituted in Eqs. (69) and (70) we obtain

for the SiGe n-leg-to-SiMo junction

$\sigma_P = 6500$ psi (tension)

$\sigma_e = 8300$ psi (compression)

for the SiGe p-leg-to-SiMo junction

$$\sigma_p = 7410 \text{ psi}$$

$$\sigma_e = -7380 \text{ psi}$$

The SiGe material has a measured capability to withstand compressive loading to approximately 130,000 psi (U.C.S.). Analysis of various couple configurations of this type indicates that the SiMo material is capable of withstanding a minimum of 20,500 psi in tension due to thermal stress loading. Furthermore, couples having more extreme variations in geometry are fabricated with no failures observed when they are brought down to room temperature.

b. Capability of Couple to Withstand Thermal Transient Requirement

Requirement: The panel shall withstand the following thermal transient test: It shall be heated to an absorber surface temperature of 1500°F as rapidly as possible when subject to the thermal flux required to achieve this hot junction temperature. Immediately after temperature equilibrium has been established, heating shall cease. The panel shall be allowed to cool to an equilibrium temperature by radiating to the surrounding walls of a liquid nitrogen cooled chamber. This cycle shall be repeated twice.

Analysis: Consider the thermal stresses produced in the couple by 1) the temperature gradient imposed at a hot junction temperature of 1500°F (816°C) and a cold junction temperature of 788°F (420°C), and 2) the isothermal state corresponding to the liquid nitrogen temperature of -311°F (-192°C).

(1) Stresses Corresponding to Hot Junction Temperature of 1500°F

Referencing the temperature to the zero stress temperature, we obtain

$$T_p = 1200 - 816 = 384°C \ (724°F)$$

$$T_e = 1200 - \frac{816 + 420}{2} = 582°C \ (1080°F)$$

(for a linear gradient)

and using the previously noted constants in Eqs. (69) and (70) gives, for the SiGe n-leg-to-SiMo junction

$$\sigma_p = 9300 \text{ psi}$$
$$\sigma_e = -11{,}900 \text{ psi}$$

and for the SiGe p-leg-to-SiMo junction

$$\sigma_p = 10{,}600 \text{ psi}$$
$$\sigma_e = -10{,}550 \text{ psi}$$

(2) Stresses Corresponding to Liquid Nitrogen Equilibrium Temperature

In this case, the couple structure is isothermal at an equilibrium temperature of -311°F (-192°C). Applying Eqs. (69) and (70) gives for the SiGe n-leg-to-SiMo junction

$$\sigma_p = 7700 \text{ psi}$$
$$\sigma_e = -9840 \text{ psi}$$

for the SiGe p-leg-to-SiMo junction

$$\sigma_p = 8800 \text{ psi}$$
$$\sigma_e = -8750 \text{ psi}$$

As before, the maximum stresses are within the allowable ranges determined for the materials. Further, it should be noted that thermoelectric couples, similar in construction, have been subjected to rapid immersion (essentially shock condition) into a liquid nitrogen bath with no failures.

IV. TEST PANEL REFERENCE DESIGN

Layout Drawings of the Reference Design Test Panel

RCA is obligated to fabricate and deliver three flat plate sections of the 150-watt SiGe solar thermoelectric generator. The reference design of the test section was changed from twelve to nine couples to provide a panel section geometry compatible with Lewis Research Center test equipment. The nine-couple test section is electrically connected in series instead of series parallel.

The following parameters will apply to the nine couple test panel when tested under specified design conditions:

Power in Load (watts)	2.81
Load Voltage (volts)	1.00
Load Resistance (ohms)	0.353
Internal Resistance (ohms)	0.295
Current (amps)	2.82
Open Circuit Voltage	2.05

Engineering drawings for the nine-couple test panel section are attached. A brief description of each drawing follows:

Test Panel Assembly (Figure 34) - Drawing of the nine-couple test panel section depicting the complete assembly with insulation.

Test Panel Base Plate Section (Figure 35) - Dimensioned drawing of the beryllium base plate for a nine-couple test panel section.

Test Panel Electrical Schematic (Figure 36) - Electrical schematic of the nine-couple test panel section showing series circuit connection.

Solar Test Panel Instrumentation Heat-Reception and Heat-Rejection Plate Thermocouples (Figure 37) - Instrumentation for the nine-couple test panel section showing heat-reception and heat-rejection plate thermocouple locations for five couples.

Solar Test Panel Instrumentation Voltage Taps and Current Leads (Figure 38) - Voltage tap and current lead locations for the nine-couple test panel section.

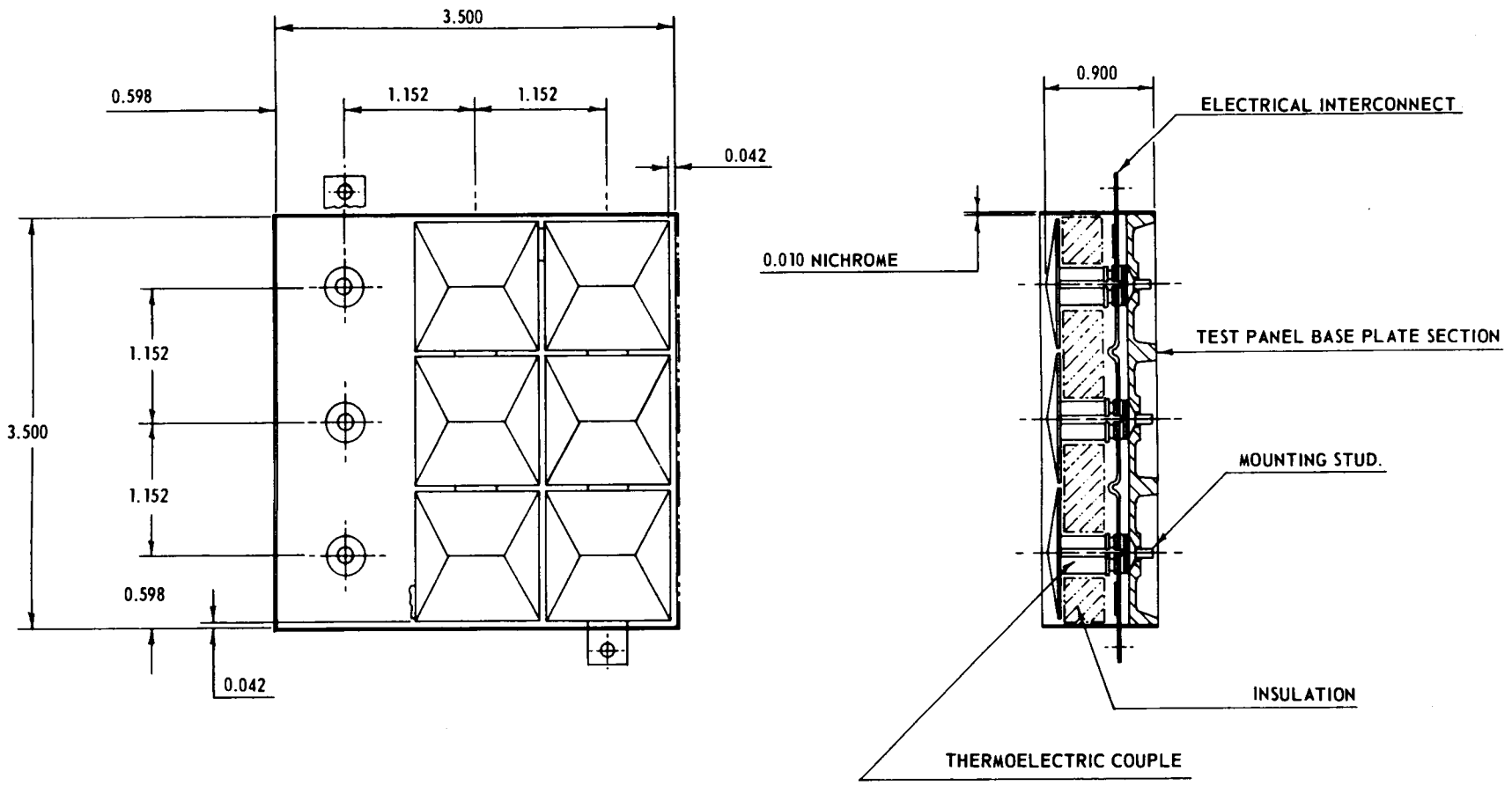

FIGURE 34. TEST PANEL ASSEMBLY

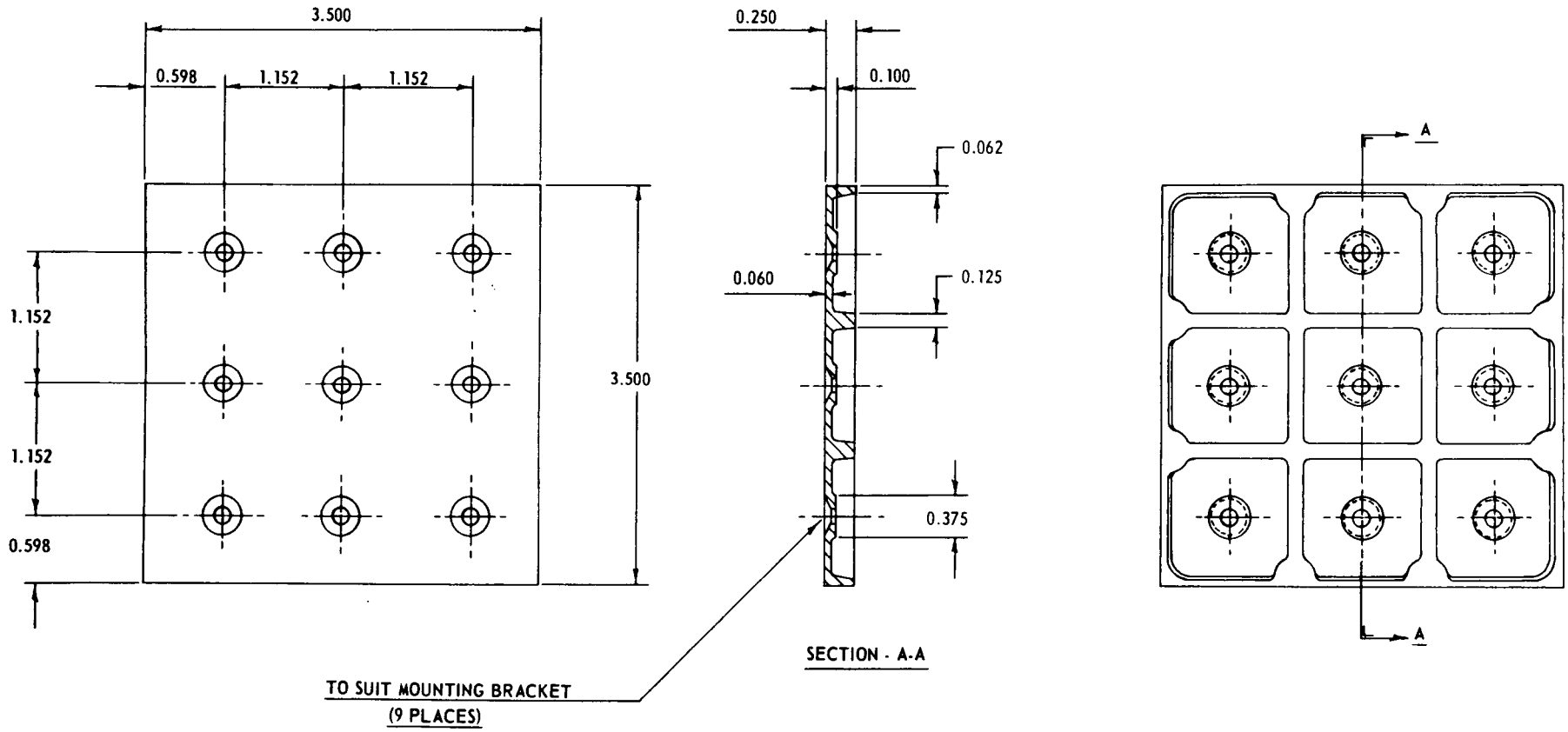

FIGURE 35. TEST PANEL BASE PLATE SECTION

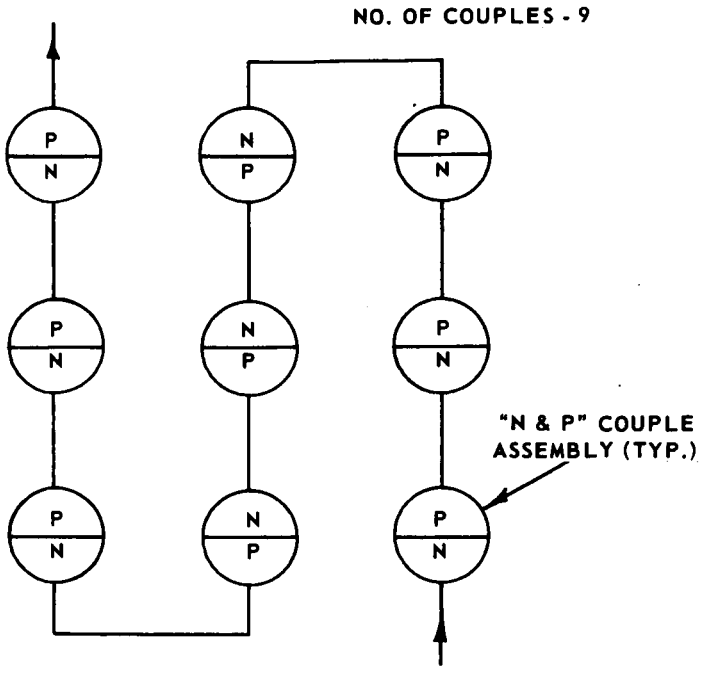

FIGURE 36. ELECTRICAL SCHEMATIC—TEST PANEL SERIES CIRCUIT

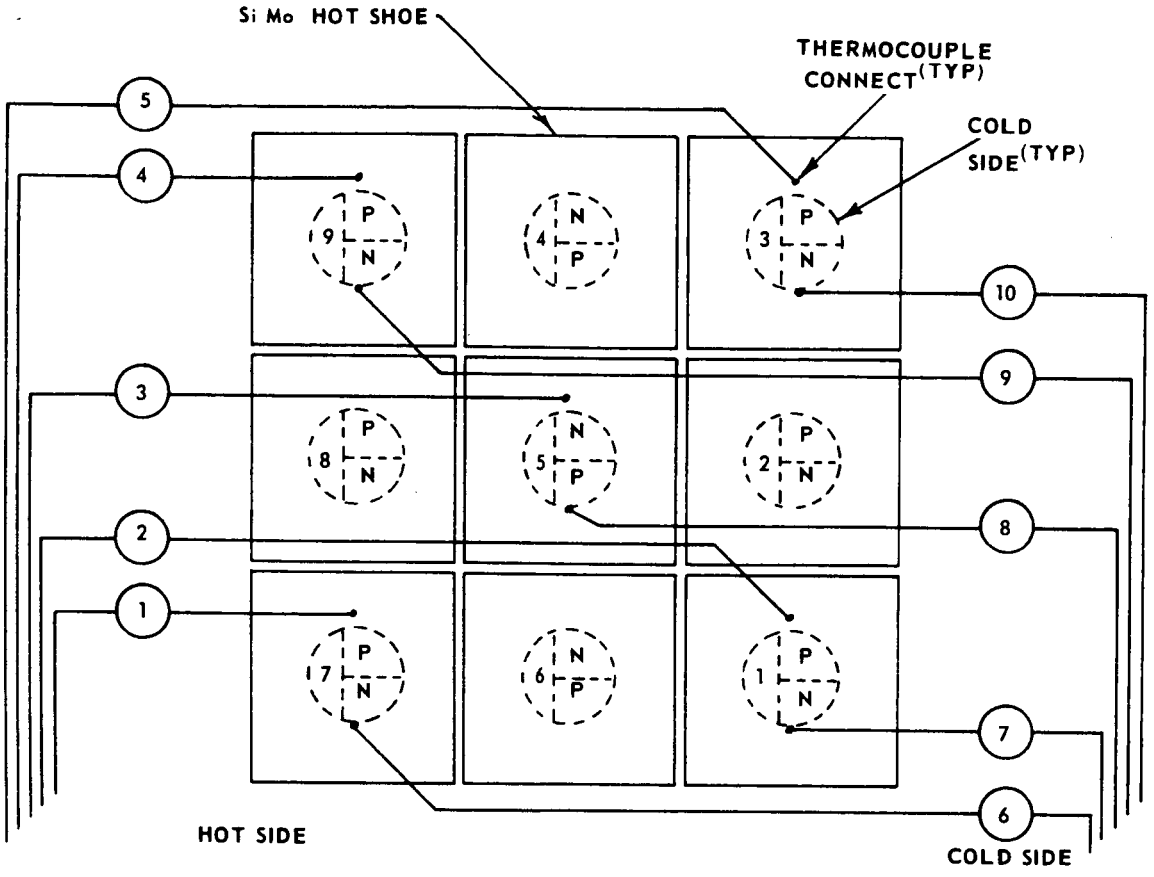

FIGURE 37. SOLAR TEST PANEL INSTRUMENTATION

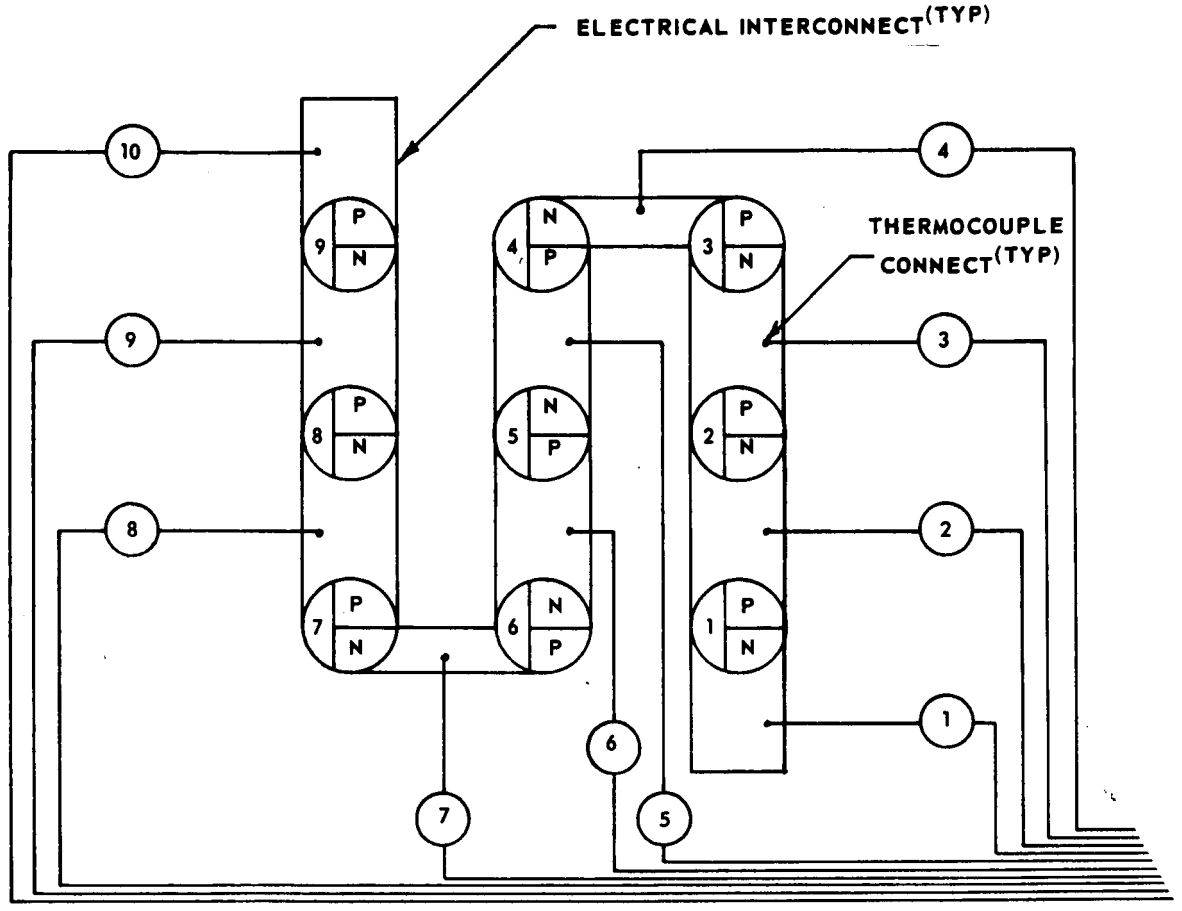

FIGURE 38. SOLAR TEST PANEL INSTRUMENTATION (VOLTAGE TAPS & CURRENT LEADS)

V. THERMOELECTRIC MATERIALS PROPERTIES

The characteristics of the n-type and p-type SiGe and SiMo alloys employed in the Solar Thermoelectric Generator design are presented in this section. In addition, a discussion of those properties of SiGe which make it attractive as a thermoelectric material is also included.

A. Silicon-Germanium Thermoelectric Material Properties

Temperature-dependent thermoelectric properties for n-type and p-type SiGe alloys which include electrical resistivity, Seebeck coefficient, and thermal conductivity are shown in Figures 39 through 41. Essential thermal and mechanical characteristics of SiGe alloys are shown in Table VI.

B. Silicon-Molybdenum Alloy Material Properties

The electrical resistivity and thermal resistivity of the silicon molybdenum alloy hot shoe material employed in the development of the silicon-germanium thermoelectric panels are shown in Figures 42 and 43.

C. Background Information on Silicon-Germanium Thermoelectrics

While the efficiency of a thermoelectric generator depends, in theory, on only a few thermoelectric properties, in practice it is necessary that the thermoelectric material possess a number of additional mechanical properties so that reliable devices can be constructed. The thermoelectric material should have reasonable strength, should be chemically stable at high temperatures, and should have a low coefficient of thermal expansion to minimize thermal stresses. In addition, means should be available for joining the thermoelectric material to other members of the thermoelectric structure so that efficient thermal and electrical flux paths can be maintained. Silicon-germanium alloys represent a major contribution to the thermoelectric art in that they combine good thermoelectric properties with an extremely favorable combination of mechanical properties, permitting construction of reliable devices with significant efficiencies.

Some of the unique features of the silicon-germanium thermoelectric alloys are that they are operable at elevated temperatures (approximately 1800 -

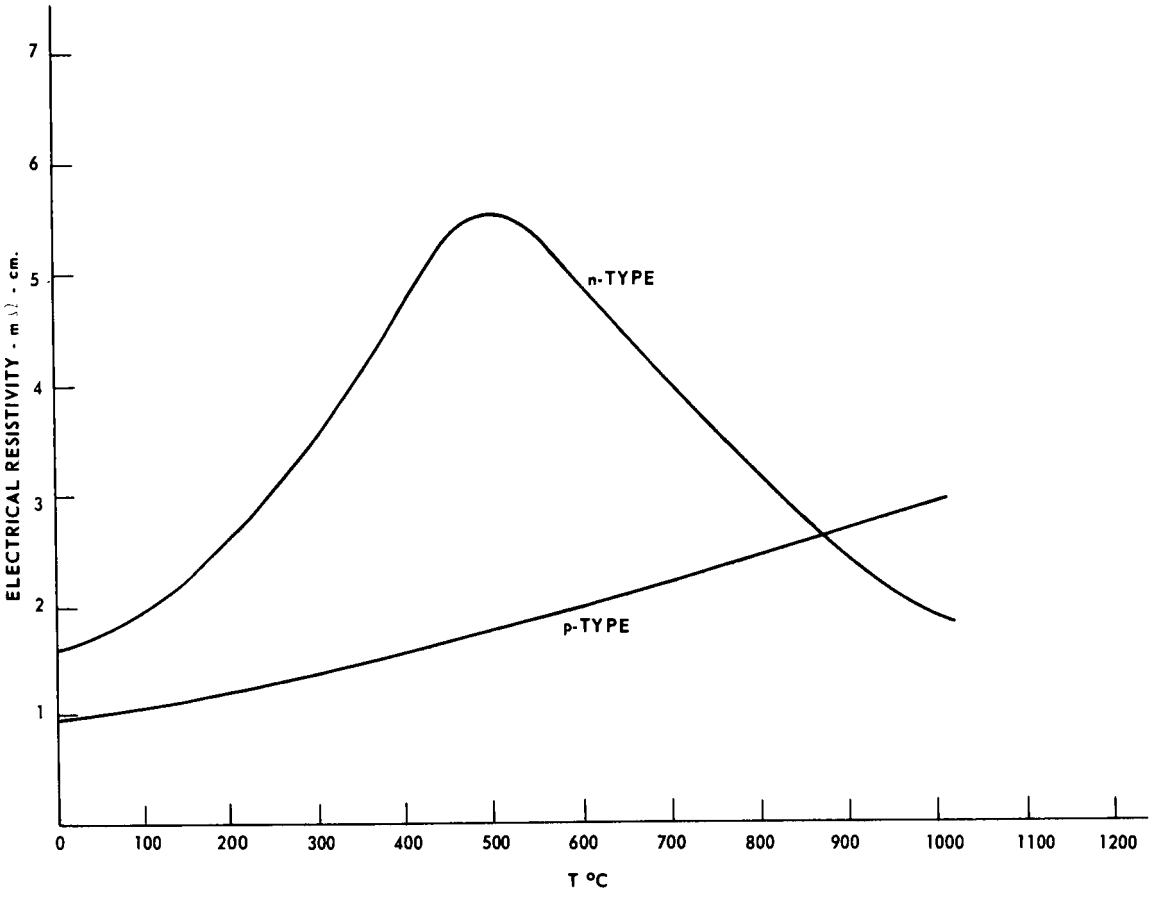

FIGURE 39. ELECTRICAL RESISTIVITY OF n- AND p-TYPE SiGe ALLOYS

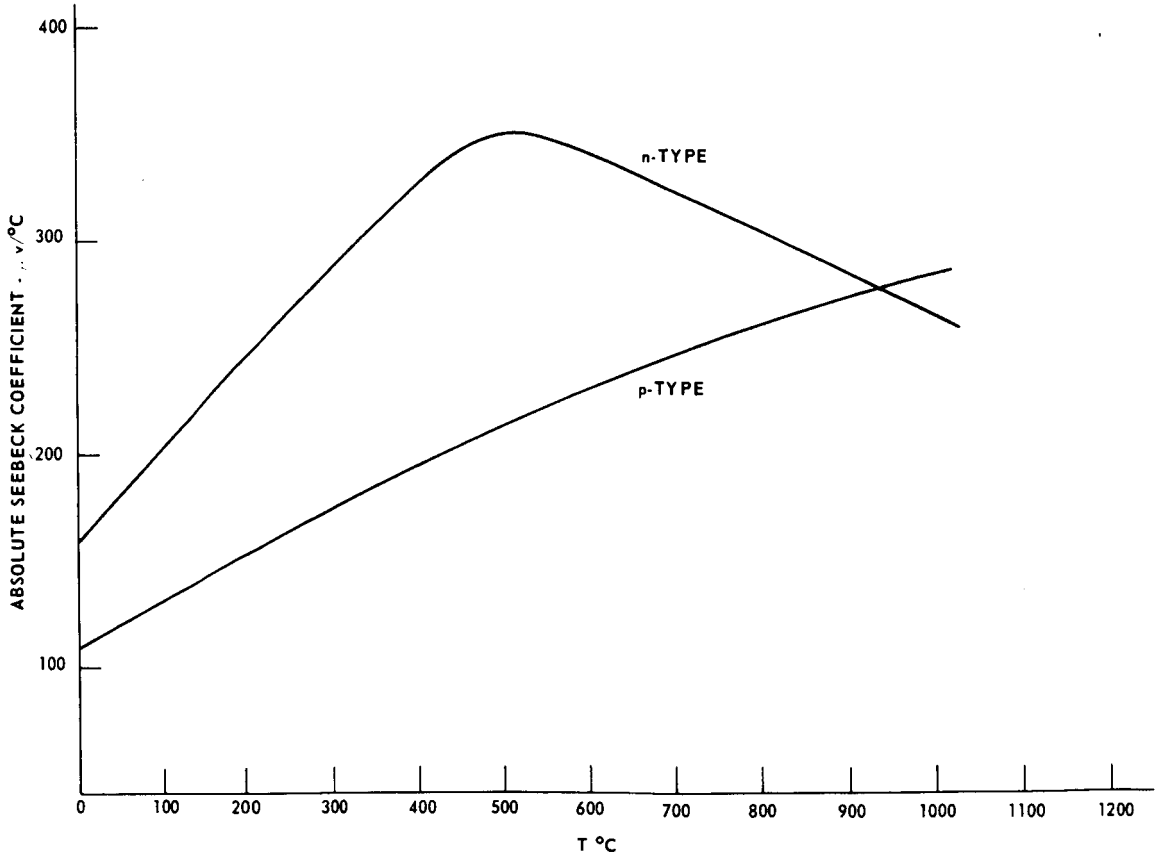

FIGURE 40. ABSOLUTE SEEBECK COEFFICIENT OF n- AND p-TYPE SiGe ALLOYS

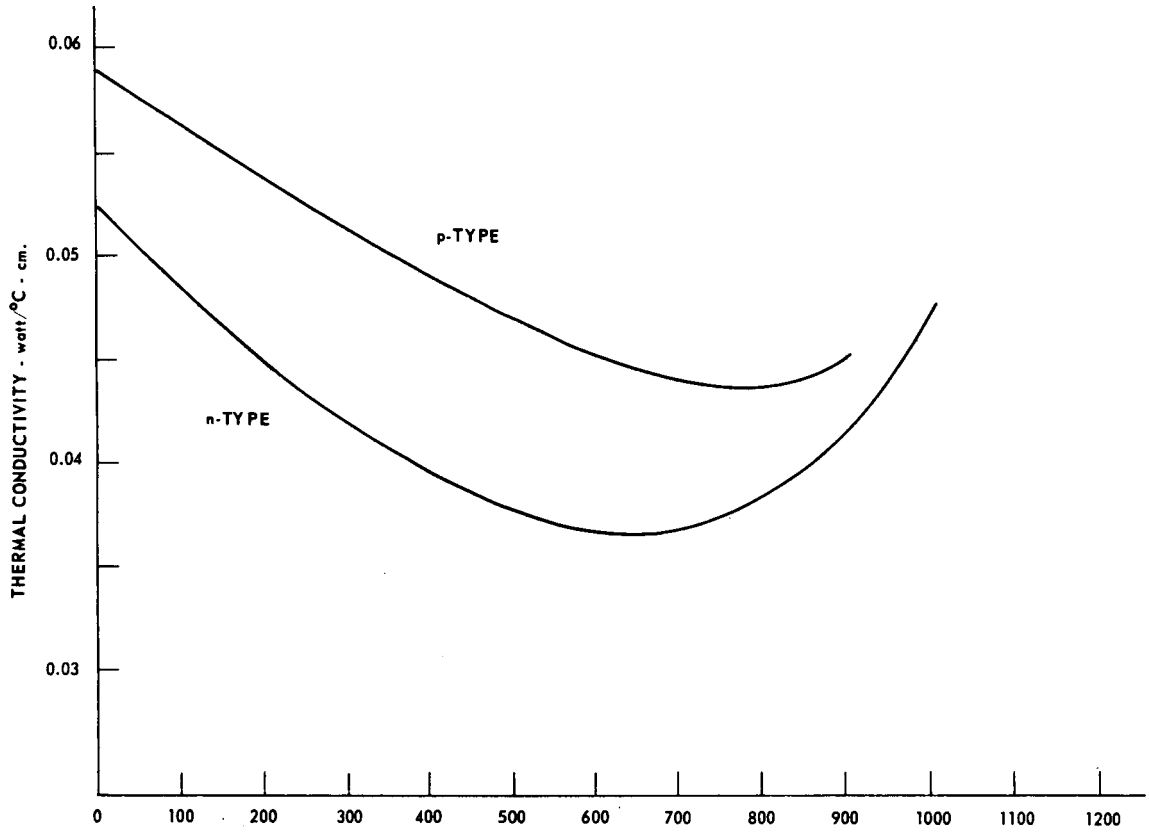

FIGURE 41. THERMAL CONDUCTIVITY OF n- AND p-TYPE SiGe ALLOYS

TABLE VI

PHYSICAL PROPERTIES - THERMOELECTRIC MATERIALS

(Approximate Values)

Property	SiGe	Si-Alloy Hot Shoe
Thermal Expansion	4.8 to 5.0 x 10^{-6} °K	Same as SiGe
Tensile Strength		
p-type: 932°F(500°C)	3900 psi	--
n-type: 932°F(500°C)	4400 psi	--
Compressive Strength	150,000 psi	--
Avg. Modulus of Rupture	3600 psi	--
Vapor Pressure	3 x 10^{-9} at 1472°F(800°C)	--
Density	3 to 3.5 g/cm.^{3}	2.6 g/cm.^{3}

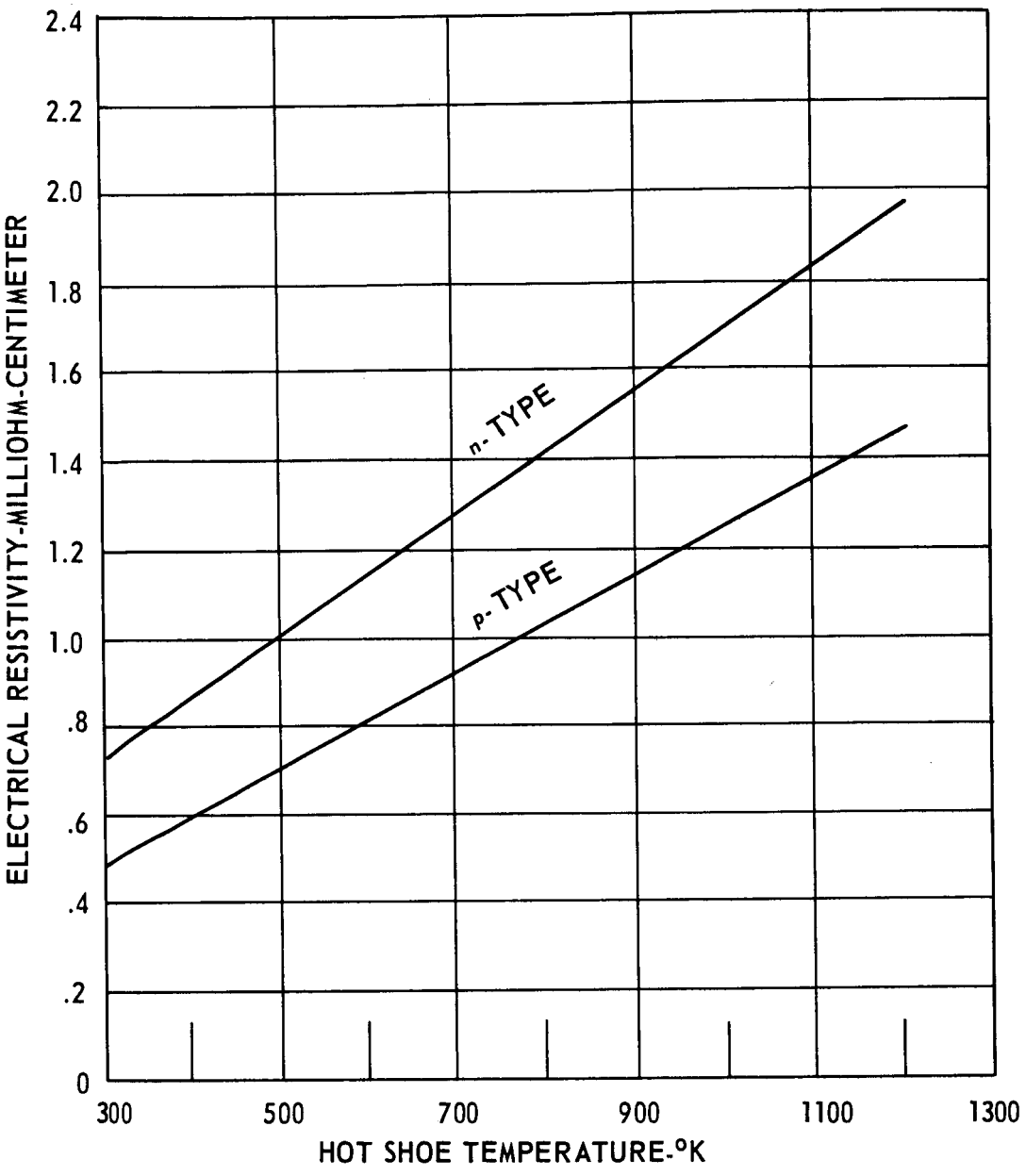

FIGURE 42. ELECTRICAL RESISTIVITY *n*-TYPE AND *p*-TYPE SILICON MOLYBDENUM ALLOY

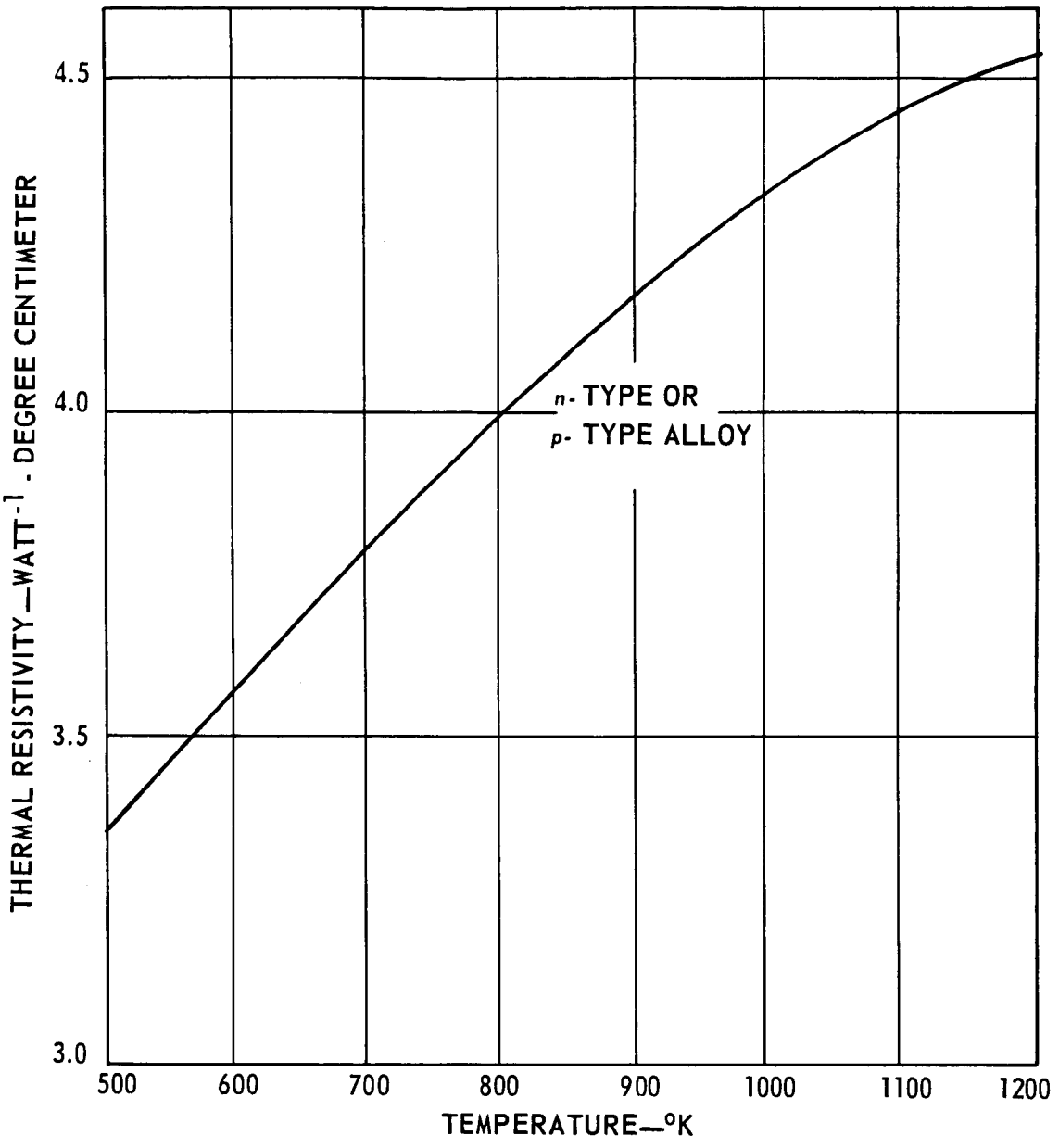

FIGURE 43. THERMAL RESISTIVITY OF SILICON MOLYBDENUM ALLOY

1900°F (1000°C); they are mechanically strong (tensile strength is many times that of conventional thermoelectric materials); they are less dense than conventional thermoelectric materials by a factor of about two and one-half times; they are relatively free from harmful oxidation effects; they are operable in vacuum and air for long periods without encapsulation; they are completely non-magnetic (both the active material and the normally-used RCA contacting materials).

Other unique features which enhance the applicability of SiGe thermoelectric materials are:

Utilization of the Material

The use of many thermoelectric materials in practical power-generating devices has been hampered by the inability to create stable, strong, low-electrical resistance contacts to the materials. However, RCA has developed an excellent ionic bond to metallic contacts for silicon germanium. This development was a key step in the utilization of the characteristics of this material in practical, operating devices. In fact, this development made it feasible to meet the design requirements of such space power supply systems as the SNAP-10A.

Efficiency

The efficiency of silicon-germanium thermoelectric material is, of course, a function of the temperature range in addition to the device design. For this reason, it is desirable to have the hot junction temperature as high as possible. Silicon-germanium alloys, with their demonstrated capability for high-temperature operation in practical device configurations, are able to take advantage of high-temperature heat sources to gain either improved thermoelectric efficiencies or high cold junction temperatures for minimizing radiator weight.

Radiation Resistance

Complete quantitative data for the radiation resistance of silicon-germanium alloys are not yet available; but initial investigations have been made. Samples of the material have been exposed to integrated neutron fluxes in

excess of 5×10^{18} nvt with only minor effects on either the Seebeck coefficient or resistivity. Although these early tests were not performed at operating temperatures, subsequent annealing of the specimens at operating temperatures for short periods removed most of the damage. Although further investigation of the effect of radiation on silicon-germanium alloys is necessary, the results to date indicate that no major problems will be encountered in this area.

Mechanical Strength

Because almost all space power systems will be subjected to severe mechanical environments during vehicle launch, the thermoelectric structures must be extremely reliable. The devices incorporating SiGe have demonstrated the same favorable mechanical characteristics as the materials themselves. For example, modules intended for use in the SNAP-10A system were tested in accordance with the mechanical tests specified for the Atlas-Agena vehicle combination. In all cases, the modules have been tested without failure to levels twice the specification limit. The test limitations indicated have generally been a limitation of available test equipment.

Density

As mentioned earlier, the silicon-germanium alloy is a low-density material. For example, the converter system alone of the SNAP-10A has a specific power of about 4 watts per pound at an efficiency of about 2 percent. The specific power of only the thermoelectric material is many times 4 watts per pound because most of the weight is incorporated in the radiators, in the liquid metal tubing, in the insulator stacks, and in associated structures. Significantly, these values are not limited by the structures but more by the available temperatures. For example, an increase in the available heat source temperature could increase both the efficiency and specific power of the device, without the need for major changes in the structure.

Nonmagnetic

Silicon-germanium thermoelectric materials are nonmagnetic. Additionally, all of the other materials employed in making usable thermocouples, including the hot and cold shoes, are nonmagnetic. As a result, no special

precautions or magnetic shielding are needed when using this material in close proximity to sensitive measurement instruments.

Summary

In the past few years, advances in thermoelectric materials and in device technology have made thermoelectric power systems technically and practically feasible. The work accomplished by RCA in thermoelectrics, supported both by Government programs and RCA funds, has contributed significantly to this advance. The development of silicon-germanium alloys and the contact and device technology attendant on their use have been demonstrated as a sound basis for reliable long-life power systems.

VI. REFERENCES

1. A. F. Ioffe, Semiconductor Thermoelements and Thermoelectric Cooling, (Infosearch Ltd., London, 1957)

2. F. E. Jaumot, Proc. Inst. Radio Engrs. 46, 538 (1958)

3. P. S. Castro and W. W. Happ, J. Appl. Phys. 31, 1314 (1960)

4. N. Fuschillo, R. Gibson, F. K. Eggleston and J. Epstein, Adv. Eng. Conv. 6, 103 (1966)

5. W. C. Lyon and C. J. Anderson, Proc. IEEE/AIAA Therm. Spec. Conf., Washington, D. C., May 1966

6. N. Fuschillo and R. Gibson, Preprint, IEEE Aerospace Conf., Seattle, Washington, July 1966

7. R. W. Cohen and B. Abeles, J. Appl. Phys. 34, 1687 (1963)

8. Machinery's Handbook, (Machinery Publishing Co., Brighton, England, 1962) p. 361

9. R. J. Roark, Formulas for Stress and Strain, (McGraw Hill, New York, 1965)

10. J. P. Den Hartog, Mechanical Vibrations, (McGraw Hill, New York, 1956)

11. C. T. Morrow, Shock and Vibration Engineering, Vol. I, (John Wiley & Son, Inc., New York, 1963)

12. B. Morrill, Mechanical Vibrations, (Ronald Press, New York, 1957) p. 142

13. Maleev and Hartman, Machine Design, (International Textbook Company, New York, 1955)

14. D. R. White and J. E. Burke, The Metal Beryllium, (ASM, New York, 1955)

15. B. E. Gatewood, Thermal Stresses, (McGraw Hill, New York, 1957)

16. Standard Publication - Gas Turbine Sound and its Reduction, NEMA Publication No. SM33 - 1964

VII. DISTRIBUTION LIST FOR CONTRACT NAS3-10600

U.S. Atomic Energy Commission
Albuquerque Operations Office
P. O. Box 5400
Albuquerque, New Mexico 87115
Attn: L. P. Gise

U.S. Atomic Energy Commission
Germantown, Maryland 20767
Attn: Leonard Topper, Capt. R. Morrow

U.S. Atomic Energy Commission
Canoga Park Area Office
P. O. Box 591
Canoga Park, California 91305

U.S. Atomic Energy Commission
Chicago Operations Office
9800 South Cass Avenue
Argonne, Illinois 60439
Attn: George H. Lee

U.S. Atomic Energy Commission
Cincinnati Area Office
P. O. Box 39188
Cincinnati, Ohio 45239
Attn: Document Accountability

U.S. Atomic Energy Commission
Division of Technical Information Extension
P. O. Box 62
Oak Ridge, Tennessee 37830

U.S. Atomic Energy Commission
AEC Library
Mail Station G-017
Washington, D. C. 20545

U.S. Atomic Energy Commission
New York Operations Office
376 Hudson Street
New York, New York 10014
Attn: Reports Librarian

U.S. Atomic Energy Commission
Oak Ridge Operations Office
Mail and Document Accountability Section
P. O. Box E
Oak Ridge, Tennessee 37830
Attn: Document Library

U.S. Atomic Energy Commission
Office of Assistant General
Counsel for Patents
Washington, D. C. 20545
Attn: Roland A. Anderson

Aerojet-General Corporation
P. O. Box 296
Azusa, California 91702
Attn: Myra T. Grenier,
Corporate Librarian

Aerojet-General Corporation
P. O. Box 15847
Sacremento, California 95813
Attn: M.S. Nylin, Technical Library

Aerojet-General Corporation
San Ramon Plant
P. O. Box 86
San Ramon, California 94583
Attn: Sandra L. Johnson,
Document Custodian

Aeronautical Systems Division
Research & Technology Div. (SEPIR)
Wright-Patterson Air Force Base,
Ohio 45433
Attn: Augustus Daniels

Aerospace Corporation
P. O. Box 95085
Los Angeles, California 90045
Attn: Neil Crow, Supr. Reports
Acquisitions Group

Headquarters
U.S. Air Force (AFRSTG)
Washington, D. C. 20330
Attn: Chief, Nuclear Div.

Air Force Weapons Laboratory (WLIL)
Kirtland Air Force Base, New Mexico 87117
Attn: M.F. Canova

Air University Library
Maxwell Air Force Base, Alabama 36112
Attn: Mrs. E.C. Pittman, AUL3T-7143

Allison Division-GMC
P. O. Box 24013
Indianapolis, Indiana 46224
Attn: R.R. Blackwell, Security Coordinator

Argonne National Laboratory
9700 South Cass Avenue
Argonne, Illinois 60439
Attn: E.N. Pettitt

Headquarters
U.S. Army Ballistic Research Labs.
Aberdeen Proving Ground, Maryland 21005
Attn: Security Officer

Chief of Research & Development
Headquarters
Department of the Army
Washington, D. C. 20310
Attn: Chief, Nuclear, Chemical-Biological Division

Commanding Officer
U.S. Army Materials Research Agency
Watertown, Massachusetts 02172
Attn: AMXMR-ATL

Redstone Scientific Information Ctr.
U.S. Army Missile Command
Redstone Arsenal, Alabama 35809
Attn: Chief, Document Section

Nuclear Power Field Office
U.S. ARMY Engineer Reactors Group(USAERDL)
Fort Belvoir, Virginia 22060
Attn: Security Officer

Atomics International
A Div. of North American Aviation, Inc.
P. O. Box 309
Canoga Park, California 91304
Attn: Technical Library

Battelle Memorial Institute
Columbus Laboratories
505 King Avenue
Columbus, Ohio 43201
Attn: Dr. Stan J. Paprocki

Battelle Memorial Institute
Pacific Northwest Laboratory
P. O. Box 999
Richland, Washington 99352
Attn: Technical Information Section

Brookhaven National Laboratory
Technical Information Division
Upton, L.I., New York 11973
Attn: Classified Documents Group

Office of the Director of Defense
Research and Engineering
Room 3E-1071, Pentagon
Washington, D. C. 20301
Attn: Frank J. Thomas, Ass't. Director, Nuclear Programs

E.I. duPont de Nemours and Company
Savannah River Laboratory
Document Transfer Station 703-A
Aiken, South Carolina 29801

General Atomic Division
General Dynamics Corporation
P. O. Box 1111
San Diego, California 92112
Attn: Chief, Technical Information Serv.

General Electric Company
Nuclear Materials & Propulsion Opr.
P. O. Box 132
Cincinnati, Ohio 45215
Attn: J.W. Stephenson

General Electric Company
FPD Technical Information Center
Building 700 N-32
Cincinnati, Ohio
Attn: James J. Brady, Manager

General Electric Company
Missile and Space Division
P. O. Box 8555
Philadelphia, Pennsylvania 19101
Attn: C. Nemec, ANSO Library

General Electric Company
Atomic Power Equipment Department
P. O. Box 1131
San Jose, California 95108
Attn: Alleen Thompson

Institute for Defense Analyses
400 Army-Navy Drive
Arlington, Virginia 22202
Attn: Patricia W. Andrews

Jet Propulsion Laboratory
4800 Oak Grove Drive
Pasadena, California 91103
Attn: Louis Canter, Mgr. Library Section

The Johns Hopkins University
Applied Physics Laboratory
8621 Georgia Avenue
Silver Spring, Maryland 20910
Attn: Boris W. Kuvshinoff

Los Alamos Scientific Laboratory
P. O. Box 1663
Los Alamos, New Mexico 87544
Attn: Report Librarian

Martin Company
Division of Martin Marietta Corp.
Nuclear Products
P. O. Box 5042
Middle River, Maryland 21220
Attn: AEC Document Custodian

Minnesota Mining & Mfg. Company
P. O. Box 7565
H. C. Zeman, Security 235
St. Paul, Minnesota 55119

Monsanto Research Corporation
Mound Laboratory
P. O. Box 32
Miamisburg, Ohio 45342
Attn: Records Management Section

National Aeronautics & Space Admin.
Washington, D. C. 20546
Attn: Dr. F. Schulman (Code RNP)
Arvin H. Smith (Code RNP)

NASA-Ames Research Center
Moffett Field, California 94035
Attn: Library
A. C. Wilbur, M.S. N244-6

National Aeronautics & Space Admin.
Goddard Space Flight Center
Glenn Dale Road
Greenbelt, Maryland 20771
Attn: Librarian
Joseph Epstein

National Aeronautics & Space Admin.
Langley Research Center
Langley Station
Hampton, Virginia 23365
Attn: Associate Director

National Aeronautics & Space Admin.
Lewis Research Center
21000 Brookpark Road
Cleveland, Ohio 44135
Attn: Dr. Bernard Lubarsky M.S. 500-201
Roger Mather M.S. 500-309
James Ward M.S. 500-309
William Bifano M.S. 500-309
John Milko M.S. 500-201
Technology Utilization
Office M.S. 3-19
John E. Dilley M.S. 500-309
Library M.S. 60-3

National Aeronautics & Space Admin.
Manned Spacecraft Center
Houston, Texas 77058
Attn: Ass't. Chief for Technical
Information Programs

National Aeronautics & Space Admin.
George C. Marshall Space Flight Center
Huntsville, Alabama 35812
Attn: Lois M. Robertson, MS-IL

National Aeronautics & Space Admin.
Scientific & Technical Information Facility
P. O. Box 33
College Park, Maryland 20740
Attn: NASA Representative

National Aeronautics & Space Admin.
Washington, D. C. 20546
Attn: Document Control Officer, USS-10

National Reactor Testing Station (INC)
P. O. Box 2869
NRTS Technical Library
Idaho Falls, Idaho 83401
Attn: Document Control

Naval Facilities Engineering Command Hqrts.
Department of the Navy
Washington, D. C. 20390
Attn: Code 042, Director, Nuclear
Power Division

Director, Atomic Energy Division
Office of the Chief of Naval Operations
Department of the Navy
Washington, D. C. 20350

Commanding Officer and Director
U.S. Naval Radiological Defense Laboratory
San Francisco, California 94135

Director
U.S. Naval Research Laboratory
Washington, D. C. 20390
Attn: Classified Material Control Branch

Naval Ship Systems Command Hqrts.
Navships 08
Navy Department
Washington, D. C. 20360
Attn: Irene P. White

Nuclear Materials & Equipment Corp.
P. O. Box 354
Lewiston, New York 14092
Attn: Rudolph Placentino, Security
Officer

Pratt and Whitney Aircraft Division
United Aircraft Corporation
400 Main Street
East Hartford, Connecticut 06108
Attn: William H. Podolny

Radio Corporation of America
Electronic Components and Devices
415 South Fifth Street
Harrison, New Jersey 07029
Attn: M.J. Hegarty

Radio Corporation of America
Astro Electronics Division
P. O. Box 11
Cranbury, New Jersey 08512
Attn. Joseph E. Hanlon

Director, USAF Project Rand
Via: Air Force Liaison Office
The Rand Corporation
1700 Main Street
Santa Monica, California 90406
Attn: Frank R. Collbohn

Power Conversion Department
Republic Aviation Division
Fairchild Hiller Corporation
Farmingdale, New York 11735
Attn: Alfred E. Kunen or
Alfred Schock

Sandia Corporation
P. O. Box 5800
Albuquerque, New Mexico 87115
Attn: Mail Services Section
Warren Windle Division 9333
Howard Gerwin Division 9333

Thermo Electron Engineering Corp.
Jerome H. Weinstein/John Dunlay
P. O. Box 482
Waltham, Massachusetts 02154

Tracerlab
Division of Laboratory for Electronics, Inc.
2030 Wright Avenue
Richmond, California 94804
Attn: Leon Leventhal, Div. Mgr. Technical
Services

Union Carbide Corporation
Nuclear Division
X-10 Laboratory Records Department
P. O. Box X
Oak Ridge, Tennessee 37830

University of California
Lawrence Radiation Laboratory
P. O. Box 808
Livermore, California 94551
Attn: Technical Information Division

Westinghouse Electric Corporation
Aerospace Electrical Division
P. O. Box 7
Lima, Ohio 45802
Attn: George L. Arensman

Westinghouse Electric Corporation
Astronuclear Laboratory
P. O. Box 10864
Pittsburgh, Pennsylvania 15236
Attn: Florence McKenna, Librarian

Westinghouse Electric Corporation
Astronuclear Laboratory
P. O. Box 1064
Pittsburgh, Pennsylvania 15236
Attn: AEC Document Custodian

General Dynamics
Fort Worth Division
P. O. Box 748
Fort Worth, Texas 76101
Attn: Keith G. Brown or B.S. Fain